The certain generalized stresses method for assessment of variability of plate and shell structures

Mahyunirsyah Mahjudin

Par **Mahyunrisyah MAHJUDIN**

The certain generalized stresses method for assessment of variability of plate and shell structures

Thèse présentée en cotutelle
pour l'obtention du grade
de Docteur de l'UTC

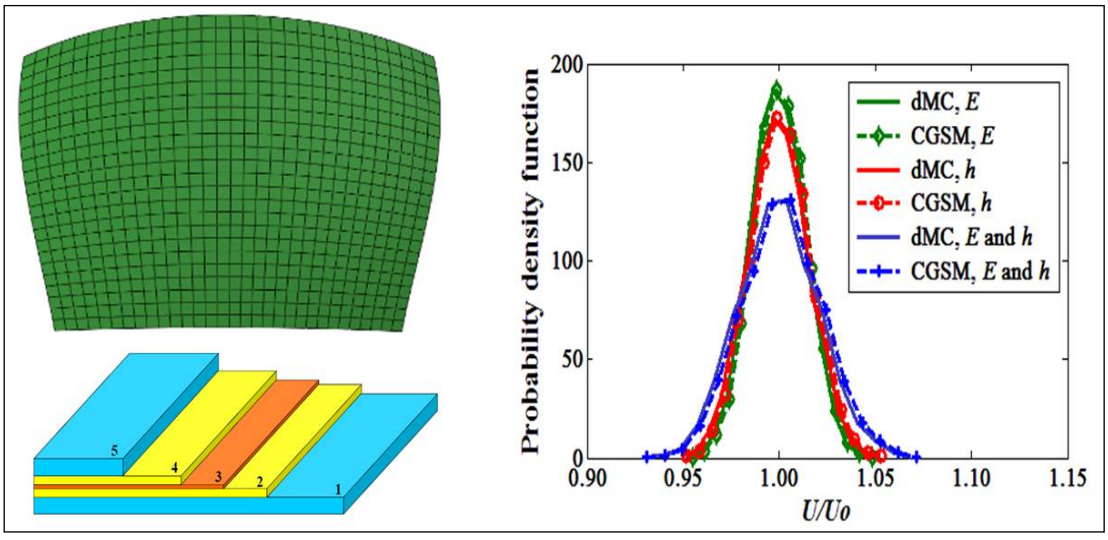

Soutenue le 30 octobre 2015
Spécialité : Mécanique Avancée

D2252

The certain generalized stresses method for assessment of variability of plate and shell structures

Par Mahyunrisyah MAHJUDIN

Soutenue le 30 octobre 2015 devant le jury composé de :

M. J-L. BATOZ (Président)
M. I. KATILI (Directeur de thèse)
M. P. LARDEUR (Directeur de thèse)
M. Y. LI (Rapporteur)
M. T. TISON (Rapporteur)
M. F. DRUESNE
M. H. SUHARTANTO

Invité : M. D. PRIADI

Acknowledgements

I am grateful to the Indonesian Government, the Embassy of France in Indonesia and the University of Technology of Compiègne for the financial support. I am also grateful to Professor Jean-Louis Batoz and Professor Irwan Katili who initiated the collaborative research program between University of Technology of Compiègne and Universitas Indonesia.

I would like to thank Professor Pascal Lardeur, Professor Irwan Katili and Professor Frédéric Druesne for their guidance, constant encouragement and mentorship throughout my doctoral studies. Their suggestions, comments and many hours of enthusiastic discussions have been instrumental in enhancing my understanding and appreciation of the subject of my thesis.

I wish to thank the reviewers Professor Thierry Tison and Professor Yuming Li for approving my thesis. Thanks are also due to Professor Jean-Louis Batoz, Professor Dedi Priadi, and Professor Heru Suhartanto, for their suggestions during my defense.

I want to thank my colleagues and friends from UTC: Djihad Rial, Kheris Fatah, Amine Tiar, Sui Liqi, Ha Manh Hung, Qi Yin, Brigitte Duch, and more generally the members of the Department of Mechanical Engineering and the Department of Mechanical Systems. I want to thank my colleagues and friends from UI: Riana Lumingkewas, Lita Barus, Toha Saleh, Surya Dharma, Hendriko, Mona Arif Muda, and more generally the members of the DDIP Program.

I would like to thank my family and especially my parents for all their love and support. Above all, I am deeply indebted to my dear wife Yonia who was bearing the brunt of work during my doctoral studies. Thank you for everything, most notably for being such a caring mother to our children.

Contents

Notations

n	number of finite elements
nk	number of layers
nX	number of random inputs
N	number of trials
KL	number of terms of Karhunen-Loève expansion
P	number of terms of polynomial chaos expansion
E	elasticity modulus
G	shear modulus
v	Poisson's ratio
L	characteristic dimension of the structure
h	thickness
A	area
V	volume
k_s	transverse shear correction factor
π_{int}	strain energy
π_{int}^{m}	membrane strain energy
π_{int}^{b}	bending strain energy
π_{int}^{tsh}	transverse shear strain energy
π_{int}^{i}	strain energy of element i
$\langle\varepsilon\rangle$	strain vector which contains the terms $\varepsilon_{xx}, \varepsilon_{yy}, \varepsilon_{zz}, \gamma_{xy}, \gamma_{xz}$ and γ_{yz}
$\langle e\rangle$	membrane strain vector which contains the terms e_x, e_y and e_{xy}

$\langle\chi\rangle$	bending strain vector which contains the terms χ_x, χ_y and χ_{xy}
$\langle\gamma\rangle$	transverse shear strain vector which contains the terms γ_{xz} and γ_{yz}
U	displacement
F	load applied at point P
$\langle N\rangle$	axial forces vector which contains the terms N_x, N_y, and N_{xy}
$\langle N'\rangle$	axial forces vector due to loads applied on the whole structure except at point P in the direction of interest which contains the terms N_x', N_y' and N_{xy}'
$\langle N^{"}\rangle$	axial forces vector due to a unitary load applied at point P in the direction of interest which contains the terms $N_x^{"}$, $N_y^{"}$ and $N_{xy}^{"}$
$\langle M\rangle$	moments vector which contains the terms M_x, M_y and M_{xy}
$\langle M'\rangle$	moments vector due to loads applied on the whole structure except at point P in the direction of interest which contains the terms M_x', M_y' and M_{xy}'
$\langle M^{"}\rangle$	moments vector due to a unitary load applied at point P in the direction of interest which contains the terms $M_x^{"}$, $M_y^{"}$ and $M_{xy}^{"}$
$\langle T\rangle$	transverse shear forces vector which contains the terms T_x and T_y
$\langle T'\rangle$	transverse shear forces vector due to loads applied on the whole structure except at point P in the direction of interest which contains the terms T_x' and T_y'

$\langle T^{"} \rangle$	transverse shear forces vector due to a unitary load applied at point P in the direction of interest which contains the terms $T_x^{"}$ and $T_y^{"}$
$[H]$	plane stress elasticity matrix
$[H_s]$	transverse shear elasticity matrix
$[A]$	generalized membrane stiffness matrix
$[B]$	membrane-bending coupling stiffness matrix
$[D]$	bending stiffness matrix
$[F]$	transverse shear stiffness matrix
$[H^k]$	plane stress elasticity stiffness matrix for layer k
$[Hs^k]$	transverse shear elasticity stiffness matrix for layer k
E_k	elasticity modulus for layer k
h_k	z-coordinate of bottom of layer k
$[H_0]$	mean value of the constitutive matrix
$[B_s]$	strain-displacement matrix
$[K]$	stiffness matrix
$[K_0]$	nominal stiffness matrix
$[K']$	first derivative of stiffness matrix
$[K'']$	second derivative of stiffness matrix
$\{F\}$	load vector
$\{F_0\}$	nominal load vector
$\{F^{'}\}$	first derivative of load vector
$\{F^{''}\}$	second derivative of load vector
$\{U\}$	displacement vector
$\{U_0\}$	nominal displacement vector
$\{U^{'}\}$	first derivative of displacement vector

$\{U''\}$	second derivative of displacement vector
$\psi_j(\theta)$	polynomial chaos expansion
Ω	sample space
ω	outcome
X	random variable
$F(x)$	cumulative distribution function
$f(x)$	probability density function
$P(X)$	probability of random variable X
$m(X)$	mean of random variable X
$\sigma(X)$	standard deviation of random variable X
$Var(X)$	variance of random variable X
$c.o.v.(X)$	coefficient of variation of random variable X
$Cov[X_1, X_2]$	covariance between two random variables X_1 and X_2
$[COV]$	autocovariance matrix
$H(x, \theta)$	random field
$\widehat{H}(x, \theta)$	random field discretization
$h(x)$	a set of basis functions used in the random field discretization
λ	eigenvalues of the autocovariance function
κ	eigenfunctions of the autocovariance function
$[U], [V]$	orthonormal eigenvectors of $[COV][COV]^T$ and $[COV]^T[COV]$
$[S]$	square roots of eigenvalues from $[U]$ or $[V]$
x	spatial coordinates
θ	randomness
$\rho[X_1, X_2]$	coefficient of correlation between X_1 and X_2
τ	absolute distance between two points

τ_1	difference between the x coordinates of two points
τ_2	difference between the y coordinates of two points
λ	correlation length
err	error
$err1^e$	first error criteria on the strain energy of an element
$err2^e$	second error criteria on the strain energy of an element
CGSM	Certain Generalized Stresses Method
MC	Monte Carlo
dMC	direct Monte Carlo
MCS	Monte Carlo Simulation

Abstract

Taking into account uncertainties in structural mechanics is a real challenge and leads to intensive research activities. The aim is to increase the predictive capability of numerical models coupling computational mechanics and uncertainties. In this thesis, aleatory uncertainties are considered and uncertain inputs are defined by probabilistic laws. The outputs are statistical quantities: mean value, standard deviation and probability density functions of the structural responses.

The objective of this research is to develop a methodology based on the Certain Generalized Stresses Method (CGSM), for the static finite element analysis of plates and shells with variability. The basic assumption is that the generalized stresses do not depend on input parameters perturbations. The CGSM is a non-intrusive method that requires only one finite element analysis with some load cases to calculate the variability of mechanical quantities of interest. The statistical results are obtained by Monte Carlo simulations, using a semi-analytical formula. The uncertain input parameters are elasticity moduli, Poisson's ratios and thicknesses. Uniform random parameters as well as random fields have been considered. The output parameters retained for the study are displacements and strains.

Several examples of membrane plates, bending plates, and homogeneous as well as multilayered shells, are treated. The results are compared with the direct Monte Carlo Simulation considered as a reference. Very satisfactory results are obtained for the mean value, standard deviation and probability densities of displacements and strains. The limitations of the methodology developed are also highlighted, in particular some discrepancies have been observed when random fields and very small correlation lengths are considered.

In summary the CGSM has several advantages. It allows an easy interfacing with standard finite element software, a large reduction of the high computational costs that characterize most of the existing approaches, and leads to accurate results. Consequently, application of the CGSM to real industrial examples is a promising perspective.

Résumé

La prise en compte des incertitudes en mécanique des structures constitue un challenge et mène à une importante activité de recherche. L'objectif est d'accroître la capacité prédictive des modèles numériques en couplant le calcul éléments finis et les incertitudes. Dans cette thèse, les incertitudes de type aléatoire sont considérées et les entrées incertaines sont définies par des lois statistiques. En sortie, les résultats sont des quantités statistiques : moyenne, écart-type et densité de probabilité des réponses de la structure.

L'objectif de cette recherche est de développer une méthodologie basée sur la méthode des efforts généralisés certains (CGSM) pour l'analyse statique par éléments finis des plaques et coques avec variabilité. L'hypothèse de base est que les efforts généralisés ne dépendent pas des perturbations des paramètres d'entrée. La méthode CGSM est non intrusive et ne nécessite qu'une seule analyse par éléments finis avec un certain nombre de cas de charge pour calculer la variabilité des quantités d'intérêt. Les résultats statistiques sont obtenus par simulations de Monte Carlo, en utilisant une formule semi-analytique. Les paramètres d'entrée incertains sont les modules d'élasticité, les coefficients de Poisson et les épaisseurs. Des variables aléatoires uniformes ainsi que des champs aléatoires sont considérés. Les résultats observés sont les déplacements et les déformations.

Plusieurs exemples de plaques en membrane, de plaques en flexion, de coques homogènes ou multicouche, ont été traités. Les résultats sont comparés avec des simulations de Monte Carlo directes. Des résultats très satisfaisants sont obtenus pour la moyenne, l'écart-type et la densité de probabilité des déplacements et des déformations. Les limitations de la méthodologie développée sont aussi mises en évidence, en particulier des écarts ont été observés lorsque des champs aléatoires avec de très petites longueurs de corrélation sont considérés.

En résumé, la méthode CGSM présente plusieurs avantages. Elle permet un interfaçage facile avec un logiciel éléments finis standard, une diminution très importante des temps de calcul élevés qui caractérisent la plupart des approches existantes et elle fournit des résultats précis. Par conséquent, l'application de la méthode CGSM à des exemples industriels constitue une perspective prometteuse.

Chapter 1
Introduction

1.1. Background

Improvement of the predictive capabilities of numerical models is currently a relevant challenge. Taking into account uncertainty and variability is one way to describe more closely the physical phenomena and so to increase the predictive capabilities of the numerical models. In an industrial context, several experimental studies have been performed and highlight uncertainty and variability phenomena, in particular in the vibration and acoustics domains. Some authors, namely Wood and Joachim [1] and Kompella and Bernhard [2] published experimental results highlighting this phenomenom, in particular in the vibration and acoustic behavior of automotive systems. Indeed, the structural acoustic behaviour of complex built-up structures such as cars is known to be highly variable. Lionnet and Lardeur [3] proposed a hierarchical approach to the assessment of the variability of interior noise levels measured in passenger cars. Scigliano et al. [4] and Arnoult et al. [5] studied the effect of the temperature changes on the windscreen vibration behaviour. The aim of these researches is to understand and then control the variability of industrial objects performances. In a mechanical system, there are a lot of potential sources of uncertainty and variability. Indeed boundary conditions, loading, constitutive material laws, physical properties and geometry are generally nondeterministic.

The basic principle of computational mechanics is constructing mathematical and then numerical models describing the physical reality as well as possible in order to reproduce the experimental observations. Performance of numerical models continuously increases along with the advances of the technologies and the computational methods. However as stated by Sudret [6]:

...despite the increase in the accuracy of the representations and in the power of computers, models will never be able to catch comprehensively the complexity of the real world. Indeed, they always rely upon simplifying assumptions that are usually validated a posteriori by experimental evidence...

The complexity of computational mechanics is due to the inherent uncertainty in the system computational modeling. Figure 1-1 gives a classification of sources and types of uncertainty in mechanics. This figure also highlights the contribution domain of the thesis. We distinguish here between mechanical modeling uncertainty, numerical modeling uncertainty and parametric uncertainty. Mechanical modeling uncertainty is due to the assumptions which lead to the mathematical model retained. It comprises namely the type of finite elements, constitutive laws including potential damage and rupture, boundary conditions and loading. Numerical modeling uncertainty is due to numerical choices. In particular the finite element mesh refinement level is a key point of this issue. In this thesis, we assumed that the mathematical model is correct, so the mechanical modeling uncertainty is not taken into account. However numerical modeling uncertainty is taken into account through the mesh issue. Parametric uncertainty comes from uncertainty of input parameters of the model: thicknesses, material properties... Parametric uncertainty is the main issue of this thesis. This problem can not be solved only by a classical deterministic calculation, but it needs a non deterministic approach. This process requires the identification of the input uncertainties in order to ensure results that are consistent with the physical reality. There are some constraints in the process of identification of the input uncertainties, such as the restrictions of budget, resources, knowledge and time [7].

Uncertainty is classified in two types: aleatoric uncertainty and epistemic uncertainty. This issue is detailed and discussed in chapter 2.

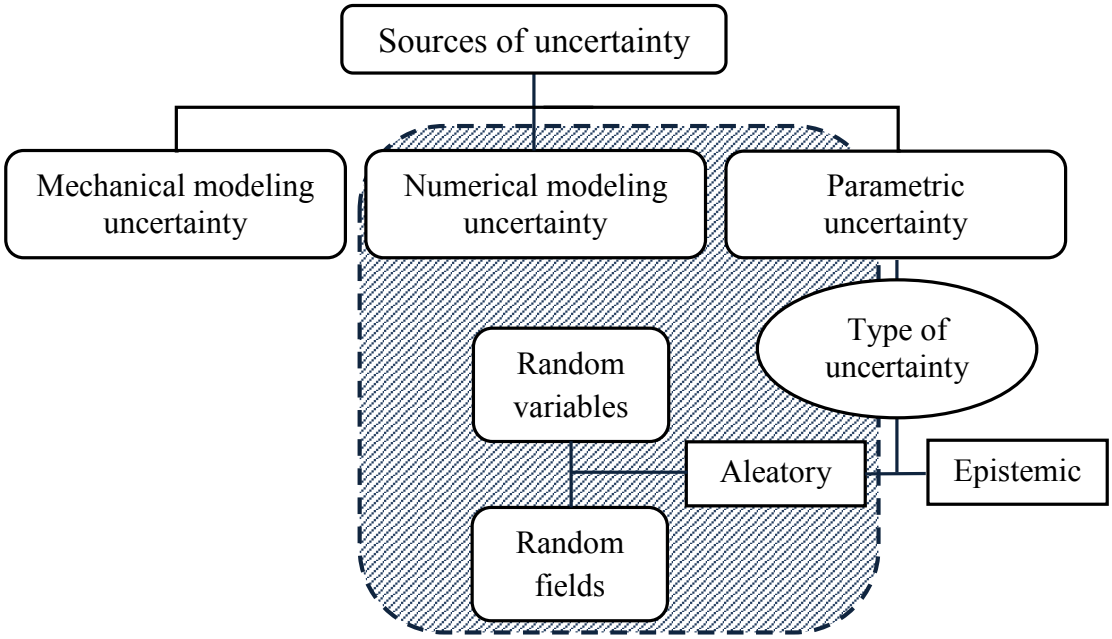

Figure 1-1 Classification of sources and types of uncertainty in mechanics – contribution domain of the thesis

Recently, the interest for solving uncertain problems in computational mechanics has grown. The stochastic finite element method is a solution to resolve uncertain problems. The stochastic finite element method is an extension of the classical finite element method, described for example in Batoz and Dhatt [8] and Katili [9], where the deterministic finite element computation is combined with the non deterministic computation to solve uncertain problems. Until now intensive researches have been conducted to develop reliable, accurate and efficient stochastic finite element methods.

As already mentioned, taking into account uncertainty is useful to improve the predictive capability of numerical models. The impact of the benefits is a better understanding of real systems behaviors, enhanced confidence in system analysis results, improvement in a decision making situation, and robust system for possible uncertainties [7]. Consequently taking into account uncertainty is one way to progress in the Verification and Validation process of finite element models. [10-13]. Indeed the major objective of this methodology is to increase the predictive capability of models. In particular validation which is the process of determining the degree to which a model is an accurate representation of the real world from the

perspective of the intended uses of the model, is clearly improved if uncertainty is considered.

1.2. Problem statement

Non deterministic finite element analysis leads to the following difficulties:

a. It is generally expensive in terms of computational time, in particular for industrial examples with a large number of degrees of freedom and a large number of uncertain parameters.
b. The results are not always accurate, in particular when the input variability level is large.
c. Numerous non deterministic methods are not compatible with standard finite element software.
d. Consequently, up to now, the application of stochastic methods to industrial examples is limited. In particular, the development of variability for industrial applications involving plate and shell structures is a real challenge.

1.3. Objectives and scope of research

The global objective of this research is to develop a numerical method to account variability of material and physical properties for plate and shell structures in static analysis. The proposed method uses the Certain Generalized Stresses Method (CGSM). The CGSM was introduced by Lardeur et al. [14-16] for bar and beam structures. This method is based on the assumption that the generalized forces are independent of uncertain parameters. The CGSM applied to bar and beam structures has several advantages: it needs only one finite element analysis in the nominal configuration, and gives very accurate results.

The first goal of this research is to develope the CGSM formulation for plate and shell structures. The second goal is to form a stochastic finite element computation by combining Monte Carlo simulation with the CGSM. The method proposed is compatible with any standard finite element software.

1.4. Thesis outline

The structure of this thesis is organized as described hereafter.

Chapter 2 presents the literature review of stochastic finite element (SFE) methods. It gives an overview of the quantification and discretization of uncertainty, classification of SFE methods, and the advantages and disadvantages of the existing SFE methods.

Chapter 3 presents methodological aspects in relation with the CGSM. It contains the principle of the CGSM and introduces the necessary mathematical tools. It describes the global process for the CGSM formulation of displacement, for uncertainty modeling. Error criteria to assess the CGSM assumption are proposed. Finally, the specific cases when the CGSM assumption is exactly verified, are identified.

Chapter 4 presents the formulation and applications of CGSM for membrane plates, chapter 5 for bending plates and chapter 6 for shells. All of these chapters begin with the description of the formulation of CGSM to calculate variability of displacements and strains. Then examples are treated. The results are compared with those given by the direct Monte Carlo Simulation considered as a reference.

Chapter 7 summarizes the contributions and conclusions of this research. Finally, some directions for future research are outlined.

Chapter 2
Literature Review

First, review papers and books relative to our research issue are presented in this paragraph. The following papers give a review of research in stochastic finite element approaches : Schuëller [17], Matthies et al. [18], Sudret and Der Kiureghian [19], Keese [20], Stefanou [21], Moens and Hanss [22], and Li and Chen [23]. Some books and doctorate manuscripts also deal with uncertainty: stochastic methods in structural dynamics [24, 25], probability methods [26-28], general Stochastic Finite Element Method [29, 30], Monte Carlo methods [31, 32], spectral methods [33, 34], perturbation methods [35], random fields [36, 37], uncertainty quantification and propagation [38, 39], and interval methods [40]. Papers relative to specific isues are presented in the next sections.

2.1. Input uncertainties

2.1.1. Different types of input uncertainties

Uncertainty may be due to inherent variability (irreducible uncertainty) or lack of knowledge (reducible uncertainty) [11]. In mechanical problems, many types of input parameters may be uncertain: material properties (elasticity modulus, Poisson's ratio, yield stress), physical properties (thicknesses), geometry, loading, boundary conditions… The quality of uncertainty representation is a key point for the accuracy of the propagation of uncertainties that leads to the variability of outputs of interest.

Based on Oberkampf et al. [41, 42], uncertainty can be classified in two types, namely aleatoric uncertainty and epistemic uncertainty. Aleatoric uncertainty can be described as an inherent variation that is associated with the physical system

or the environment. Random input and output variables are generally represented by statistical distributions, leading to a probabilistic approach. In this case, the probabilistic methods may be used if the experts can ensure the distribution. One distinguishes between discrete random variables and continuous random fields. Stefanou [21] distinguishes between three types of probabilistic methods: the Monte Carlo simulation, the perturbation stochastic finite element method, and the spectral stochastic finite element method. Epistemic uncertainty is caused by the lack of knowledge or information. Uncertain input and output parameters are defined by intervals. Moens and Hanss [22] or Mulani [39] distinguish between several types of possibilistic methods, in particular interval analysis and fuzzy set theory. Other approaches which associate probabilistic and possibilistic concepts, for example the evidence theory [2], are developed.

The mathematical framework for propagation uncertainties is dependent on uncertainty characterization. Generally one distinguishes between three types of uncertainty characterization, namely: interval, probability distribution and membership function, as shown in Figure 2-1. The input uncertainties can be identified with data assimilation process [13]. The data sources can come from results experimental observations, theoretical arguments, expert opinions.

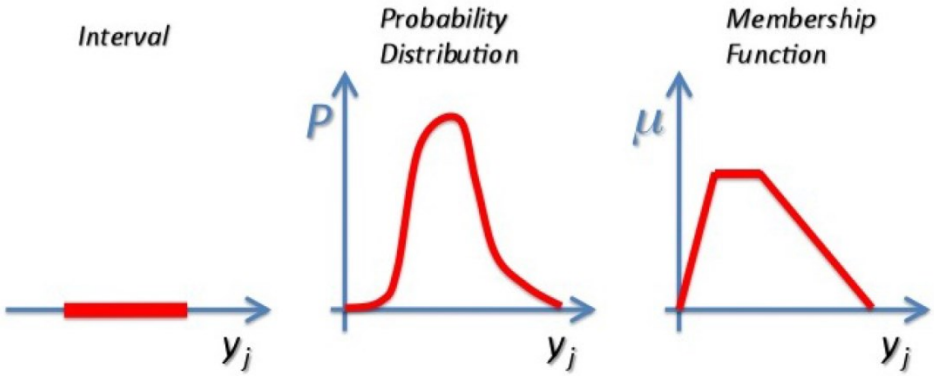

Figure 2-1 Different types of uncertainty characterization [13]

2.1.2. Probabilistic uncertainty quantification

In the probabilistic methods, the input variables X are defined by statistical laws. Several distribution laws exist: Gaussian or normal, uniform, lognormal, Weibull, etc. The distribution model selection depends on the characteristics of

uncertainty model consideration [43]. Log normal distribution may be used for properties to be modeled that are always positive [44]. A lot of physical parameters are well modeled by Gaussian distributions. This is namely justified by the existence of the central limit theorem. Hills et al. [45] presented a statistical analysis of the response distribution of nominally identical automotive vehicles. The distribution of acoustic transfer functions was shown to be a good fit to a Gaussian probability density function. The Gaussian distribution is probably the most commonly used model for random phenomena [29]. To prevent mathematical difficulties due to potential extreme values, truncated Gaussian laws are generally used.

A random field $\{H(x,\theta)\}$ is a collection of random variables X where x represents the spatial coordinates, θ represents a random process. Discretizing the random field $\{H(x,\theta)\}$ consists in approximating it by $\{\widehat{H}(x,\theta)\}$, which is defined by means of a finite set of random variables $(X_1, X_2, X_3, \dots, X_{nX})$ [46], grouped in a random vector $\{X(\theta)\}$:

$$\{H(x,\theta)\} \xrightarrow{\text{discretization}} \{\widehat{H}(x,\theta)\} = \{f(x,\{X(\theta)\})\} \qquad \textbf{2-1}$$

In general, the discretization methods can be divided into two groups: point discretization methods and average discretization methods. The objective of these methods mentioned below is to calculate the autocovariance matrix $[COV]$. In point discretization methods, $\{H(x,\theta)\}$ is represented by a vector at some given points in the domain of discretization. According to Panayirci [43], the accuracy and efficiency depend on the ratio between the correlation length and the size of the finite element used in the model, consequently the selection of the mesh is important. There are several point discretization methods: midpoint method (Der Kiureghian and Ke [47]), shape function or interpolation method (Liu et al. [48, 49], integration point method (Brenner and Bucher [50]). In the midpoint method, the random field is discretized at the centroid of each element. This method is simple and applicable with any probability distribution. Many researchers used this method such as Lee and Mosalam [51], Charmpis et al. [52], Ching and Phoon [53], etc. In the shape function or interpolation method, the random field can be

discretized at selected points as a nodal coordinate. Compared to the midpoint method, the advantage is that the continuity of the random field is better respected. In the integration point method, the random field is discretized at the integration points of the finite elements. Matthies et al. [18] stated the advantage of this method is its applicability for short correlation lengths.

In average discretization methods, the random variables are weighted integrals of $\{H(x,\theta)\}$ over a domain. Several methods are classified in the average discretization methods: optimal linear estimation method (OLE) (Li and Der Kiureghian [54]), local average method (Vanmarcke et al. [55, 56]), weighted integral method (Deodatis [57], and Deodatis and Shinozuka [58]).

When one of these point discretization methods or averaged discretization methods has been exploited, the random field is generally represented by series discretization methods. These series involve random variables and deterministic spatial functions. The random field $\{H(x,\theta)\}$ can be defined in the general form:

$$\{H(x,\theta)\} = \{m(X)\} + \sum_{i=1}^{nX} h_i(x)\{X_i(\theta)\} \qquad \textbf{2-2}$$

where x represents the spatial coordinates, $\{m(X)\}$ is the mean of the random field, θ represents a random process, *nX* is the number of random variables, $\{X_i(\theta)\}$ is a vector of random variables, and $h_i(x)$ is a basis function.

Several series discretization methods exist: singular value decomposition (Gerbrands [59]), Karhunen-Loève expansion (Loève [60], Ghanem and Spanos [33]), spectral representation (Shinozuka and Deodatis [61], Grigoriu [62]), and polynomial chaos expansion (Wiener [63], Sakamoto and Ghanem [64]). The singular value decomposition is described in more detail in section 3.8.2. The advantage of series discretization methods is they are able to reduce high dimensional and variable set of data points to a lower dimensional space [65].

In the Karhunen-Loève expansion, the set of basis functions used $h_i(x)$ (equation 2-2) is:

$$h_i(x) = \sqrt{\lambda_i}\,\kappa_i(x) \qquad \textbf{2-3}$$

where λ_i and κ_i are the eigenvalues and the eigenfunctions of the autocovariance matrix $[COV]$. Phoon et al. [66] and Pranesh and Gosh [67] proposed improvements to increase the efficiency of this method. Li et al. [68] developed it for the simulation of non-Gaussian random fields.

The spectral representation method proposed by Grigoriu [62] expands the random field as a sum of trigonometric functions with random phase and amplitudes:

$$\{\widehat{H}(x,\theta)\} = \sum_{i=0}^{nX-1} A_i \, cos(\omega_i\{x\} + \{X_i(\theta)\}) \qquad \textbf{2-4}$$

where $A_i = \sqrt{2\, S(\omega_i)\, \Delta\omega}$, $\omega_i = n\, \Delta\omega$, $\Delta\omega = \frac{\omega_i}{nX}$ and i = 0,1,2,..,nX-1.

The polynomial chaos expansion was proposed by Wiener [63] and Sakamoto and Ghanem [64]. The advantage of this method is its ability to generate sample function of non-Gaussian distribution by using classical polynomial chaos decomposition [21], with a random vector (equation 2-1):

$$\{\widehat{H}(x,\theta)\} = \sum_{i=0}^{p} h_i(x)\, \psi_i\{X_i(\theta)\} \qquad \textbf{2-5}$$

where $\psi_i\{X_i(\theta)\}$ is the chaos basis function and $h_i(x)$ refers to deterministic coefficients.

2.2. Propagation approaches and methods for stochastic analysis

2.2.1. Probabilistic and possibilistic approaches

In section 2.1.1, as shown in Figure 2-1, three types of uncertainty characterization have been distinguished. The propagation approaches are generally classified in two main types: probabilistic and possibilistic, the interval and the fuzzy approaches being considered as possibilistic ones. To compute the uncertainty ouput or response requires two processes: the uncertainty quantification and the propagation ones. Moreover one distinguishes between intrusive and non-

intrusive methods. Non intrusive methods are compatible with the use of standard finite element software (ex: Nastran, Abaqus …). Intrusive methods lead to the development of specific stochastic finite element software. Model errors, including the system modeling and numerical errors, have also to be considered. This global process is described in Figure 2-2.

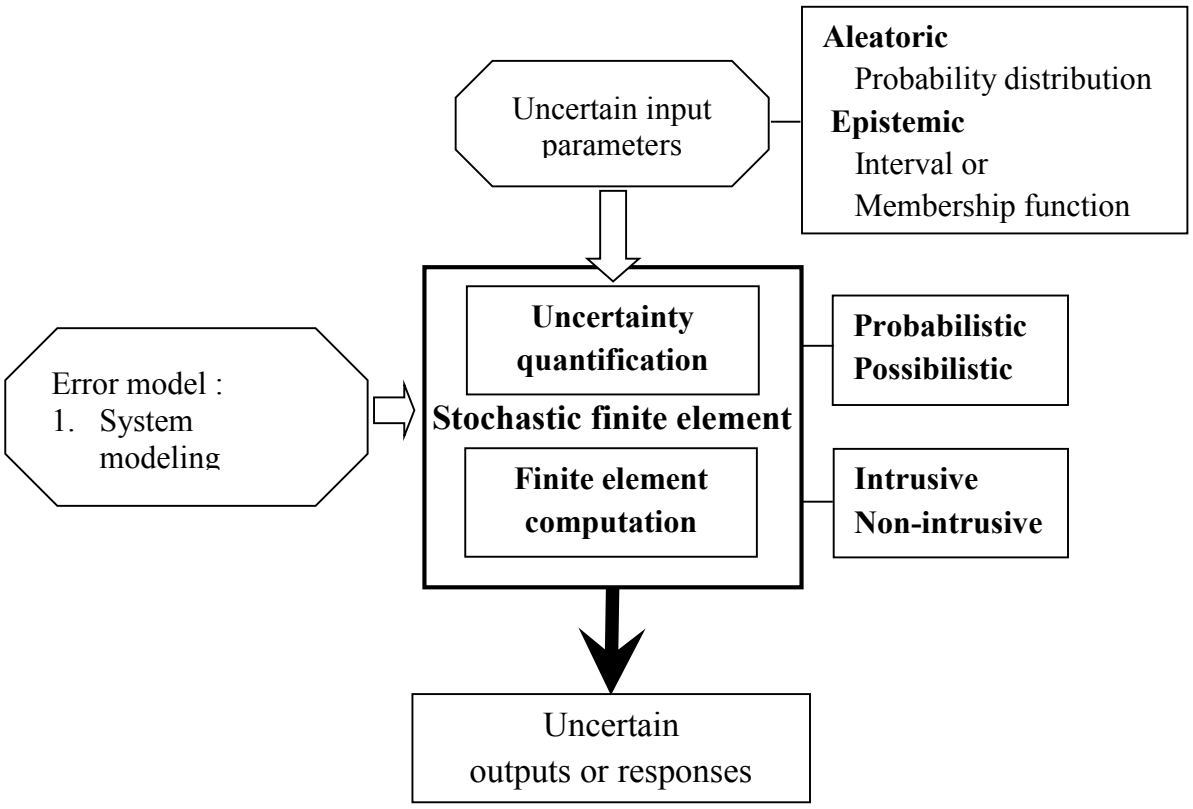

Figure 2-2 Global process for stochastic finite element problems

As mentioned in section 2.1.1, the uncertainty approaches can be classified into two major categories: probabilistic and possibilistic. For each type of approach, a large number of methods exist. In this section, the following methods: Monte Carlo simulation, perturbation, spectral finite element method, interval, fuzzy, CGSM, are presented.

2.2.2. Monte Carlo simulation

The Monte Carlo simulation was first proposed by Metropolis and Ulam [69]. The Monte Carlo simulation (MCS) has several advantages: it is the most robust method, it is simple to implement and it is adaptable to any discipline. Due to its robustness and simplicity, MCS is often used in the literature as a reference method in order to check the accuracy of other approaches. It is based on random sampling, where the laws of statistics are exploited to derive information on the variability of the response. The statistical outputs are obtained by generating samples of the random input parameters X_i that meet the statistical distribution retained, and using deterministic computation for each trial.

The Monte Carlo simulation leads to the evaluation of the output distribution. It allows the identification of the classical statistical quantities of interest: the mean $m(Y)$, the variance $Var(Y)$, the standard deviation $\sigma(Y)$, and then the coefficient of variation $c.o.v.(Y)$. If N is the number of trials, these quantities can be calculated as follows:

$$m(Y) = \frac{1}{N}\sum_{i=1}^{N} Y_i \qquad \textbf{2-6}$$

$$Var(Y) = \frac{1}{N-1}\sum_{i=1}^{N}\left(Y_i - m(Y_i)\right)^2 \qquad \textbf{2-7}$$

$$\sigma(Y) = \sqrt{Var[Y]} \qquad \textbf{2-8}$$

$$c.o.v.(Y) = \frac{\sigma(Y)}{m(Y)} \qquad \textbf{2-9}$$

The main drawback of this method is that it requires a lot of trials, leading to an expensive computational cost. Schenk and Schuëller [30] state the estimation error of the Monte Carlo simulation is arround $N^{-\frac{1}{2}}$.

Several techniques were developed to accelerate the convergence of the Monte Carlo simulation. The first type of approach leads to a reduction of the number of trials: latin squares (latin hypercube sampling, LHS) [70, 71], adaptive sampling [72], subset simulation [73-75], line sampling [76] and Sobol method [77, 78]. The second type of approach leads to the reduction of the computational time

for each trial, by using for example the spectral representation for uncertainty quantification [79-82] or by using Neumann expansion method [83-85]. Another well-known approach consists in using design of experiments and surface response models. In this case, the trials are performed using the response surface model rather than the finite element model.

2.2.3. Perturbation method

The perturbation approach [35, 48, 49, 86-93] is based on a Taylor series expansion of the response vector. The Taylor series expansion of the stiffness in the stochastic system can be expressed as:

$$[K] = [K_0] + \sum_{i=1}^{nX} [K_i'] X_i + \frac{1}{2} \sum_{i=1}^{nX} \sum_{j=1}^{nX} [K_{ij}''] X_i X_j + \cdots \quad \textbf{2-10}$$

where

$$[K_i'] = \left. \frac{[\partial K]}{\partial X_i} \right|_{X=0} \quad \text{and} \quad [K_i''] = \left. \frac{[\partial^2 K]}{\partial X_i \partial X_j} \right|_{X=0} \quad \textbf{2-11}$$

and $\{X_i\} = (X_1, X_2, X_3, \dots, X_{nX})$ is a random vector containting the random variables.

Similiarly the loading and the response can be defined by:

$$\{F\} = \{F_0\} + \sum_{i=1}^{nX} \{F_i'\} X_i + \frac{1}{2} \sum_{i=1}^{nX} \sum_{j=1}^{nX} \{F_{ij}''\} X_i X_j + \cdots \quad \textbf{2-12}$$

$$\{U\} = \{U_0\} + \sum_{i=1}^{nX} \{U_i'\} X_i + \frac{1}{2} \sum_{i=1}^{nX} \sum_{j=1}^{nX} \{U_{ij}''\} X_i X_j + \cdots \quad \textbf{2-13}$$

If the loading is considered deterministic ($\{F\} = \{F_0\}$ and $\{F_i'\} = \{F_{ij}''\} = 0$) , the displacement is:

$$\{U_0\} = [K_0]^{-1} \{F_0\} \quad \textbf{2-14}$$

$$\{U_i'\} = [K_0]^{-1} (-[K_i'] \{U_0\}) \quad \textbf{2-15}$$

$$\{U_{ij}''\} = [K_0]^{-1} \left(-[K_i'] \{U_j'\} - [K_j'] \{U_i'\} - [K_{ij}''] \{U_0\}\right) \quad \textbf{2-16}$$

The second order estimate of the mean of displacement is:

$$\{m(U)\} = \{U_0\} + \frac{1}{2}\sum_{i=1}^{nX}\sum_{j=1}^{nX}\{U_{ij}''\}\ Cov(X_i, X_j) \quad \textbf{2-17}$$

where $Cov(X_i, X_j)$ is the covariance between X_i and X_j as defined in equation 3-22.

Initially the perturbation method was applicable for small variations (< 10%) of the input variables [19]. The computational cost may be high for large problems due to the calculation of the partial derivatives $[K_i']$ and $[K_i'']$ [21]. Some authors, for example Falsone and Impollonia [89], proposed improvements of the perturbation method to overcome this drawback.

2.2.4. Spectral stochastic finite element method

The Spectral Stochastic Finite Element Method (SSFEM) was proposed by Ghanem and Spanos [33, 94]. This method uses Karhunen-Loève expansion (see equations 2-2 and 2-3) to model the uncertain input parameters and polynomial chaos expansion to calculate the propagation of response. In the SSFEM, the stiffness matrix of an element is expressed as:

$$[K] = \sum_{i=0}^{\infty}[K_i]\, X_i(\theta) \quad \textbf{2-18}$$

where $[K_0]$ is the nominal stiffness matrix, θ represents a random process, X_i are uncorrelated Gaussian random variables (except for $i = 0$ indeed $X_0 = 1$), $[K_i]$ are deterministic matrices defined as:

$$[K_i] = \sqrt{\lambda_i(x)}\int_{\Omega_i}\kappa_i(x)\,[B]^T\,[H_0]\,[B]\,d\Omega_i \quad \textbf{2-19}$$

where $[B]$ is the strain-displacement matrix and $[H_0]$ is the mean value of the constitutive matrix. For $\lambda_i(x)$ and $\kappa_i(x)$ see equation 2-3. Using polynomial chaos expansion, the stochastic displacement vector $U(\theta)$ can be written as:

$$\{U(\theta)\} = \sum_{j=0}^{\infty}\{U_j\}\ \psi_j(\theta) \quad \textbf{2-20}$$

where $\{U_j\}$ is a set of nodal displacement coefficients and $\psi_j(\theta)$ are orthonormal polynomials that define the so-called series polynomial chaos. The finite element equilibrium for deterministic loading is given by:

$$\left(\sum_{i=0}^{\infty}[K_i]\,X_i(\theta)\right).\left(\sum_{j=0}^{\infty}\{U_j\}\;\psi_j(\theta)\right)-\{F\}=\;0 \qquad \textbf{2-21}$$

For computational purpose, the series expansion in the equation 2-21 are truncated with a finite number of terms using *KL*+1 terms of Karhunen-Loève expansion for the stiffness matrix expansion and *P* terms of polynomial chaos expansion for the displacement vector expansion. The solution of equation 2-21 is obtained by minimizing the residual in a mean square sense [19].

In its initial version, the SSFEM was limited and only applicable for a small number of degrees of freedom. There were several attempts to solve equation 2-21 more efficiently by using block diagonal-sparse for matrix $[K]$, Krylov-type iterative techniques to reduce matrix-vector products [95, 96], and ad hoc iterative solution techniques [97, 98]. Several studies on the non-intrusive approach in the SSFEM have been proposed, such as Ghiocel and Ghanem [99] who used projection method and Berveiller et al. [100] and Blatman and Sudret [78] who used regression method. The disadvantage of the SSFEM is the quality of the results depends on the dimension of polynomials.

2.2.5. Interval analysis

The interval analysis was initiated by Moore [40] in 1958. In the interval analysis, the uncertain variables are described by upper and lower bounds. The aim of the interval analysis is to find upper and lower bound of any of the response variables. There are essentially two approaches in the interval analysis [22], namely interval arithmetic approach and global optimisation approach.

Interval arithmetic approach is conducted by using interval arithmetic operations. For example, considering two intervals $X1 = [X1_{min}, X1_{max}]$ and $X2 = [X2_{min}, X2_{max}]$, the operations on $X1$ and $X2$ can be defined by [101]:

$$X1 + X2 = [X1_{min} + X2_{min}, X1_{max} + X2_{max}]$$

$$X1 - X2 = [X1_{min} - X2_{max}, X1_{max} - X2_{min}]$$

$$X1.X2 = \begin{bmatrix} min(X1_{min}X2_{min}, X1_{min}X2_{max}, X1_{max}X2_{min}, X1_{max}X2_{max}) \\ max(X1_{min}X2_{min}, X1_{min}X2_{max}, X1_{max}X2_{min}, X1_{max}X2_{max}) \end{bmatrix} \quad \textbf{2-22}$$

$$\frac{X1}{X2} = [X1_{min}, X1_{max}].[1/X2_{max}, 1/X2_{min}]$$

A well-known problem is that the interval arithmetic overestimates the response interval. As reported by Moens and Hanss [22], attempts have been made to limit this conservatism [102-104].

The global optimisation approach can also be used for the interval analysis. Indeed, the objective of an interval analysis is to identify the lower and bigger bounds of an output quantity of interest, leading to minimization and maximization problems. Several studies contributed to this approach: Majumder and Rao [105], Xu and Qiu [106], and Santoro et al. [107].

2.2.6. Fuzzy set theory

Zadeh [108] initiated the development of the fuzzy set theory. Moens and Vandepitte [109] presented a review of the main methods developed in this domain. A fuzzy set can be interpreted as an extension of a conventional interval. Where a classical set clearly distinguishes between members and non-members of the set, the fuzzy set introduces a degree of membership, represented by the membership function. This membership function describes the grade of membership to the fuzzy set for each element in the domain. The concept allows membership values comprised between zero and one. This enables the representation of a value that is only to a certain degree member of the set (α). Examples of membership functions are given in Figure 2-3.

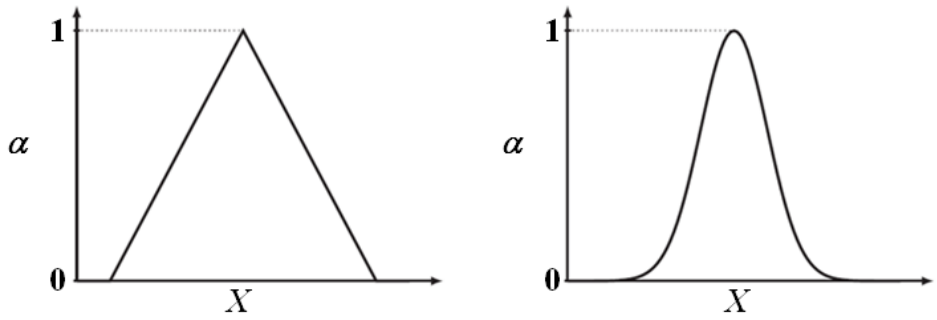

Figure 2-3 Triangular and Gaussian fuzzy membership functions [22]

A discretized approximation of the output membership functions can be obtained by repeating the α-cut procedure at a number of membership levels. Consequently, a fuzzy numerical analysis can be replaced by a sequence of interval numerical analyses. Illustration of this procedure can be seen in Figure 2-4.

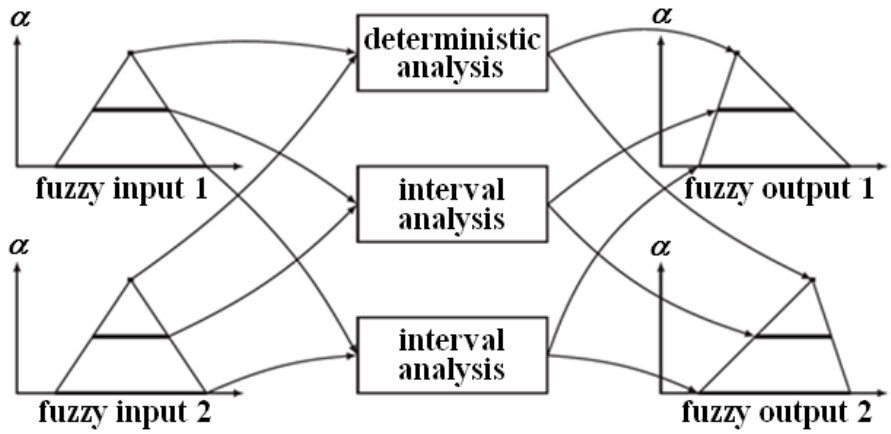

Figure 2-4 α-cut procedure applied at three membership levels on a function with two inputs and two outputs [22]

Several papers deal with recent advances in fuzzy finite element methods. Sawyer and Rao [110] studied the strength-based reliability of fuzzy structural and mechanical systems. Massa et al. [111, 112] used optimisation technique and Taylor expansion to speed up the exact goal function. Farkas et al. [113] studied reanalysis-based FEM with the purpose of reducing computational cost of the repeated deterministic FE solutions that arise in a fuzzy FE analysis.

2.2.7. The Certain Generalized Stresses Method

The CGSM was initiated by Lardeur et al. [14-16]. This method accelerates the mechanical computation in the stochastic finite element approach. Up to now this method has essentially been developed in the context of a probabilistic approach. Applications have been conducted on bar and beam structures [14-16]. In this thesis the CGSM is developed and evaluated for membrane plates, bending plates and shells. For shells, single-layered as well as multilayered structures, made of isotropic materials, are considered.

Chapter 3
Methodological Aspects

3.1. Introduction

This chapter introduces the main methodological aspects which are necessary for the approaches based on the CGSM developed in this study; these methodological aspects are exploited in chapters 4, 5 and 6. First the principle of the CGSM is recalled. Then the first and second Castigliano's theorems are described. Namely, the second Castigliano's theorem is exploited for the CGSM. Lardeur et al. [14-16] developed the CGSM formulations which uses the Castigliano's second theorem, for calculating the displacement variability in structures made of bars and beams. In this study we develop the CGSM formulations for more complex structures, namely membrane plates, bending plates, and homogeneous as well as heterogeneous shells. Some general comments are given about the nominal finite element analysis required in the CGSM. The relations between the generalized stresses and strains are also described, for the homogeneous as well as the heterogeneous case. The description of the different types of uncertain input parameters taken into account is given. In this study, material and physical parameters may be uncertain. Uncertainty modeling is also described. In particular, one distinguishes between random variables and random fields. Random fields require a specific treatment and the methodology used to describe random fields is detailed. The spatial discretization is also a key point of the finite element analysis with variability. Our approach about this issue is presented. Finally several error criteria are used to assess the CGSM. These criteria are described and justified.

3.2. Principle of the Certain Generalized Stresses Method

The flowchart of the CGSM is shown in Figure 3-1. The principal process described in this figure is valid for all types of thin-walled structures: bars, beams, plates and shells. The CGSM is based on the assumption that the generalized stresses are independent of the uncertain parameters. Thanks to this assumption, only one finite element run with some load cases, in the nominal configuration, is necessary to calculate the generalized stresses. It is then possible to calculate the internal strain energy of the system for all values of uncertain parameters without further finite element analysis. The displacement of a point of the structure is evaluated using Castigliano's theorem. A simplified expression of the displacement is then obtained. By using this expression, a Monte Carlo simulation is performed to calculate the mean value, standard deviation and distribution of the displacement. For some types of structures, the mean value and the standard deviation can also be obtained analytically. The CGSM is a non intrusive method and it is compatible with the use of any standard finite element software. In this study, Abaqus [114] has been used to treat the examples. In particular, the finite elements S3 and S4 of Abaqus have been used. Moreover, the finite element DKMQ [115] has been implemented in Abaqus as a user's element.

Finally, the CGSM can be considered as a post-treatment of one standard finite element calculation. In this study, Abaqus is used for the nominal finite element analysis and Matlab [116] is exploited for the post-treatment stage. To calculate the variability at n points, one finite element analysis with $2n$ load cases at most are needed. This finite element analysis is performed in the nominal configuration, so for the different load cases the stiffness matrix is always the same and consequently, this matrix has to be inverted only once. This is an advantage from the computational time point of view.

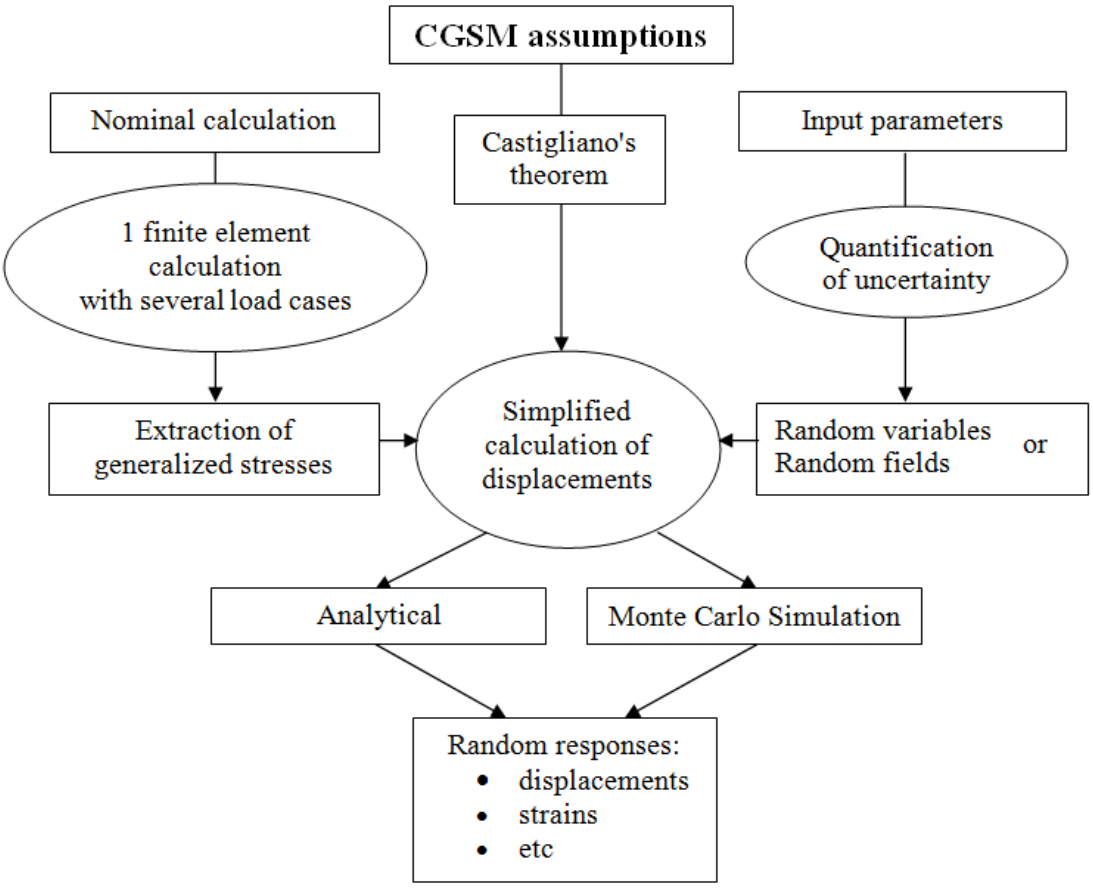

Figure 3-1 Principle of the CGSM method for calculating variability

3.3. Castigliano's theorem

Castigliano's theorem is conducted by an Italian engineer Alberto Castigliano in 1879. It allows the computation of a deflection at any point in a structure. There are two theorems [117]:

I. Castigliano's first theorem

The first partial derivative of the total internal energy (strain energy) in a structure with respect to any particular deflection component at a point is equal to the force applied at that point and in the direction corresponding to that deflection component.

$$F = \frac{\partial \pi_{int}}{\partial U} \qquad \textbf{3-1}$$

This first theorem is applicable to linear or nonlinear elastic structures in which the temperature is constant and the supports are unyielding.

II. Castigliano's second theorem

The first partial derivative of the total internal energy in a structure with respect to the force applied at any point is equal to the deflection at the point of application of that force in the direction of its line of action.

$$U = \frac{\partial \pi_{int}}{\partial F} \quad \textbf{3-2}$$

The second theorem of Castigliano is applicable to linear elastic (Hookean material) structures with constant temperature and unyielding supports.

In order to apply the Castigliano's theorem for calculating the displacement U at a point P in a given direction, generalized stresses are decomposed into two contributions:

$$F_{gs} = F_{gs}' + F F_{gs}'' \quad \textbf{3-3}$$

where F is the load applied at point P in the direction of interest; F_{gs} are the generalized stresses; F_{gs}' are the generalized stresses due to loads on the whole structure except at point P in the direction of interest; F_{gs}'' are the generalized stresses due to a unit load applied at point P in the direction of interest.

3.4. Derivation of CGSM formulation for displacement

In this section the main steps of the derivation of the CGSM formulation for calculating the variability of displacements are given.

a. Writing the expression of the total strain energy which contains the nominal generalized stresses and all the uncertain parameters (material properties, thicknesses…):

$$\pi_{int} = f_1(N, M, T, E, v, h) \quad \textbf{3-4}$$

b. Decomposing generalized stresses into two contributions, the total strain energy formulation becomes:

$$\pi_{int} = f_2(N', M', T', N'', M'', T'', F, E, v, h) \quad \textbf{3-5}$$

c. From equations 3-2 and 3-5, one obtains an explicit and simplified expression of the displacement:

$$U = f_3(N', M', T', N'', M'', T'', F, E, v, h) \quad \textbf{3-6}$$

d. A fast Monte Carlo Simulation is performed by exploiting equation 3-6.

The CGSM also allows the calculation of the variability of strains. This issue is discussed in detail in chapter 4.

3.5. Nominal finite element analysis

The CGSM only requires one nominal finite element analysis with several load cases for the calculation of the displacement variability. The detailed processes have been explained in the section 3.2. The CGSM needs the nominal generalized stresses. These generalized stresses may be obtained with any finite element software and are exported in a development software (ex: Matlab) for the treatment of variability. Moreover, any type of element (triangular or quadrilateral) is compatible with the CGSM. Finally the CGSM is a non-intrusive method.

3.6. Generalized constitutive laws

Relationship between generalized stresses and strains depends on the type of material. Homogeneous as well as heterogeneous materials are considered.

The relationship between the generalized stresses $\langle N\ M\ T \rangle$ and strains $\langle \varepsilon\ \ \chi\ \ \gamma \rangle$ for a homogeneous and isotropic material is given hereafter.

a. Membrane: relationship between axial forces $\{N\}$ and in-plane strains $\{\varepsilon\}$:

$$\{N\} = h[H]\{\varepsilon\} \quad \textbf{3-7}$$

$$\begin{Bmatrix} N_x \\ N_y \\ N_{xy} \end{Bmatrix} = \frac{Eh}{1-v^2} \begin{bmatrix} 1 & v & 0 \\ v & 1 & 0 \\ 0 & 0 & \frac{1-v}{2} \end{bmatrix} \begin{Bmatrix} \varepsilon_x \\ \varepsilon_y \\ \gamma_{xy} \end{Bmatrix}$$

b. Bending: relationship between moments $\{M\}$ and curvatures $\{\chi\}$:

$$\{M\} = \frac{h^3}{12}[H]\{\chi\}$$

$$\begin{Bmatrix} M_x \\ M_y \\ M_{xy} \end{Bmatrix} = \frac{Eh^3}{12(1-v^2)} \begin{bmatrix} 1 & v & 0 \\ v & 1 & 0 \\ 0 & 0 & \frac{1-v}{2} \end{bmatrix} \begin{Bmatrix} \chi_x \\ \chi_y \\ \chi_{xy} \end{Bmatrix} \quad \textbf{3-8}$$

c. Transverse shear: relationship between transverse shear forces $\{T\}$ and out-of-plane shear strains $\{\gamma\}$:

$$\{T\} = k_s[H_s]\{\gamma\}$$

$$\begin{Bmatrix} T_x \\ T_y \end{Bmatrix} = k_s G\, h \begin{bmatrix} 1 & 0 \\ 0 & 1 \end{bmatrix} \begin{Bmatrix} \gamma_{xz} \\ \gamma_{yz} \end{Bmatrix} \quad \textbf{3-9}$$

$$G = \frac{E}{2\,(1+v)} \quad \textbf{3-10}$$

where $[H]$ is the plane stress elasticity matrix, $[H_s]$ is the transverse shear elasticity matrix, h is the thickness, E is the elasticity modulus, v is the Poisson's ratio, G is the shear modulus, and k_s is the transverse shear correction factor.

As far as multilayered composite structures are concerned, several references give detailed information leading to the generalized constitutive laws. These details are not given here, the reader can refer for example to the following books: Ashton and Whitney [118], Nettles [119], Reddy [120], Berthelot [121]. The relationship between the generalized stresses $\langle N\ M\ T \rangle$ and strains $\langle \varepsilon\ \ \chi\ \ \gamma \rangle$ for a multilayered isotropic structure made of isotropic materials is:

$$\begin{Bmatrix} N_x \\ N_y \\ N_{xy} \\ M_x \\ M_y \\ M_{xy} \\ T_x \\ T_y \end{Bmatrix} = \left[\begin{array}{ccc|ccc|cc} A_{11} & A_{12} & A_{13} & B_{11} & B_{21} & B_{31} & 0 & 0 \\ A_{12} & A_{22} & A_{23} & B_{12} & B_{22} & B_{32} & 0 & 0 \\ A_{13} & A_{23} & A_{33} & B_{13} & B_{23} & B_{33} & 0 & 0 \\ \hline B_{11} & B_{12} & B_{13} & D_{11} & D_{12} & D_{13} & 0 & 0 \\ B_{21} & B_{22} & B_{23} & D_{12} & D_{22} & D_{23} & 0 & 0 \\ B_{31} & B_{32} & B_{33} & D_{13} & D_{23} & D_{33} & 0 & 0 \\ \hline 0 & 0 & 0 & 0 & 0 & 0 & F_{11} & F_{12} \\ 0 & 0 & 0 & 0 & 0 & 0 & F_{12} & F_{22} \end{array}\right] \begin{Bmatrix} e_x \\ e_y \\ e_{xy} \\ \chi_x \\ \chi_y \\ \chi_{xy} \\ \gamma_{xz} \\ \gamma_{yz} \end{Bmatrix} \quad \textbf{3-11}$$

where:

$$\begin{aligned} A_{ij} &= \sum_{i=1}^{nk} H_{ij}^k (h_k - h_{k-1}) \\ B_{ij} &= \frac{1}{2} \sum_{i=1}^{nk} H_{ij}^k (h_k^2 - h_{k-1}^2) \\ D_{ij} &= \frac{1}{3} \sum_{i=1}^{nk} H_{ij}^k (h_k^3 - h_{k-1}^3) \\ F_{ij} &= k_s \sum_{i=1}^{nk} Hs_{ij}^k (h_k - h_{k-1}) \end{aligned} \quad \textbf{3-12}$$

where $[A]$, $[B]$, $[D]$, and $[F]$ are respectively the generalized membrane stiffnesses, membrane-bending coupling stiffnesses, bending stiffnesses and transverse shear stiffnesses; nk is the number of layers; $[H^k]$ is the plane stress elasticity stiffnesses for layer *k*; $[Hs^k]$ is the transverse shear elasticity stiffnesses for layer *k*; E_k is the elasticity modulus for layer *k*; h_k is the z-coordinate of bottom of layer *k*; and k_s is the transverse shear correction factor.

3.7. Uncertain input parameters

The uncertain input parameters are the material and physical properties. The uncertain material properties are the elasticity modulus *E* and Poisson's ratio ν, the uncertain physical property is the thickness *h*. These uncertain parameters can be quantified by using random variables or random fields.

3.8. Uncertainty modelling

Stochastic models are considered for material and physical properties as explained in the previous section. This thesis uses a probabilistic approach. The CGSM is compatible with any distribution law without any specific difficulty, in this study essentially truncated Gaussian laws are exploited. In this study the truncation meets the so-called $\pm 3\sigma$ rule. Indeed, as stated in section 2.1.2, the Gaussian distribution is the most commonly used model for random phenomena. There are two models of uncertainty which are considered, namely random variables and random fields.

3.8.1. Gaussian random variables

Random variables are defined by a Cumulative Distribution Function (CDF), $F(x)$:

$$F(x) = P(X \leq x), \qquad -\infty \leq x \leq \infty \tag{3-13}$$

or its Probability Density Function (PDF), $f(x)$:

$$P(a \leq X \leq b) = \int_{-\infty}^{\infty} f(x)\, dx \tag{3-14}$$

with function $f(x)$ for Gaussian distribution:

$$f(x) = \frac{1}{\sqrt{2\pi}\,\sigma} exp\left[-\frac{1}{2}\left(\frac{x - m(X)}{\sigma}\right)^2\right], \quad -\infty \leq x \leq \infty \tag{3-15}$$

The relation between $f(x)$ and the Cumulative Distribution Function (CDF) is:

$$f(x) = \frac{dF(x)}{dx} \tag{3-16}$$

with:

$$F(x) = \frac{1}{\sqrt{2\pi}\,\sigma} \int_{-\infty}^{\infty} exp\left[-\frac{1}{2}\left(\frac{x - m(X)}{\sigma}\right)^2\right] dx \tag{3-17}$$

The first moment is the mean of X, defined by:

$$m(X) = \int_{-\infty}^{\infty} x\, f(x)\, dx \qquad \textbf{3-18}$$

a. Probability density function b. Cumulative distribution function

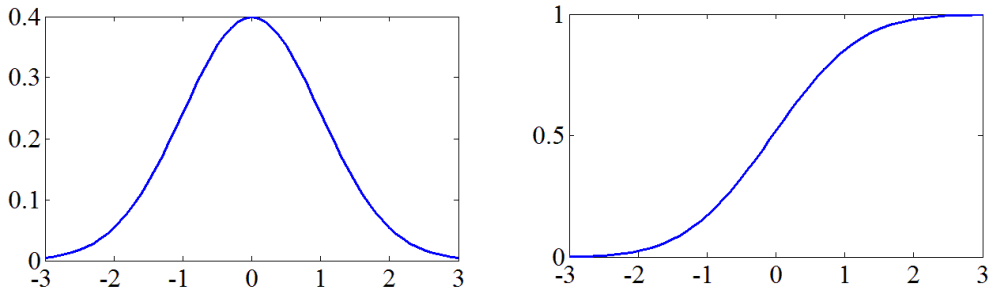

Figure 3-2 Probability density function (PDF) and cumulative distribution function (CDF) of Gaussian distribution

Variance, standard deviation and coefficient of variation of a random variable *X* are respectively defined by:

$$Var[X] = m\,[(X - m(X))(X - m(X))] = \int_{-\infty}^{\infty} (x - m(X))^2\, f(x) dx \qquad \textbf{3-19}$$

$$\sigma(X) = \sqrt{Var[X]} \qquad \textbf{3-20}$$

$$c.o.v.(X) = \frac{\sigma(X)}{m(X)} \qquad \textbf{3-21}$$

3.8.2. Random fields

Random fields allow continous random variations of inputs with the multiple probabilistic variables $(X_1, X_2, X_3, \dots, X_n)$. The covariance of two variables X_i and X_j is defined by:

$$Cov[X_i, X_j] = m\,[(X_i - m(X_i))(X_j - m(X_j))] \qquad \textbf{3-22}$$

The autocovariance matrix $[COV]$ of *nX* random variables is:

$$[COV] = \begin{bmatrix} Var[X_1] & Cov[X_1, X_2] & \dots & Cov[X_1, X_{nX}] \\ Cov[X_2, X_1] & Var[X_2] & \dots & Cov[X_2, X_{nX}] \\ \vdots & \vdots & \ddots & \vdots \\ Cov[X_{nX}, X_1] & Cov[X_{nX}, X_2] & \dots & Var[X_{nX}] \end{bmatrix} \quad \textbf{3-23}$$

where $[COV]$ is a positive definite and symmetric matrix.

The autocorrelation of the multiple probabilistic variables is obtained by normalizing the autocovariance by the respective standard deviation:

$$\rho[X_i, X_j] = \frac{Cov[X_i, X_j]}{\sigma(X_i)\sigma(X_j)} \quad \textbf{3-24}$$

or the autocovariance $Cov[X_i, X_j]$ is defined by:

$$Cov[X_i, X_j] = \sigma(X_i)\sigma(X_j)\rho[X_i, X_j] \quad \textbf{3-25}$$

Generally random fields are assumed to be homogeneous and isotropic. In this case, the mean and covariance of the field are constant over the whole domain and the autocorrelation function depends on the absolute distance between two positions. Several types of correlation functions are used:

$$\rho[X_i, X_j] = \exp\left(-\frac{\tau}{\lambda}\right) \quad \text{(exponential)} \quad \textbf{3-26}$$

$$\rho[X_i, X_j] = \exp\left(-\frac{\tau^2}{\lambda^2}\right) \quad \text{(square exponential)} \quad \textbf{3-27}$$

where $\tau = (|x_i - x_j|)$ is the absolute distance between two positions relative to X_i and X_j, and λ is the correlation length, which may be written $\lambda = bL$, where b is a coefficient and L is a characteristic dimension of the structure.

Random fields can also be anisotropic, in this case the correlation function may be defined as follows:

$$\rho[X_i, X_j] = \exp\left[-\left(\frac{|\tau_x|}{\lambda_x} + \frac{|\tau_y|}{\lambda_y}\right)\right] \quad \text{(exponential)} \quad \textbf{3-28}$$

$$\rho[X_i, X_j] = (1 - \zeta)\exp[-(\zeta)] \quad \text{(square exponential)} \quad \textbf{3-29}$$

with

$$\zeta = \left(\frac{\tau_x}{\lambda_x}\right)^2 + \left(\frac{\tau_y}{\lambda_y}\right)^2 \quad \textbf{3-30}$$

where τ_x and τ_y represent the distances along the *x* and *y* axes, $\lambda_x = b_1 L$ and $\lambda_y = b_2 L$ are the correlation lengths associated with the *x* and *y* axes respectively.

Discretization method used is the midpoint method, and the random field is discretized at the centers of gravity of elements. This technique is widely used in applications primarily because of its simplicity. The main disadvantage of this method is that it requires one variable per element, leading to a large number of random variables when the mesh is fine.

Singular value decomposition is utilized to decompose the autocovariance matrix. Singular value decomposition is based on a theorem from linear algebra [65]. The autocovariance matrix can be decomposed into the product of three matrices: an orthogonal matrix $[U]$, a diagonal matrix $[S]$ and the transpose of orthogonal matrix $[V]$. The singular value decomposition equation is defined by:

$$[COV] = [U][S]^{\frac{1}{2}}[V]^T \quad \textbf{3-31}$$

where $[U]^T[U] = [I]$; $[V]^T[V] = [I]$; the columns of $[U]$ and $[V]$ are orthonormal eigenvectors of $[COV][COV]^T$ and $[COV]^T[COV]$; $[S]$ is a diagonal matrix containing the square roots of eigenvalues from $[U]$ or $[V]$ in descending order.
To decompose the autocovariance matrix the following equation is used:

$$dc[COV] = [U][S]^{\frac{1}{2}} \quad \textbf{3-32}$$

The random field $H(x, \theta)$ can be described by:

$$\{\widehat{H}(x, \theta)\} = \{m(X)\} + dc[COV]\{X(\theta)\} \quad \textbf{3-33}$$

where x represents the spatial coordinates, θ represents a random process, $\{X(\theta)\}$ is a set of independent random variables to be determined, $dc[COV]$ is the decomposition of the autocovariance matrix.

In summary the process for calculating the random fields is defined by five steps as follows:

- calculation of the distance between the centers of gravity of all the elements τ or τ_i and τ_j,
- calculation of the terms $\rho[X_i, X_j]$ of the autocorrelation matrix (equations 3-26, 3-27, 3-28, 3-29, and 3-30),
- calculation of the terms $Cov[X_i, X_j]$ of the autocovariance matrix $[COV]$ (equation 3-25),
- calculation of the autocovariance decomposition matrix by using singular value decomposition (equation 3-32),
- calculation of the random field $\{\widehat{H}(x, \theta)\}$ (equation 3-33).

3.9. Influence of the spatial discretization

Spatial discretization is an important issue in the finite element analysis of structures, particularly in presence of uncertainties. Using an optimal finite element mesh leads to an increase of the efficiency and to a reduction of the computational time. In an approach with variability, the objective is to find the optimal mesh for an accurate calculation of statistical quantities of the results observed (displacements, strains, stresses). In particular, the convergence conditions for the mean value or the standard deviation of these quantities must be met. Matthies et al. [18] recommend the use of a uniform mesh for computing variability, in particular when input parameters are defined by random fields. A homogeneous mesh refinement is performed until achieving convergence conditions. The main disadvantage of this approach is that it leads to meshes with a large number of elements and so the mesh may be not optimal.

In this study, it is assumed that an optimal mesh for the nominal calculation is also convenient for the variability evaluation. Therefore, the strategy adopted here is finding the optimal mesh for the nominal configuration and then exploit it to calculate the variability. In the examples section, the relevance of this strategy is discussed. Two approaches have been tested. The first approach leads to a classical refinement study, with a more or less homogeneous mesh. The second one consists in using adaptive mesh techniques that can minimize the number of elements for a

given precision. Adaptive mesh may involve a heterogeneous mesh and thus significant variations in the dimensions of the elements, especially in stress concentration areas. The adaptive mesh procedure available in the Abaqus software [114] is applied. The error based on the strain energy density of each element indicator is selected. For some examples described in chapters 4, 5 and 6, adaptive meshing technique is used.

3.10. Error criteria

This section presents the error criteria (in %) that are used for the examples. The errors due to the spatial discretization and those related to the CGSM assumption are distinguished. On the one hand, three global criteria and two local criteria are defined for the errors due to the variability calculation, on the other hand three criteria are defined for the error due to the spatial discretization.

The three global error criteria associated to variability concern the mean value, standard deviation and coefficient of variation. The CGSM results are compared with the direct Monte Carlo ones. These criteria are evaluated for a given mesh. They are defined as:

$$err\big(m(U)\big) = \left(\frac{m_{CGSM}(U) - m_{dMC}(U)}{m_{dMC}(U)}\right) \text{x } 100 \qquad \textbf{3-34}$$

$$err\big(\sigma(U)\big) = \left(\frac{\sigma_{CGSM}(U) - \sigma_{dMC}(U)}{\sigma_{dMC}(U)}\right) \text{x } 100 \qquad \textbf{3-35}$$

$$err\big(c.o.v.(U)\big) = \left(\frac{c.o.v._{CGSM}\,(U) - c.o.v._{dMC}\,(U)}{c.o.v._{dMC}\,(U)}\right) \text{x } 100 \qquad \textbf{3-36}$$

To further analyze the quality of the results obtained by the CGSM measured with the global error criteria defined in equations 3-34; 3-35; and 3-36, two local error criteria are proposed. These criteria are based on the strain energy and calculated on each finite element. The strain energy results calculated with the CGSM and the direct Monte Carlo simulations are compared.

Two variants are proposed. The first criteria evaluates the relative error due to the CGSM assumption:

$$err1^{e}(\pi_{int}) = m\left|\frac{\pi^{e}_{int_{CGSM}} - \pi^{e}_{int_{dMC}}}{\pi^{e}_{int_{dMC}}}\right| \text{x } 100 \qquad \textbf{3-37}$$

In equation 3-37**,** the error is expressed in relation to the strain energy of the element considered. This criteria measures the intrinsic error due to the CGSM assumption. For the second criteria calculated in each element, the error on the strain energy is expressed in relation to a reference strain energy. This reference energy is calculated considering the strain energy throughout the structure ($\pi^{T}_{int_{MCd}}$), weighted by the element size. This error is written:

$$err2^{e}(\pi_{int}) = m\left|\frac{\pi^{e}_{int_{CGSM}} - \pi^{e}_{int_{dMC}}}{\pi^{T}_{int_{dMC}}\left(\frac{A_e}{A_T}\right)}\right| \text{x } 100 \qquad \textbf{3-38}$$

This criteria gives an indication of the contribution of each element to the error on the strain energy. It focuses on the areas where the strain energy density is high.

Error criteria due to the spatial discretization are also defined. As explained in section 3.9, the strategy adopted here is finding the optimal mesh for the nominal configuration and then exploit it to calculate the variability. The error associated with the nominal displacement at one specific point, for a given mesh, is defined as:

$$err_{mesh}(U) = \left(\frac{U_{nom} - U_{ref}}{U_{ref}}\right) \text{x } 100 \qquad \textbf{3-39}$$

When the optimal mesh has been identified for the nominal configuration, the next stage consists in checking whether this mesh is adapted to calculate the variability. In this context, it is necessary to calculate the errors on the mean value and the standard deviation of displacement, due to the spatial discretization. The errors are defined as:

$$err_{mesh}\big(m(U)\big) = \left(\frac{m(U)_{nom} - m(U)_{ref}}{m(U)_{ref}}\right) \text{x } 100 \qquad \textbf{3-40}$$

$$err_{mesh}\big(\sigma(U)\big) = \left(\frac{\sigma(U)_{nom} - \sigma(U)_{ref}}{\sigma(U)_{ref}}\right) \text{x } 100 \qquad \textbf{3-41}$$

3.11. Influence of input variability on the generalized stresses

In the general case, the generalized stresses depend more or less on random input parameters. In this section specific cases where the CGSM assumption is exact, are higlighted. In these cases, the generalized stresses are certain and do not depend on the value of the random parameters. Three types of parameters are considered: the thickness h, the elasticity modulus E and the Poisson's ratio v. Random variables as well as random fields are considered. Results are shown in Table 3-1.

	Statically determined structure	**1 uniform random variable**			***nX* uniform random variables**	**Random field**
	thickness *h,* elasticity modulus *E,* Poisson's ratio υ	thickness h	elasticity modulus E	Poisson's ratio υ	thickness *h,* elasticity modulus *E,* Poisson's ratio υ	thickness *h,* elasticity modulus *E,* Poisson's ratio υ
Membrane plate	certain	certain	certain	uncertain	uncertain	uncertain
Bending plate	certain	uncertain	certain	uncertain	uncertain	uncertain
Single-layered shell	certain	uncertain	certain	uncertain	uncertain	uncertain
Multi-layered shell	certain	uncertain	uncertain	uncertain	uncertain	uncertain

Table 3-1 Influence of input variability on the generalized stresses

Chapter 4
Formulation and Applications of CGSM for Membrane Plates

4.1. Formulation of the CGSM for membrane plates

4.1.1. Displacement variability

In this section, the CGSM is developed for the three-node triangles (T3) and the four-node quadrilaterals (Q4), whatever the details of the formulation of these elements.

The objective here is to describe the calculation of the variability of displacement. First the strain energy is expressed as:

$$\pi_{int}^{m} = \frac{1}{2}\int_{V} \langle e\rangle\,[H]\,\{e\}\,dV = \frac{1}{2}\int_{A} h\langle e\rangle\,[H]\,\{e\}\,dA \qquad \textbf{4-1}$$

where $\langle e\rangle = \langle e_x \;\; e_y \;\; e_{xy}\rangle$ are the axial strains, V is the volume of the structure ($dV = h\,dA$), $[H]$ is the plane stress elasticity matrix for an isotropic material:

$$[H] = \frac{E}{1-v^2}\begin{bmatrix} 1 & v & 0 \\ v & 1 & 0 \\ 0 & 0 & \dfrac{1-v}{2} \end{bmatrix} \qquad \textbf{4-2}$$

where E is the elasticity modulus, and v is the Poisson's ratio.

The relationship between strains $\{e\}$ and axial forces $\{N\}$ is:

$$\{e\} = \frac{1}{h}[H]^{-1}\{N\} \qquad \textbf{4-3}$$

with $\langle N\rangle = \langle N_x \;\; N_y \;\; N_{xy}\rangle$.

Substituting equation 4-3 into equation 4-1 gives:

$$\pi_{int}^{m} = \frac{1}{2}\int_{A} \frac{1}{h} \langle N \rangle [H]^{-1} \{N\}\, dA \qquad \textbf{4-4}$$

or:

$$\pi_{int}^{m} = \frac{1}{2}\int_{A} \frac{1}{Eh} \langle N_x \quad N_y \quad N_{xy} \rangle \begin{bmatrix} 1 & -v & 0 \\ -v & 1 & 0 \\ 0 & 0 & 2(1+v) \end{bmatrix} \begin{Bmatrix} N_x \\ N_y \\ N_{xy} \end{Bmatrix} dA \qquad \textbf{4-5}$$

Equation 4-5 can be simplified into:

$$\pi_{int}^{m} = \frac{1}{2}\int_{A} \frac{1}{Eh} \left({N_x}^2 - 2vN_xN_y + {N_y}^2 + 2(1+v){N_{xy}}^2 \right) dA \qquad \textbf{4-6}$$

Considering that the domain is spatially discretized and the mesh contains *n* finite elements, equation 4-6 can be written as:

$$\pi_{int}^{m} = \frac{1}{2}\sum_{i=1}^{n} \int_{A_i} \frac{1}{E_i h_i} \left({N_{x_i}}^2 - 2v_i N_{x_i} N_{y_i} + {N_{y_i}}^2 + 2(1+v_i){N_{xy_i}}^2 \right) dA \qquad \textbf{4-7}$$

where *i* is the element number; N_{x_i}, N_{y_i} and N_{xy_i} are the axial forces; A_i is the area; E_i is the elasticity modulus; h_i is the thickness and v_i is the Poisson's ratio.

In order to apply the Castigliano's theorem for calculating the displacement U at a point P in a given direction, the axial forces of each element are decomposed into two contributions:

$$\begin{aligned} N_{x_i} &= N_{x_i}' + F N_{x_i}^{"} \\ N_{y_i} &= N_{y_i}' + F N_{y_i}^{"} \\ N_{xy_i} &= N_{xy_i}' + F N_{xy_i}^{"} \end{aligned} \qquad \textbf{4-8}$$

where *i* is the element number; *F* is the load applied at point *P* in the direction of interest (*F* is a force or a moment if the variability of a displacement or a rotation must be assessed respectively); N_{x_i}, N_{y_i} et N_{xy_i} are the axial forces; N_{x_i}', N_{y_i}' et N_{xy_i}' are the axial forces due to loads on the whole structure except at point *P* in the direction of interest; $N_{x_i}^{"}$, $N_{y_i}^{"}$, and $N_{xy_i}^{"}$ are the axial forces due to a unitary load applied at point *P* in the direction of interest, as shown in Figure 4-1.

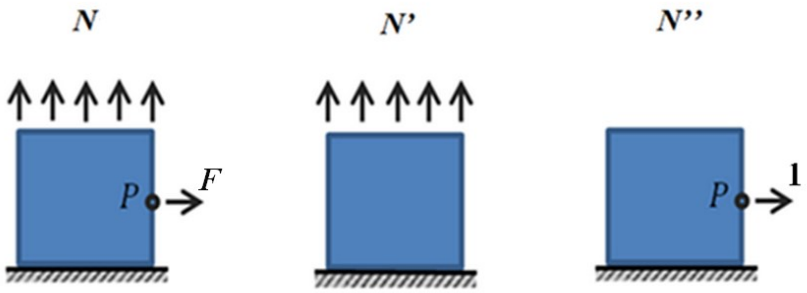

Figure 4-1 Square plate under tension – decomposition of loading and axial forces

Substituting equation 4-8 into equation 4-7 gives:

$$\pi_{int}^{m} = \frac{1}{2}\sum_{i=1}^{n}\int_{A}\frac{1}{E_i h_i}\left(\left(N_{x_i}' + FN_{x_i}^{"}\right)^2 - 2v_i\left(\begin{matrix}N_{x_i}'N_{y_i}' + FN_{x_i}'N_{y_i}^{"} \\ +FN_{x_i}^{"}N_{y_i}' + F^2N_{x_i}^{"}N_{y_i}^{"}\end{matrix}\right) + \left(N_{y_i}' + FN_{y_i}^{"}\right)^2 + 2(1+v_i)\left(N_{xy_i}' + FN_{xy_i}^{"}\right)^2\right)dA \qquad \textbf{4-9}$$

Our objective is to consider simple interpolations of axial forces; these interpolations are independent of the initial formulation of the element. Indeed, it is assumed that the nominal finite element analysis is performed with a standard software and consequently, precise information about the formulation of the element is not available. For T3 and Q4 elements considered here, the axial forces are assumed to be constant over one element. Equation 4-9 becomes:

$$\pi_{int}^{m} = \frac{1}{2}\sum_{i=1}^{n}\frac{A_i}{E_i h_i}\left(\left(N_{x_i}' + FN_{x_i}^{"}\right)^2 - 2v_i\left(\begin{matrix}N_{x_i}'N_{y_i}' + FN_{x_i}'N_{y_i}^{"} \\ +FN_{x_i}^{"}N_{y_i}' + F^2N_{x_i}^{"}N_{y_i}^{"}\end{matrix}\right) + \left(N_{y_i}' + FN_{y_i}^{"}\right)^2 + 2(1+v_i)\left(N_{xy_i}' + FN_{xy_i}^{"}\right)^2\right) \qquad \textbf{4-10}$$

To obtain the displacement at a point P in a given direction, the Castigliano's theorem is applied:

$$U_m = \frac{\partial \pi_{int}^{m}}{\partial F} \qquad \textbf{4-11}$$

$$U_m = \sum_{i=1}^{n} \frac{A_i}{E_i h_i} \Big(N_{x_i}^{"} \big(N_{x_i}' + F N_{x_i}^{"} \big) - v_i \Big(N_{x_i}' N_{y_i}^{"} + N_{x_i}^{"} N_{y_i}' + 2F N_{x_i}^{"} N_{y_i}^{"} \Big) + N_{y_i}^{"} \Big(N_{y_i}' + F N_{y_i}^{"} \Big) + 2(1+v_i) N_{xy_i}^{"} \Big(N_{xy_i}' + F N_{xy_i}^{"} \Big) \Big) \quad \textbf{4-12}$$

or:

$$U_m = \sum_{i=1}^{n} \frac{A_i}{E_i h_i} \Big(N_{x_i}^{"} \big(N_{x_i}' + F N_{x_i}^{"} \big) + N_{y_i}^{"} \Big(N_{y_i}' + F N_{y_i}^{"} \Big) + 2 N_{xy_i}^{"} \Big(N_{xy_i}' + F N_{xy_i}^{"} \Big) + v_i \Big(2 N_{xy_i}^{"} \Big(N_{xy_i}' + F N_{xy_i}^{"} \Big) - \Big(N_{x_i}' N_{y_i}^{"} + N_{x_i}^{"} N_{y_i}' + 2F N_{x_i}^{"} N_{y_i}^{"} \Big) \Big) \Big) \quad \textbf{4-13}$$

The expression of U_m given in equation 4-13 is used for each trial of the CGSM+Monte Carlo simulation, to calculate the displacement variability at a point of a membrane plate. This expression of U_m is compatible with any distribution law for the Monte Carlo Simulation. As mentioned in section 3.8, in this study essentially truncated Gaussian laws are exploited.

4.1.2. Strains variability

The CGSM also allows to calculate the strains variability. Two methods are proposed. In both cases the strains are calculated at the center of each element.

4.1.2.1. Method 1

The strains in an element are calculated using nominal axial forces, using equation 4-3:

$$\{e\} = \frac{1}{h} [H]^{-1} \{N_o\} \quad \textbf{4-14}$$

This expression only requires the nominal axial forces in the element concerned. Consequently only one finite element analysis in the nominal configuration is

required. The equation 4-14 is applied for each trial of the Monte Carlo simulation. The accuracy of this method is tested in section 4.2.2.4.

4.1.2.2. Method 2

The strains are calculated from the values of displacements at the nodes of the element concerned, according to the classical expression:

$$\{e\} = [B]\{U\} \qquad \textbf{4-15}$$

The matrix $[B]$ contains derivatives of the displacement shape functions. Simple linear or bilinear shape functions are chosen. This method also requires, for each trial, the calculation of $\{U\}$ which contains the displacements at three or four nodes for T3 or Q4 elements respectively. At each node, the membrane displacements components (u and v) are calculated with the CGSM. It is then necessary to run 1 finite element analysis with twelve or sixteen load cases at most in the nominal configuration, for T3 or Q4 elements respectively. Then the equation 4-15 is applied for each trial of the Monte Carlo simulation. The results obtained with this method are also given in section 4.2.2.4.

4.2. Membrane plates examples

4.2.1. Square plate under tension

4.2.1.1. Presentation of the example

Let us consider a square plate under tension (Figure 4-2). The plate has a dimension L = 1 (data are provided in dimensionless form) and is subjected to a uniformly distributed load p = 1. Poisson's ratio is 0.3 and the average modulus is $m(E)$ = 1. The elasticity modulus E is defined by a random field. The coefficient of variation $c.o.v.(E)$ varies between 5% and 15% and different correlation lengths are considered. The direct Monte Carlo simulations and CGSM are carried out with 10,000 trials. This number of trials is sufficient to guarantee the convergence of the

Monte Carlo process, leading to very small errors (less than 1%) on the mean and standard deviation of the quantities of interest.

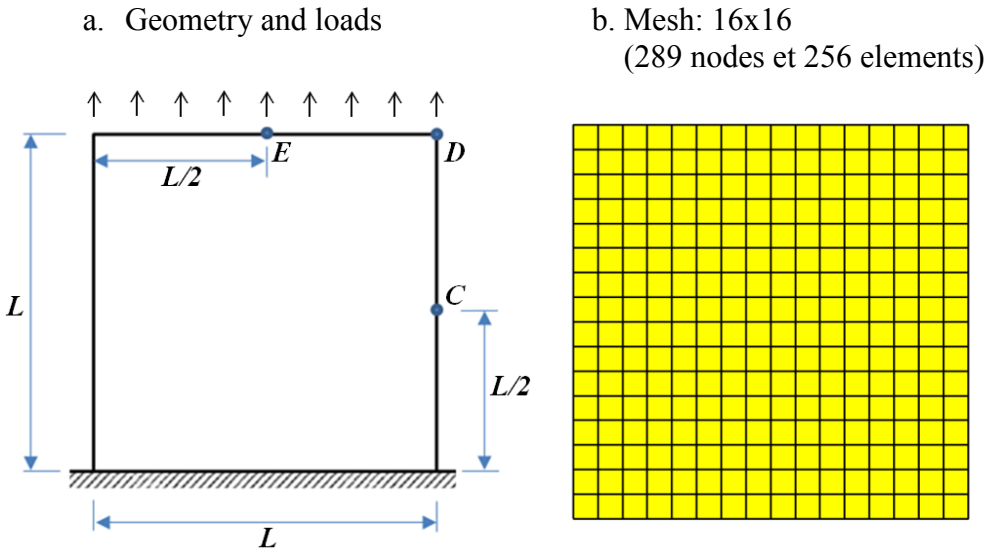

Figure 4-2 Square plate under tension

4.2.1.2. Finite element mesh

The global strategy applied here to identify an optimal mesh has been described in section 3.9. In this example, the elements S4 available in Abaqus [114] are used. Firstly a convergence analysis is performed with the CGSM formulation (equation 4-13), in the nominal configuration. Table 4-1 shows the results of a convergence study of nominal displacements at 3 nodes *C*, *D* and *E* highlighted in Figure 4-2. The maximum error accepted for nominal displacement is 0.5%. The reference is given by a very fine mesh Q4_64x64 (4096 nodes and 4225 elements). The optimal mesh for the nominal calculation is Q4_16x16 (256 nodes and 289 elements). Consequently this mesh is exploited to calculate the variability. Tests are performed a posteriori to ensure that this mesh is suitable for the calculation of the variability (see section 4.2.1.3).

Node		Q4_8x8		Q4_16x16		Q4_32x32		Q4_64x64
		Displacement	Error (%)	Displacement	Error (%)	Displacement	Error (%)	Displacement (reference)
C	*x*	-1.450E-01	1.0	-1.460E-01	0.3	-1.462E-01	0.1	-1.464E-01
	y	5.000E-01	0.1	5.002E-01	0.1	5.004E-01	0.0	5.005E-01
E	*y*	9.814E-01	0.3	9.831E-01	0.1	9.838E-01	0.0	9.841E-01
D	*x*	-1.560E-01	0.4	-1.555E-01	0.1	-1.554E-01	0.0	-1.553E-01
	y	9.912E-01	0.1	9.921E-01	0.1	9.925E-01	0.0	9.927E-01

Table 4-1 Square plate under tension – study of convergence of displacements in the nominal configuration

4.2.1.3. Displacement variability

The CGSM results are compared with those obtained by Rahman and Rao [87] and with a reference solution obtained by direct Monte Carlo simulation. For the correlation function equation 3-28 is used, with $b_1 = 1$, $b_2 = 2$, and the correlation length $\lambda = L$. The variability level is defined by $c.o.v.(E) = 12\%$. Table 4-2 shows CGSM provides highly accurate results for the mean and the variance. The maximum errors are worth 0.2% and 1.3% for the mean and variance of the displacement respectively. The results obtained by Rahman and Rao [87] lead to significant errors. This discrepancy is certainly due to the fact that they used a too coarse mesh.

Node			Rahman and Rao [87]		CGSM		direct Monte Carlo
			Results	Error (%)	Results	Error (%)	Reference
C	*x*	$m(U)$	-1.477E-01	0.3	-1.479E-01	0.1	-1.481E-01
		$\sigma^2(U)$	8.394E-04	6.3	8.960E-04	0.0	8.957E-04
	y	$m(U)$	5.056E-01	0.3	5.079E-01	0.2	5.071E-01
		$\sigma^2(U)$	3.772E-03	7.7	4.137E-03	1.3	4.086E-03
D	*x*	$m(U)$	-1.577E-01	0.7	-1.570E-01	0.2	-1.566E-01
		$\sigma^2(U)$	5.868E-03	11	6.673E-03	1.2	6.591E-03
	y	$m(U)$	1.002E+00	0.5	1.009E+00	0.1	1.008E+00
		$\sigma^2(U)$	1.308E-02	11	1.477E-02	0.9	1.464E-02
E	*y*	$m(U)$	9.935E-01	0.2	9.966E-01	0.1	9.955E-01
		$\sigma^2(U)$	9.561E-03	9	1.065E-02	0.9	1.055E-02

Table 4-2 Square plate under tension (E random, $c.o.v.(E) = 12\%$, $\lambda = L$) – variability of displacement

The correlation length varies now between $\lambda = 0.01L$ and $100L$, and two levels of variability: $c.o.v.(E)$ = 5% or 15%, are considered. Table 4-3 shows the maximum errors on the mean and standard deviation of displacement at point C. The overall results obtained with the CGSM method are very satisfactory. We find that the error decreases when the correlation length increases. Indeed, from a theoretical point of view, when the elasticity modulus is constant over the whole plate, the CGSM assumption is verified exactly. Consequently this justifies small errors for large correlation lengths.

λ	$0.01L$		$0.1L$		L		$10L$		$100L$	
$c.o.v.(E)$ (%)	5	15	5	15	5	15	5	15	5	15
Error on $m(U)$ (%)	0.1	1.3	0.1	0.9	0.0	0.2	0.0	0.0	0.0	0.0
Error on $\sigma(U)$ (%)	0.4	5.3	0.3	3.0	0.0	0.7	0.0	0.0	0.0	0.0

Table 4-3 Square plate under tension (E random, $c.o.v.(E)$ = 12%) – errors on the statistical results of the displacement at point C, for different correlation lengths and two coefficients of variation

Figure 4-3 shows the distribution of the displacement at point C, U_0 being the nominal displacement. For both levels of variability 5% and 15% with the correlation length $\lambda = L$, the CGSM method provides results very close to those obtained by the direct Monte Carlo simulation results.

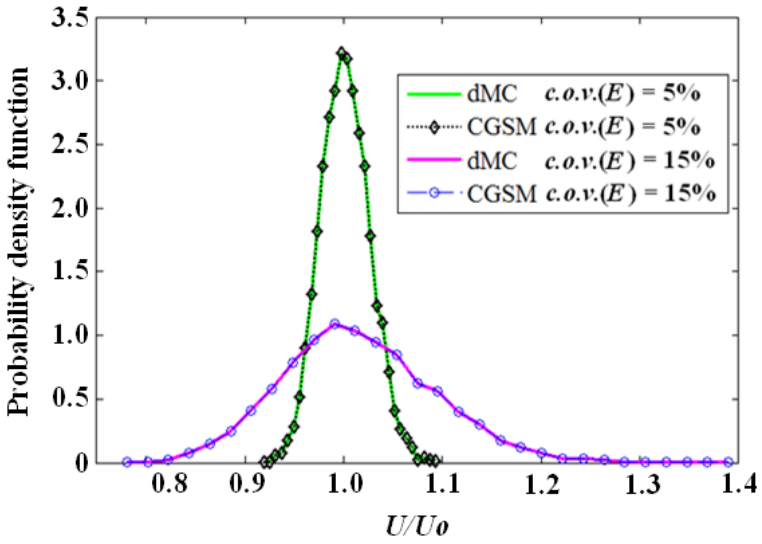

Figure 4-3 Square plate under tension (E random, $c.o.v.(E)$ = 5% and 15%, $\lambda = L$) – probability density of the displacement at point C

4.2.1.4. Influence of the mesh for variability calculation

Here we verify a posteriori whether the Q4_16x16 mesh is also correct for the calculation of the variability. This study is conducted with the CGSM. Table 4-4 compares the results obtained with this mesh and the reference mesh. For most cases considered, the errors are less than 2% for the mean and standard deviation of displacement. Only the case with a correlation length $\lambda = 0.01L$ leads to more significant errors and would justify a finer mesh. This is due to the fact that the variation of the elasticity modulus is very fast in this case. These results show that the strategy which consists in identifying the optimal mesh for the nominal case and use it for the calculation of the variability is valid, except when the correlation length is extremely small. However this extreme situation is not physically realistic and consequently this case has not been studied further.

λ	$0.01L$		$0.1L$		L		$10L$		$100L$	
c.o.v. (E) (%)	5	15	5	15	5	15	5	15	5	15
$err_{mesh}\big(m(U)\big)$ (%)	0.0	0.1	0.0	0.1	0.1	0.7	0.1	0.0	0.2	0.3
$err_{mesh}\big(\sigma(U)\big)$ (%)	140	140	0.8	1.2	0.6	1.2	1.4	1.3	0.5	1.6

Table 4-4 Square plate under tension (E random, *c.o.v.*(E) = 5% and 15%) – errors on the statistical results of the displacement at point C, for the mesh Q4_16x16 compared to the reference mesh Q4_64x64

4.2.1.5. Performance of the CGSM in computational time

Regarding the calculation time, for this example, the acceleration factor obtained by the CGSM method is about 400, compared to the direct Monte Carlo simulation.

4.2.1.6. Errors on the strain energy

In this paragraph the two error criteria $err1^e(\pi_{int})$ and $err2^e(\pi_{int})$, defined in section 3.10 (equations 3-37 and 3-38) and based on the strain energy, are observed. The objective is to analyze in detail the local errors on each element due to the CGSM assumption. The analysis of these errors allow to better justify

the good performance of the method for the calculation of statistical quantities (mean, standard deviation). Tests are carried out for the extreme values of the correlation length ($\lambda = 0.01L$ and $\lambda = 100L$).

Figures 4-4 and 4-5 show the results for the error criteria $err1^e(\pi_{int})$ and $err2^e(\pi_{int})$ respectively. First we observe that for both criteria, when the length of correlation is large, local errors are very small, vice versa the errors are more significant for a small correlation length. Indeed when the correlation length is large, the random variable is almost uniform over the whole studied area. As already stated, if we consider a perfectly uniform variable over the whole studied area, the CGSM assumption is verified exactly. So it is logical to observe small errors for large correlation lengths and bigger errors for small correlation lengths. For a given correlation length, we also observe that the first criteria leads to slightly lower maximum errors compared to the second criteria. The maximum errors are also located in different zones.

These two criteria are complementary. The observation of these results shows that significant local errors due to the CGSM assumption lead to small errors on the mean and standard deviation of displacement (see Tables 4-2 and 4-3).

a. Correlation length, $\lambda = 0.01L$ b. Correlation length, $\lambda = 100L$

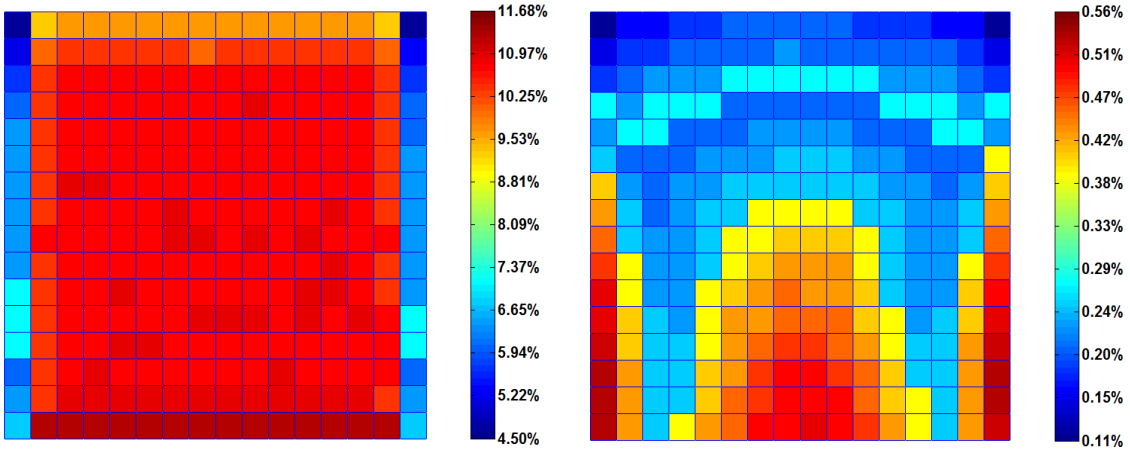

Figure 4-4 Square plate under tension – error criteria $err1^e$

a. Correlation length, $\lambda = 0.01L$ b. Correlation length, $\lambda = 100L$

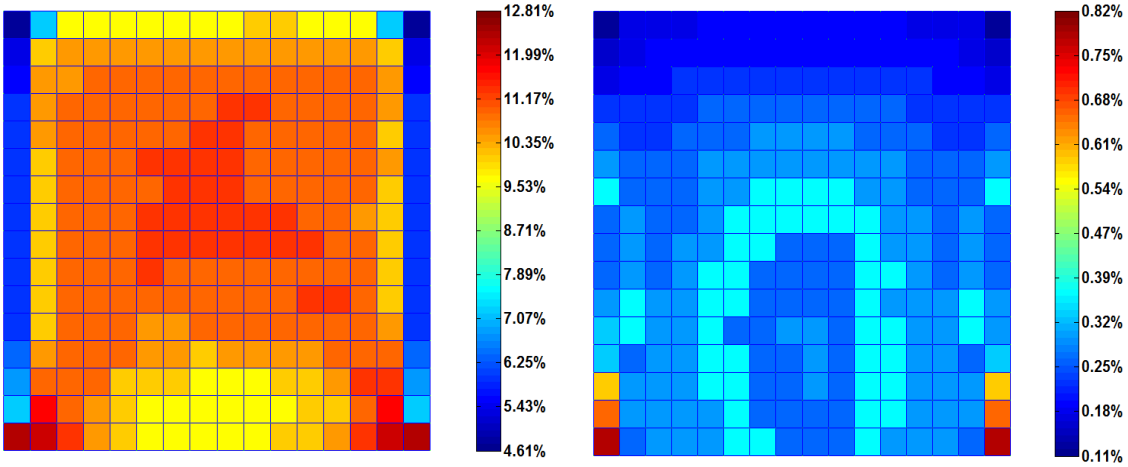

Figure 4-5 Square plate under tension – error criteria $err2^e$

4.2.2. Square plate with a circular hole under tension

4.2.2.1. Presentation of the example

The second example, a square plate with a circular hole, is shown in Figure 4-6. The plate size is $2L = 40$ (data are provided in dimensionless form), with a hole diameter $2a = 2$. It is subjected to a uniformly distributed load of intensity $p = 1$. Poisson's ratio ν is equal to 0.3. The elasticity modulus E is assumed to be described by an anisotropic or isotropic random field and the mean value of E is $m(E) = 1$. The coefficient of variation $c.o.v.(E)$ varies between 5% and 15% and various correlation lengths are considered. Direct Monte Carlo simulations and CGSM + Monte Carlo simulations are made with 10,000 runs.

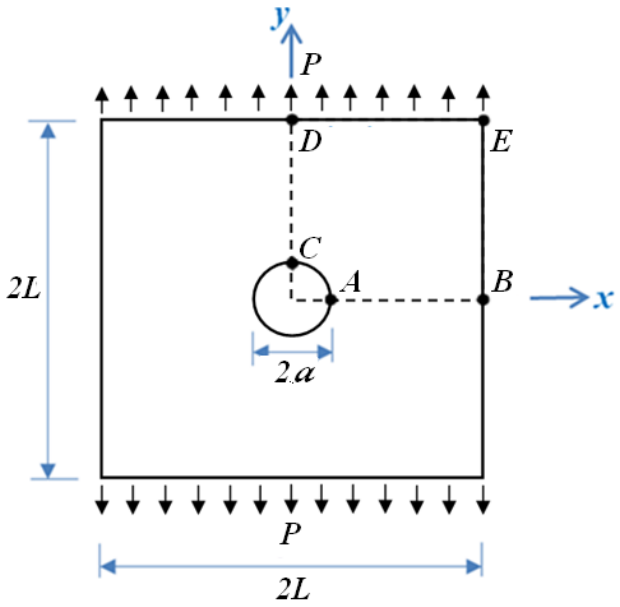

Figure 4-6 Square plate with a circular hole under tension

4.2.2.2. Finite element mesh

The global strategy applied here to identify an optimal mesh has been described in section 3.9. Firstly, thanks to a convergence analysis performed with the CGSM formulation (equation 4-13) in the nominal configuration, an adequate mesh is obtained. Then this mesh is exploited to calculate the variability. Finally tests are performed a posteriori to ensure that this mesh is suitable for the calculation of the variability (section 4.2.2.5). Two meshing techniques are used for this example: mapped mesh and adaptive mesh.

Figure 4-7 shows meshes 1 and 2 obtained with these two approaches. These meshes are sufficient to provide the nominal displacement at points of interest A, B, C, D and E, with an error $err_{mesh}(U)$ defined in equation 3-39 less than 0.5% compared to a reference value. This reference solution is obtained with a very fine mapped mesh presented in Figure 4-7. The adaptive meshing technique is interesting because it allows a significant reduction of the number of nodes, compared to the mapped meshing technique. In the next section, mesh 2 is used for the calculation of the variability.

a. Mesh 1: 1617 nodes and 1536 Q4 elements

b. Mesh 2: 785 nodes and 745 elements (726 Q4 and 19 T3)

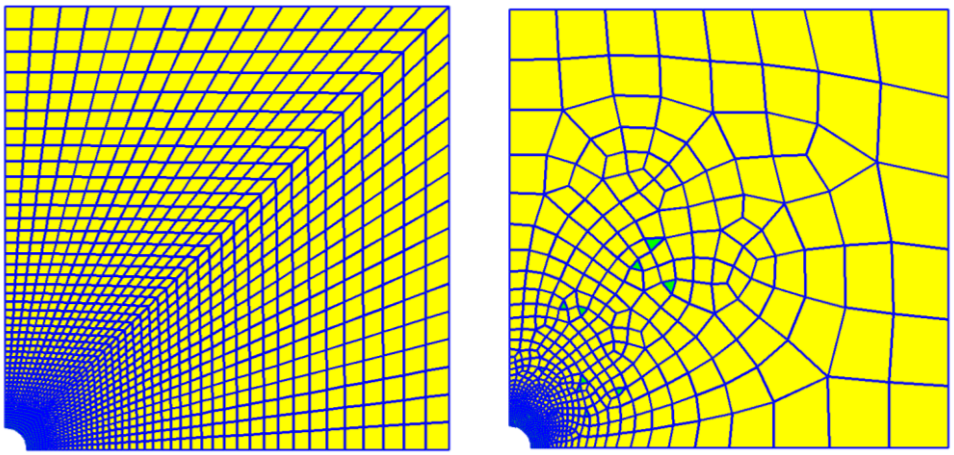

c. Reference mesh: 6305 nodes and 6144 Q4 elements

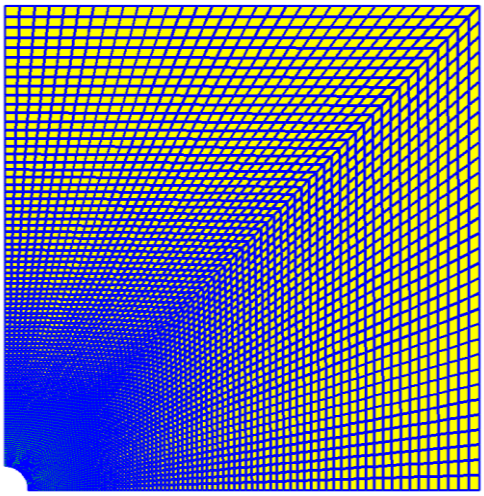

Figure 4-7 Square plate with a circular hole under tension – mapped mesh (a), adaptive mesh (b), reference mesh (c)

4.2.2.3. Displacement variability

The CGSM results are compared with the results obtained by Rahman and Xu [122] and a reference solution obtained by a direct Monte Carlo simulation. Two types of correlation functions are studied: type A (equation 3-28) with $\lambda_1 = 0.5L$, $\lambda_2 = 0.5L$ and type B (equation 3-26) with $\lambda = 0.5L$. These values correspond to an intermediate correlation length**.** Coefficient of variation of the elasticity modulus

c.o.v.(*E*) is 10%. Tables 4-5 and 4-6 show the mean value and the standard deviation results. The CGSM provides highly accurate results. The maximum errors, compared to the direct Monte Carlo simulation, are 0.5% and 0.8% for the mean value and the standard deviation of the displacement respectively. The results obtained by Rahman and Xu [122] are less accurate. As for the first example, these differences are certainly due to the mesh refinement level, indeed Rahman and Xu [122] used a relatively coarse mesh.

			Rahman and Xu [122]		CGSM		direct Monte Carlo
			Results	Error (%)	Results	Error (%)	Reference
A	*x*	$m(U)$	-9.75E-01	4.4	-1.014E+00	0.5	-1.020E+00
		$\sigma(U)$	1.12E-01	7.2	1.204E-01	0.3	1.207E-01
B	*x*	$m(U)$	-6.20E+00	0.1	-6.203E+00	0.1	-6.197E+00
		$\sigma(U)$	4.65E-01	1.5	4.606E-01	0.5	4.583E-01
C	*y*	$m(U)$	2.97E+00	2.4	3.037E+00	0.2	3.043E+00
		$\sigma(U)$	2.50E-01	7.0	2.688E-01	0.1	2.689E-01
D	*y*	$m(U)$	2.04E+01	0.1	2.047E+01	0.3	2.041E+01
		$\sigma(U)$	1.34E+00	0.4	1.342E+00	0.6	1.334E+00
E	*x*	$m(U)$	-5.84E+00	1.4	-5.952E+00	0.5	-5.922E+00
		$\sigma(U)$	5.97E-01	4.1	6.187E-01	0.6	6.223E-01
	y	$m(U)$	1.99E+01	1.0	2.016E+01	0.3	2.010E+01
		$\sigma(U)$	1.38E+00	3.3	1.433E+00	0.4	1.428E+00

Table 4-5 Square plate with a circular hole under tension (*E* random, *c.o.v.*(*E*) = 10%, type *A* with $\lambda_1 = 0.5L$, $\lambda_2 = 0.5L$) – variability of displacement at several points

The correlation length varies now, from $\lambda = 0.005L$ to $50L$ (type B), for two variability levels *c.o.v.*(*E*) = 5% and 15%. Table 4-7 shows the maximum errors on the mean and standard deviation of displacement at point *A*. All results obtained with the CGSM are very satisfactory. The maximum errors are always less than 1% and 5% for the mean value and the standard deviation of the displacement respectively.

		Rahman and Xu [122]		CGSM		direct Monte Carlo
		Results	Error (%)	Results	Error (%)	Reference
A x	$m(U)$	-9.76E-01	4.3	-1.017E+00	0.2	-1.019E+00
	$\sigma(U)$	1.18E-01	7.3	1.283E-01	0.8	1.273E-01
B x	$m(U)$	-6.20E+00	0.1	-6.216E+00	0.3	-6.196E+00
	$\sigma(U)$	4.97E-01	0.3	4.985E-01	0.0	4.983E-01
C y	$m(U)$	2.97E+00	2.2	3.042E+00	0.1	3.038E+00
	$\sigma(U)$	2.66E-01	6.4	2.843E-01	0.0	2.843E-01
D y	$m(U)$	2.04E+01	0.1	2.047E+01	0.3	2.042E+01
	$\sigma(U)$	1.45E+00	0.4	1.457E+00	0.1	1.456E+00
E x	$m(U)$	-5.85E+00	1.5	-5.953E+00	0.3	-5.938E+00
	$\sigma(U)$	6.07-01	2.8	6.267E-01	0.3	6.245E-01
y	$m(U)$	1.99E+01	1.1	2.015E+01	0.2	2.012E+01
	$\sigma(U)$	1.48E+00	2.3	1.520E+00	0.4	1.514E+00

Table 4-6 Square plate with a circular hole under tension (E random, *c.o.v.*(E) = 10%, type B with $\lambda = 0.5L$) – variability of displacement at several points

λ	$0.005L$		$0.05L$		$0.5L$		$5L$		$50L$	
c.o.v.(E) (%)	5	15	5	15	5	15	5	15	5	15
Error on $m(U)$ (%)	0.3	0.6	0.2	0.1	0.4	0.6	0.4	0.6	0.3	0.3
Error on $\sigma(U)$ (%)	0.4	4.7	0.2	2.6	0.2	1.7	0.1	1.4	0.0	0.8

Table 4-7 Square plate with a circular hole under tension (E random, *c.o.v.*(E) = 5% and 15%, type B) – errors on the statistical results of the displacement at point A

Figure 4-8 shows the probability density function of the displacement at point A. The distribution obtained with the CGSM is very close to the reference distribution obtained with the direct Monte Carlo simulation. Due to the nonlinear relation between the displacement and the random parameters from the one hand and the significant variability level from the other hand, the distribution is not exactly Gaussian.

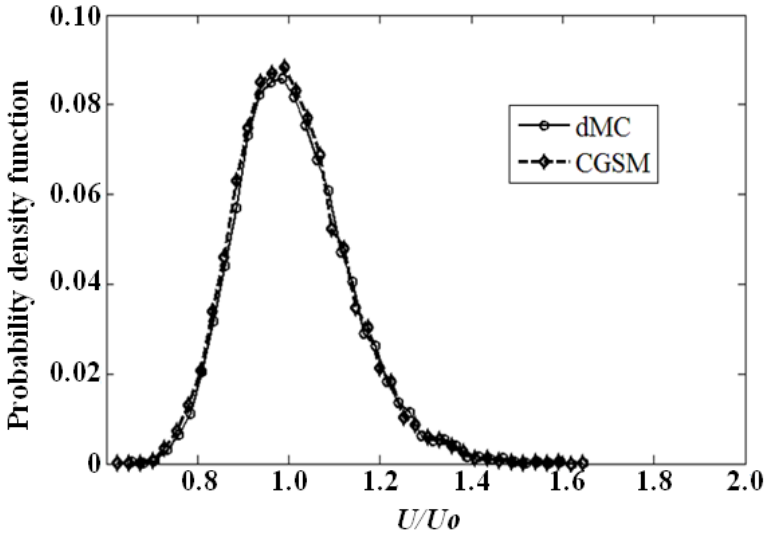

Figure 4-8 Square plate with a circular hole under tension (*E* random, *c.o.v.*(*E*) = 10%), type B with $\lambda = 0.5L$) – distribution of the displacement at point *A*

4.2.2.4. Strains variability

This section deals with the variability of strains for the square plate with a circular hole under tension. Nominal configuration tests have shown that mesh 2 is sufficiently fine for an accurate calculation of strains, so this mesh is used. The ε_{yy} component is calculated at point *A* and reference results are obtained with the direct Monte Carlo simulation. First tests are performed to compare method 1 and method 2 based on the CGSM (see section 4.1.2.1, equations 4-14 and 4-15). Table 4-8 shows that for errors on the mean value of strain ε_{yy} at point *A*, methods 1 and 2 generate similar maximum errors, 1.1% and 1.2% respectively. But some differences appear for the standard deviation. The results of method 1 are satisfactory when the correlation length is greater than *L*. However, for correlation length smaller than *L*, the difference between the CGSM results and the reference ones is significant. Method 2 provides satisfactory results for all values of correlation length. So this method is selected for further study.

The CGSM results are now compared with those obtained by Rahman and Xu [122] and with a reference solution calculated with a direct Monte Carlo simulation. Method 2 (see section 4.1.2.2) is used and the correlation function formulation is type B with $\lambda = 0.5L$. Table 4-9 shows the results obtained for the mean value and the standard deviation of strains. CGSM provides satisfactory

results, leading to maximal errors less than 1% and 3% for the mean value and the standard deviation of strains respectively. Biggest errors are observed for the results of Rahman and Xu [122]. Again, these errors are certainly due to the coarse mesh used.

	λ	0.005*L*		0.05*L*		0.5*L*		5*L*		50*L*	
	c.o.v.(*E*) (%)	5	15	5	15	5	15	5	15	5	15
Method 1	Error on $m(\varepsilon_{yy})$ (%)	0.1	1.1	0.1	0.8	0.1	0.5	0.0	0.2	0.1	0.0
	Error on $\sigma(\varepsilon_{yy})$ (%)	35	41	24	29	2	8	0.4	0.6	1.0	0.4
Method 2	Error on $m(\varepsilon_{yy})$ (%)	0.2	1.2	0.1	0.9	0.0	0.3	0.1	0.1	0.1	0.1
	Error on $\sigma(\varepsilon_{yy})$ (%)	0.1	5.1	0.2	2.7	1.3	3.6	0.5	1.5	1.2	0.2

Table 4-8 Square plate with a circular hole under tension (*E* random, *c.o.v.*(*E*) = 5% and 15%, type B) – errors on the statistical results of strain ε_{yy} at point *A*

		Rahman and Xu [122]		CGSM		direct Monte Carlo
		Results	Error (%)	Results	Error (%)	Reference
A	$m(\varepsilon_{yy})$	2.95E+00	6.5	2.782E+00	0.4	2.771E+00
	$\sigma(\varepsilon_{yy})$	2.58E-01	4.0	2.707E-01	0.7	2.689E-01
B	$m(\varepsilon_{yy})$	9.98E-01	0.3	1.006E+00	0.4	1.001E+00
	$\sigma(\varepsilon_{yy})$	8.62E-02	0.9	8.930E-02	2.6	8.702E-02
C	$m(\varepsilon_{xx})$	-7.18E-01	11	-7.994E-01	1.0	-8.077E-01
	$\sigma(\varepsilon_{xx})$	9.16E-02	12	1.032E-01	0.7	1.039E-01
D	$m(\varepsilon_{yy})$	9.90E-01	1.5	1.005E+00	0.1	1.005E+00
	$\sigma(\varepsilon_{yy})$	8.78E-02	8.9	9.742E-02	1.0	9.645E-02
E	$m(\varepsilon_{yy})$	9.79E-01	3.1	1.010E+00	0.1	1.011E+00
	$\sigma(\varepsilon_{yy})$	8.79E-02	14	1.002E-01	1.6	1.018E-01

Table 4-9 Square plate with a circular hole under tension (*E* random, *c.o.v.*(*E*) = 10%, type B with $\lambda = 0.5\ L$) – variability of strains at points *A, B, C, D* and *E*

4.2.2.5. Influence of the mesh for variability calculation

We now check that mesh 2 (adaptive mesh) is well suited also for the calculation of the variability. This study is conducted with the CGSM method. Table 4-10 compares the results obtained with this mesh and the reference mesh.

For most cases considered, the errors are less than 2.5% for the mean and standard deviation of displacement. Only the case $\lambda = 0.005L$ leads to more significant errors and justifies a finer mesh. This is due to the fact that in this case the variation of the modulus is extremely fast.

λ	$0.005L$		$0.05L$		$0.5L$		$5L$		$50L$	
c.o.v.(E) (%)	5	15	5	15	5	15	5	15	5	15
$err_{mesh}(m(U))$ (%)	0.8	0.9	0.8	1.1	0.7	1.1	0.7	0.8	0.3	0.4
$err_{mesh}(\sigma(U))$ (%)	34	35	1.6	0.9	0.7	0.8	0.6	0.3	0.4	0.5

Table 4-10 Square plate with a circular hole under tension (E random, *c.o.v.*(E) = 10%, type B) – errors on the statistical results of the displacement at point C, for mesh 2 compared to the reference mesh

4.2.2.6. Performance of the CGSM in computational time

In this example, for the computation of displacements variability, the acceleration factor obtained with the CGSM is about 600 compared to the direct Monte Carlo simulation. This acceleration factor is quite significant and is essentially due to the fact that the CGSM only requires one finite element analysis with some load cases. However, the acceleration factor can be increased further if the number of finite elements in the mesh or the number of trials used for the Monte Carlo simulation, are bigger.

4.2.2.7. Errors on the strain energy

In this paragraph the two error criteria $err1^e(\pi_{int})$ and $err2^e(\pi_{int})$, defined in section 4.2.1.6 (equations 3-37 and 3-38) and based on the strain energy, are observed. The objective is to analyze in detail the local errors on each element due to the CGSM assumption. Figures 4-10 and 4-11 show the results for the error criteria $err1^e$ and $err2^e$ respectively. In all cases, the maximal errors are located near the hole, in the stress concentration areas. For both criteria, when the correlation length is very large, errors are very small, while it is bigger for a small correlation length. This is because when the correlation length is large, the random

variable is almost uniform on the studied area. However, if a perfectly uniform variable is considered, the CGSM assumption is exactly met. Therefore it makes sense to observe more significant errors for small correlation lengths.

a. Correlation length, $\lambda = 0.005L$ b. Correlation length, $\lambda = 50L$

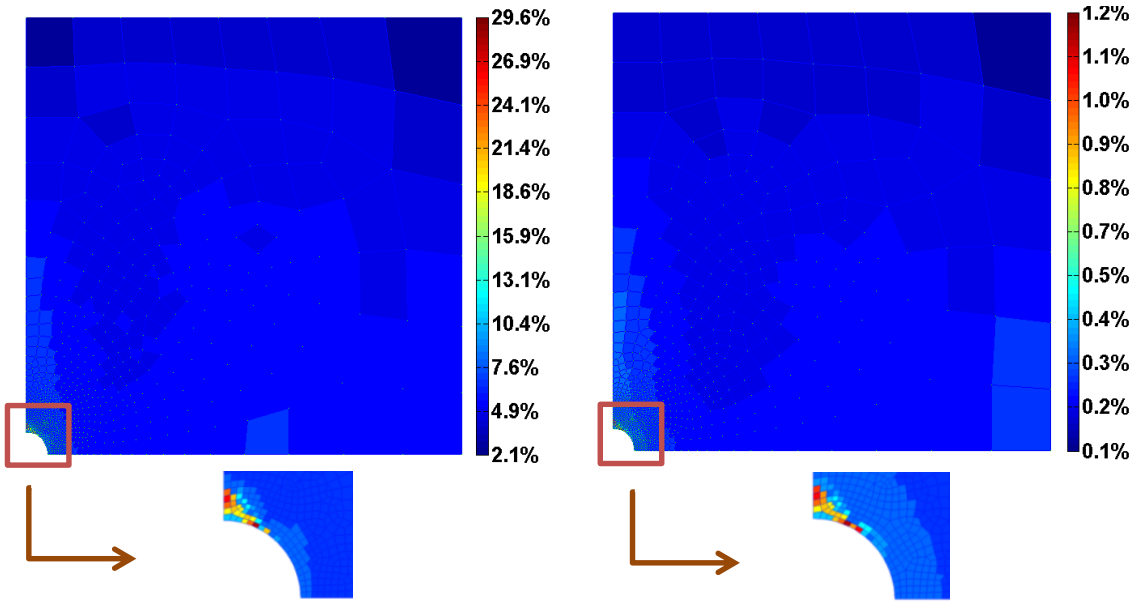

Figure 4-9 Square plate with a circular hole under tension (E random, $c.o.v.(E)$ = 10%, type B with $\lambda = 0.5\ L$) – error criteria $err1^e$

a. Correlation length, $\lambda = 0.005L$ b. Correlation length, $\lambda = 50L$

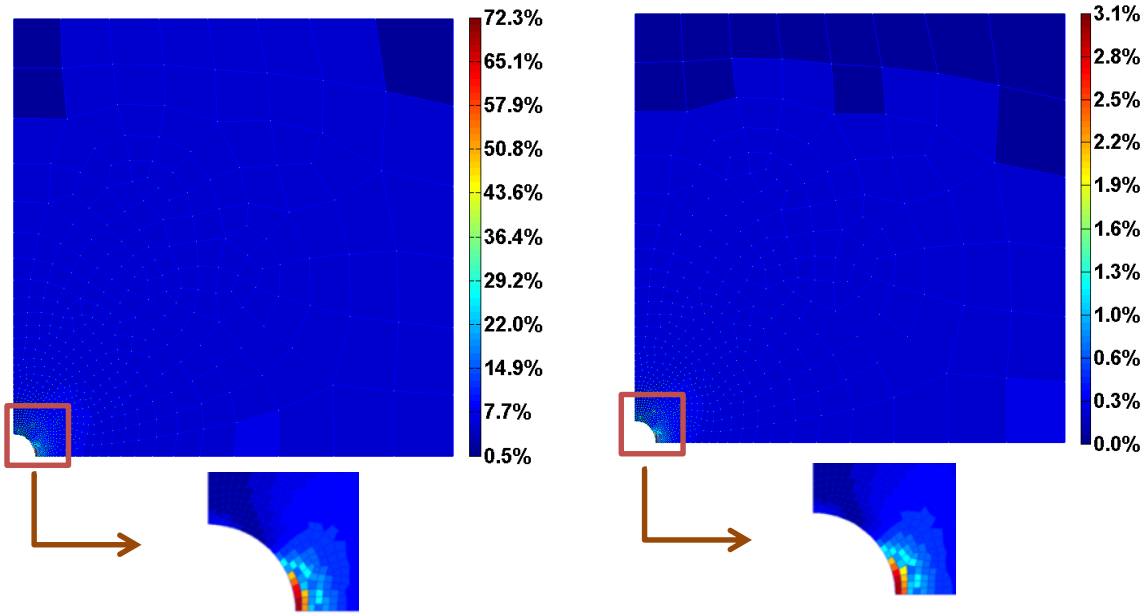

Figure 4-10 Square plate with a circular hole under tension (E random, $c.o.v.(E)$ = 10%, type B with $\lambda = 0.5\ L$) – error criteria $err2^e$

For a given correlation length one can also observe that the first criteria leads to significantly lower maximum errors than the second criteria. Indeed, compared to the first criteria, the second one amplifies the errors in high strain energy areas, in this case near the hole, (see Figure 4-9). In conclusion, when the correlation length is small, the CGSM assumption can lead to significant local errors, but the errors on the mean and standard deviation of displacement remain small (see Tables 4-5 and 4-6).

Chapter 5
Formulation and Applications of CGSM for Bending Plates

In this section, the CGSM is developed for three-node triangles (T3) and four-node quadrilaterals (Q4), whatever the formulation of these elements. A distinction is made between the thin plate case with bending effects, and the thick plate one with bending and transverse shear effects.

5.1. Formulation of the CGSM for bending plates

5.1.1. Formulation of the CGSM for thin plates

The objective is to describe the calculation of the variability of a displacement. The bending strain energy is:

$$\pi_{int}^{b} = \frac{1}{2}\int_{V} z^2 \langle\chi\rangle\,[H]\,\{\chi\}\,dV = \frac{1}{2}\int_{A} \frac{h^3}{12}\langle\chi\rangle\,[H]\,\{\chi\}\,dA \qquad \textbf{5-1}$$

where $\langle\chi\rangle = \langle\chi_x\ \ \chi_y\ \ \chi_{xy}\rangle$ are the bending strains, V is the volume of the structure ($dV = h\,dA$), $[H]$ is the plane stress elasticity matrix defined in equation 4-2 for an isotropic material.

The relationship between the bending strains $\langle\chi\rangle$ and moments $\{M\}$ is:

$$\{\chi\} = \frac{12}{h^3}[H]^{-1}\{M\} \qquad \textbf{5-2}$$

with $\langle M\rangle = \langle M_x\ \ M_y\ \ M_{xy}\rangle$.

Substituting equation 5-2 into equation 5-1 gives:

$$\pi_{int}^{b} = \frac{1}{2}\int_{A} \frac{12}{h^3}\langle M\rangle[H]^{-1}\{M\}\,dA \qquad \textbf{5-3}$$

or:

$$\pi_{int}^{b} = \frac{1}{2}\int_{A} \frac{12}{Eh^3} \langle M_x \quad M_y \quad M_{xy} \rangle \begin{bmatrix} 1 & -v & 0 \\ -v & 1 & 0 \\ 0 & 0 & 2(1+v) \end{bmatrix} \begin{Bmatrix} M_x \\ M_y \\ M_{xy} \end{Bmatrix} dA \qquad \textbf{5-4}$$

Developing equation 5-4 gives:

$$\pi_{int}^{b} = \frac{1}{2}\int_{A} \frac{12}{Eh^3} \left({M_x}^2 - 2vM_xM_y + {M_y}^2 + 2(1+v){M_{xy}}^2 \right) dA \qquad \textbf{5-5}$$

Considering that the domain is spatially discretized and the mesh contains *n* finite elements, equation 5-5 can be written as:

$$\pi_{int}^{b} = \frac{1}{2}\sum_{i=1}^{n} \int_{A_i} \frac{12}{E_i {h_i}^3} \left({M_{x_i}}^2 - 2v_iM_{x_i}M_{y_i} + {M_{y_i}}^2 + 2(1+v_i){M_{xy_i}}^2 \right) dA \qquad \textbf{5-6}$$

where *i* is the element number; M_{x_i}, M_{y_i} and M_{xy_i} are the moments; A_i is the area; E_i is the elasticity modulus; h_i is the thickness and v_i is the Poisson's ratio.

In order to apply the Castigliano's theorem for calculating the displacement U at a point *P* in a given direction, the moments in each element are decomposed into two contributions:

$$\begin{aligned} M_{x_i} &= M_{x_i}' + FM_{x_i}'' \\ M_{y_i} &= M_{y_i}' + FM_{y_i}'' \\ M_{xy_i} &= M_{xy_i}' + FM_{xy_i}'' \end{aligned} \qquad \textbf{5-7}$$

where *i* is the element number; *F* is the load applied at point *P* in the direction of interest (*F* is a force or a moment if the variability of a displacement or a rotation must be assessed respectively); M_{x_i}, M_{y_i} and M_{xy_i} are the moments; M_{x_i}', M_{y_i}' et M_{xy_i}' are the moments due to loads on the whole structure except at point *P* in the direction of interest; M_{x_i}'', M_{y_i}'' et M_{xy_i}'' are the moments due to a unitary load applied at point *P* in the direction of interest.

Substituting equation 5-7 into equation 5-6 gives:

$$\pi_{int}^{b} = \frac{1}{2}\sum_{i=1}^{n}\int_{A_i}\frac{12}{{E_i h_i}^3}\Big(\big(M_{x_i}' + FM_{x_i}^{"}\big)^2 - 2v_i\big(M_{x_i}' + FM_{x_i}^{"}\big)\Big(M_{y_i}' + FM_{y_i}^{"}\Big) + \Big(M_{y_i}' + FM_{y_i}^{"}\Big)^2 + 2(1+v_i)\Big(M_{xy_i}' + FM_{xy_i}^{"}\Big)^2\Big)\,dA \quad \textbf{5-8}$$

As for the membrane plates case, our objective is to consider simple interpolations of moments; these interpolations are independent of the initial formulation of the element. For T3 and Q4 elements considered here, the moments are assumed to be constant over one element. Equation 5-8 becomes:

$$\pi_{int}^{b} = \frac{1}{2}\sum_{i=1}^{n}\frac{12A_i}{{E_i h_i}^3}\Big(\big(M_{x_i}' + FM_{x_i}^{"}\big)^2 - 2v_i\Big(M_{x_i}'M_{y_i}' + FM_{x_i}'M_{y_i}^{"} + FM_{x_i}^{"}M_{y_i}' + F^2M_{x_i}^{"}M_{y_i}^{"}\Big) + \Big(M_{y_i}' + FM_{y_i}^{"}\Big)^2 + 2(1+v_i)\Big(M_{xy_i}' + FM_{xy_i}^{"}\Big)^2\Big) \quad \textbf{5-9}$$

To obtain the displacement at a point P in a given direction, the Castigliano's theorem is applied:

$$U_b = \frac{\pi_{int}^{b}}{\partial F} \quad \textbf{5-10}$$

Finally, for the thin bending plate case, the displacement is:

$$U_b = \sum_{i=1}^{n}\frac{12A_i}{{E_i h_i}^3}\Big(M_{x_i}^{"}\big(M_{x_i}' + FM_{x_i}^{"}\big) + M_{y_i}^{"}\Big(M_{y_i}' + FM_{y_i}^{"}\Big) + 2M_{xy_i}^{"}\Big(M_{xy_i}' + FM_{xy_i}^{"}\Big) + v_i\Big(2M_{xy_i}^{"}\Big(M_{xy_i}' + FM_{xy_i}^{"}\Big) - \Big(M_{x_i}'M_{y_i}^{"} + M_{x_i}^{"}M_{y_i}' + 2FM_{x_i}^{"}M_{y_i}^{"}\Big)\Big)\Big) \quad \textbf{5-11}$$

The expression of U_f given in equation 5-11 is used for each trial of the CGSM+Monte Carlo simulation, to calculate the displacement variability at a point of a bending plate.

5.1.2. Formulation of the CGSM for thick plates

The strain energy is:

$$\pi_{int} = \pi_{int}^{b} + \pi_{int}^{tsh} \quad \textbf{5-12}$$

The description of π_{int}^{b} is identical to that developed in section 5.1.1. The strain energy associated with the contribution of transverse shear is:

$$\pi_{int}^{tsh} = \frac{1}{2}\int_{V} \langle\gamma\rangle\,[H_s]\,\{\gamma\}\,dV = \frac{1}{2}\int_{A} h\langle\gamma\rangle\,[H_s]\,\{\gamma\}\,dA \quad \textbf{5-13}$$

where $\langle\gamma\rangle = \langle\gamma_{xz}\ \gamma_{yz}\rangle$ are the transverse shear strains, V is the volume of the structure ($dV = h\,dA$), $[H_s]$ is the transverse shear elasticity matrix. For an isotropic material, this matrix is defined by:

$$[H_s] = G\,k_s\begin{bmatrix}1 & 0\\ 0 & 1\end{bmatrix} \quad \textbf{5-14}$$

$$G = \frac{E}{2\,(1+v)} \quad \textbf{5-15}$$

where G is the shear modulus, k_s is the transverse shear correction factor, E is the elasticity modulus, and v is the Poisson's ratio.

The relationship between the transverse shear strains $\{\gamma\}$ and transverse shear forces $\{T\}$ is:

$$\{\gamma\} = h[H_s]^{-1}\{T\} \quad \textbf{5-16}$$

with $\langle T\rangle = \langle T_x \quad T_y\rangle$.

Reporting equation 5-16 into equation 5-13, one obtains:

$$\pi_{int}^{tsh} = \frac{1}{2}\int_{A} \frac{1}{h}\,\langle T\rangle[H_s]^{-1}\,\{T\}\,dA \quad \textbf{5-17}$$

or:

$$\pi_{int}^{tsh} = \frac{1}{2}\int_{A} \frac{1}{G\,k_s h}\langle T_x \quad T_y\rangle\begin{bmatrix}1 & 0\\ 0 & 1\end{bmatrix}\begin{Bmatrix}T_x\\ T_y\end{Bmatrix}\,dA \quad \textbf{5-18}$$

Developing equation 5-18 gives:

$$\pi_{int}^{tsh} = \frac{1}{2}\int_{A} \frac{2(1+v)}{E\,k_s\,h}\left({T_x}^2 + {T_y}^2\right)\,dA \quad \textbf{5-19}$$

Considering that the domain is spatially discretized and the mesh contains *n* finite elements, equation 5-19 can be written as:

$$\pi_{int}^{tsh} = \frac{1}{2}\sum_{i=1}^{n}\int_{A_i}\frac{2(1+v_i)}{E_i\,k_s\,h_i}\left({T_{x_i}}^2 + {T_{y_i}}^2\right)\,dA \qquad \textbf{5-20}$$

where *i* is the element number; T_{x_i} and T_{y_i} are the transverse shear forces; A_i is the area; E_i is the elasticity modulus; k_s is the transverse shear correction factor; h_i is the thickness and v_i is the Poisson's ratio.

In order to apply the Castigliano's theorem for calculating the displacement *U* of a point *P* in a given direction, the shear forces of each element are decomposed into two contributions:

$$\begin{aligned} T_{x_i} &= T_{x_i}' + FT_{x_i}^{"} \\ T_{y_i} &= T_{y_i}' + FT_{y_i}^{"} \end{aligned} \qquad \textbf{5-21}$$

where *i* is the element number; *F* is the load applied at point *P* in the direction of interest (*F* is a force or a moment if the variability of a displacement or a rotation must be assessed respectively), T_{x_i} and T_{y_i} are the shear forces, T_{x_i}' and T_{y_i}' are the shear forces due to loads on the whole structure except at point *P* in the direction of interest, $T_{x_i}^{"}$ and $T_{y_i}^{"}$ are the shear forces due to a unitary load applied at point *P* in the direction of interest.

Substituting-equation 5-21 into equation 5-20 gives:

$$\pi_{int}^{tsh} = \frac{1}{2}\sum_{i=1}^{n}\int_{A_i}\frac{2(1+v_i)}{E_i\,k_s\,h_i}\left(\left(T_{x_i}' + FT_{x_i}^{"}\right)^2 + \left(T_{y_i}' + FT_{y_i}^{"}\right)^2\right)\,dA \qquad \textbf{5-22}$$

As for the membrane plate and the thin bending plate cases, our objective is to consider here simple interpolations of transverse shear forces; these interpolations are independent of the initial formulation of the element. For T3 and Q4 elements considered here, the transverse shear forces are assumed to be constant over one element. Equation 5-22 becomes:

$$\pi_{int}^{tsh} = \frac{1}{2}\sum_{i=1}^{n}\frac{2(1+v_i)A_i}{E_i\,k_s\,h_i}\left(\left(T_{x_i}' + FT_{x_i}^{"}\right)^2 + \left(T_{y_i}' + FT_{y_i}^{"}\right)^2\right) \qquad \textbf{5-23}$$

To obtain the displacement at a point P in a given direction, the Castigliano's theorem is applied:

$$U = U_b + U_{tsh} = \frac{\partial \pi_{int}^{b}}{\partial F} + \frac{\partial \pi_{int}^{tsh}}{\partial F} \quad \textbf{5-24}$$

U_b is obtained by equation 5-11 and the displacement due to transverse shear effects U_{tsh} is:

$$U_{tsh} = \frac{\partial \pi_{int}^{tsh}}{\partial F} \quad \textbf{5-25}$$

Taking into account equation 5-23 leads to the following expression of the displacement due to transverse shear effects:

$$U_{tsh} = \sum_{i=1}^{n} \frac{2A_i(1+v_i)}{E_i\, k_s\, h_i} \left(T_{x_i}^{"} \left(T_{x_i}^{'} + F T_{x_i}^{"} \right) + T_{y_i}^{"} \left(T_{y_i}^{'} + F T_{y_i}^{"} \right) \right) \quad \textbf{5-26}$$

Finally, for the thick bending plate case, the displacement U is:

$$\begin{aligned} U = \sum_{i=1}^{n} \frac{12A_i}{E_i {h_i}^3} \Bigg(& M_{x_i}^{"} \left(M_{x_i}^{'} + F M_{x_i}^{"} \right) + M_{y_i}^{"} \left(M_{y_i}^{'} + F M_{y_i}^{"} \right) + 2 M_{xy_i}^{"} \left(M_{xy_i}^{'} + F M_{xy_i}^{"} \right) \\ & + v_i \left(2 M_{xy_i}^{"} \left(M_{xy_i}^{'} + F M_{xy_i}^{"} \right) - \left(M_{x_i}^{'} M_{y_i}^{"} + M_{x_i}^{"} M_{y_i}^{'} + 2F M_{x_i}^{"} M_{y_i}^{"} \right) \right) \Bigg) \\ & + \frac{2A_i(1+v_i)}{E_i\, k_s\, h_i} \left(T_{x_i}^{"} \left(T_{x_i}^{'} + F T_{x_i}^{"} \right) + T_{y_i}^{"} \left(T_{y_i}^{'} + F T_{y_i}^{"} \right) \right) \end{aligned} \quad \textbf{5-27}$$

5.2. Bending plates examples

5.2.1. Square bending plate under uniformly distributed load

5.2.1.1. Presentation of the example

The first example is a square bending plate (Figure 5-1), simply supported and subjected to a uniformly distributed load q = 10 (data are provided in dimensionless form). This example has been treated by Noh [123]. The geometric

characteristics are as follows: L = 10 and h = 1, so the plate is rather thick. The random parameters are the elasticity modulus E and the Poisson's ratio v, represented by isotropic random fields. The mean values of these parameters are $m(E)$ = 10.29 x 10^3 and $m(\nu)$ = 0.2. The coefficients of variation $c.o.v.(E)$ and $c.o.v.(\nu)$ are equal to 10%. An isotropic exponential correlation function defined in equation 3-29 and several correlation lengths $\lambda = 0.001L$ to $100L$ are considered. The direct Monte Carlo simulations and the CGSM + Monte Carlo simulations are made with 10,000 runs. The variability of the vertical displacement of the central point A is calculated. As mentioned by Noh [123], the symmetry of the structure is disturbed by random fields but this asymmetry is limited because the coefficients of variation of the random parameters are small. Consequently, as suggested by Noh [123] and in order to compare our results with this reference, only a quarter of the plate is discretized.

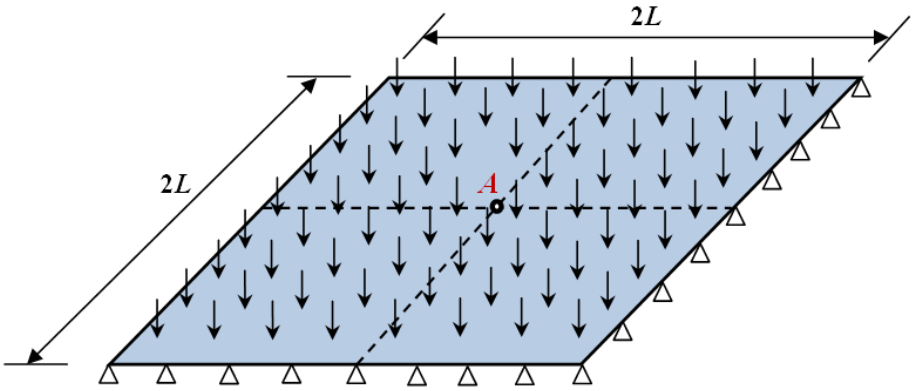

Figure 5-1 Simply supported square bending plate under uniformly distributed load

5.2.1.2. Finite element mesh

The global strategy to identify an optimal mesh, described in section 3.9 and already exploited for membrane plates in section 4.2.1.2, is applied here again. In this example, the DKMQ element proposed by Katili [115] is used and all the results presented below have been obtained with this element. Some complementary tests have shown that similar results are obtained with the S4 element of Abaqus [114]. Firstly a convergence analysis is performed with the

CGSM formulation in the nominal configuration (equation 5-27). Table 5-1 shows the results of a convergence study of nominal displacements at point *A*. The reference is given by a very fine mesh (48x48). The 24x24 mesh (Figure 5-2), leading to an error of 0.6%, is considered as satisfactory for the nominal calculation. Consequently this mesh is exploited to calculate the variability. We will check a posteriori whether this mesh is also well suited for the calculation of the variability (section 5.2.1.4).

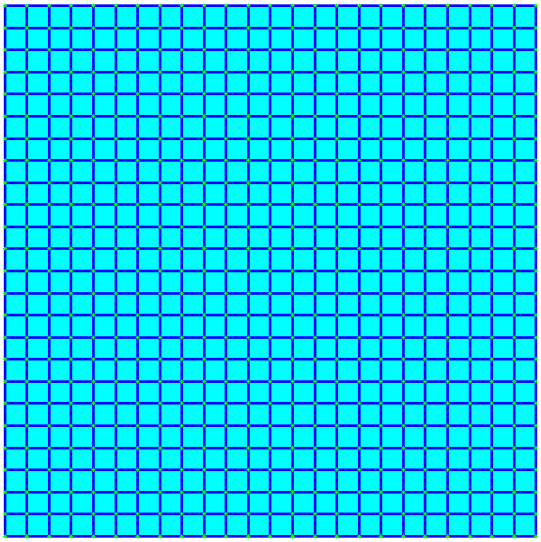

Figure 5-2 Simply supported square bending plate under uniformly distributed load – the 24x24 mesh (625 nodes and 576 elements)

Node	Mesh: 6x6		Mesh: 12x12		Mesh: 24x24		Mesh: 48x48
	Displacement	Error (%)	Displacement	Error (%)	Displacement	Error (%)	Displacement (reference)
A	7.524	2.3	7.555	1.9	7.659	0.6	7.703

Table 5-1 Simply supported square bending plate under uniformly distributed load – convergence study of displacement at node *A* in nominal configuration

5.2.1.3. Displacement variability

The CGSM results are compared to reference solutions obtained by direct Monte Carlo simulations. In the first case, the random parameter is *E* and several correlation lengths are considered. For each correlation length, the mean value,

standard deviation and coefficient of variation of displacement at point A are reported in Table 5-2. Errors are given in Table 5-3. The CGSM provides very accurate results for the whole correlation length range. Nevertheless the errors slightly increase when the correlation length is smaller than L.

In the second case, the random parameter is v and again several correlation lengths are considered. Table 5-4 shows the mean value, standard deviation and coefficient of variation of displacement obtained by the CGSM and the Monte Carlo simulations. Errors, reported in Table 5-5, are always very small.

λ	0.01L		L		10 L		100 L	
	CGSM	dMC	CGSM	dMC	CGSM	dMC	CGSM	dMC
$m(U)$	7.738	7.726	7.739	7.748	7.751	7.778	7.734	7.764
$\sigma(U)$	4.280E-02	4.180E-02	5.896E-01	5.860E-01	7.712E-01	7.732E-01	7.989E-01	8.018E-01
c.o.v.(U) (%)	0.55	0.54	7.62	7.56	9.95	9.94	10.33	10.33

Table 5-2 Simply supported square bending plate under uniformly distributed load (E random, *c.o.v.*(E) = 10%) – variability of displacement at point A

λ	0.01L	L	10 L	100 L
Error on $m(U)$ (%)	0.2	0.1	0.3	0.4
Error on $\sigma(U)$ (%)	2.4	0.6	0.3	0.4
Error on *c.o.v.*(U) (%)	2.2	0.7	0.1	0.0

Table 5-3 Simply supported square bending plate under uniformly distributed load (E random, *c.o.v.*(E) = 10%) – errors on the statistical results of displacement at point A

λ	0.01L		L		10 L		100 L	
	CGSM	dMC	CGSM	dMC	CGSM	dMC	CGSM	dMC
$m(U)$	7.659	7.687	7.658	7.685	7.658	7.684	7.659	7.686
$\sigma(U)$	8.902E-03	8.901E-03	7.600E-02	7.590E-02	7.280E-02	7.230E-02	7.100E-02	7.090E-02
c.o.v.(U) (%)	0.16	0.16	0.99	0.99	0.95	0.94	0.93	0.92

Table 5-4 Simply supported square bending plate under uniformly distributed load (v random, *c.o.v.*(v) = 10%) – variability of displacement at point A

λ	0.01*L*	*L*	10 *L*	100 *L*
Error on $m(U)$ (%)	0.4	0.4	0.3	0.3
Error on $\sigma(U)$ (%)	0.0	0.1	0.7	0.1
Error on *c.o.v.*(U) (%)	0.4	0.5	1.0	0.5

Table 5-5 Simply supported square bending plate under uniformly distributed load (ν random, *c.o.v.*(ν) = 10%) – errors on the statistical results of displacement at point *A*

Figure 5-3 shows the evolution of the coefficient of variation of displacement at point *A*, when the correlation length varies. The variability of the displacement increases non-linearly with the correlation length. For small correlation lengths, the variability level is very low. This is due to a compensation phenomenon. It is also observed that the variability of displacement is much higher in the case where the elasticity modulus is random with respect to the one where the uncertain parameter is the Poisson's ratio. CGSM provides results very close to those obtained by the direct Monte Carlo simulation. The CGSM results are also similar with those presented by Noh [123].

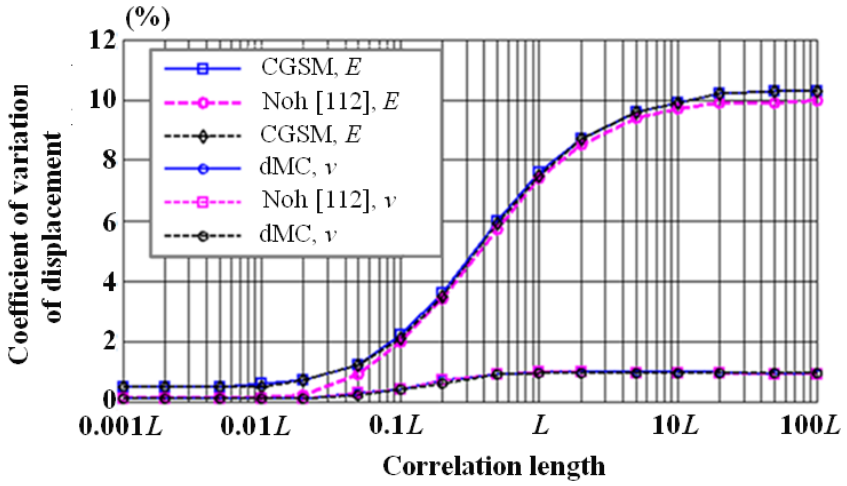

Figure 5-3 Simply supported square bending plate under uniformly distributed load (*E* and ν random, *c.o.v.*(E) = 10%, *c.o.v.*(ν) = 10%) – variability of displacement at point *A*

Figure 5-4 shows the probability density function of the displacement at point *A*, with *E* or ν considered as uncertain. As for both examples of chapter 4 (sections 4.2.1.3 and 4.2.2.3), the distributions obtained with the CGSM are very

close to the reference distributions obtained with the direct Monte Carlo simulation. Again, for the same reasons as described in sections 4.2.1 and 4.2.2, the output distributions are not exactly Gaussian.

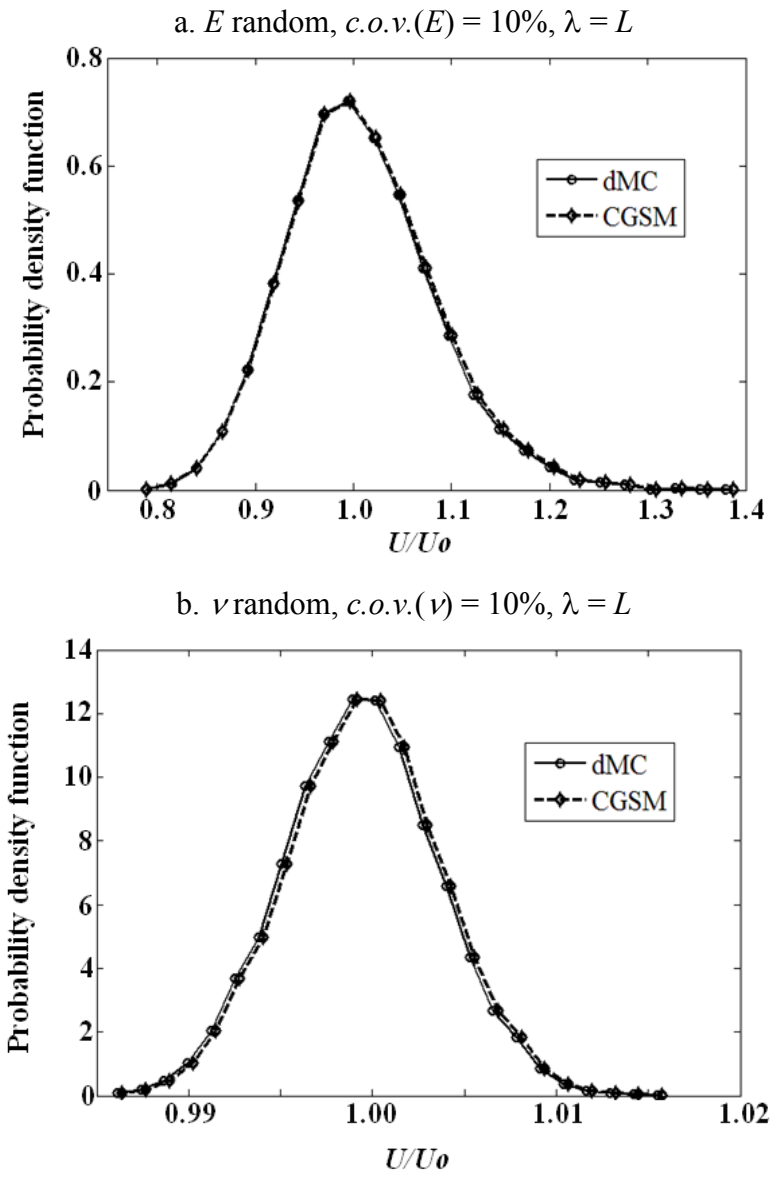

Figure 5-4 Simply supported square bending plate under uniformly distributed load – distribution of the displacement at point *A*

5.2.1.4. Influence of the mesh for variability computation

In section 5.2.1.2 the 24x24 mesh has been exploited. The objective of the tests presented in this section is to verify a posteriori whether this mesh is also correct for the calculation of variability. Again, this study is performed with the CGSM. In the first case, the random parameter is the elasticity modulus ($c.o.v.(E)$ = 10%) and in the second case, the random parameter is the Poisson's ratio ($c.o.v.(\nu)$ = 10%). The differences between the results obtained with the 24x24 mesh and the 48x48 mesh (reference mesh) on the mean value and standard deviation of displacement at point A, are shown in Tables 5-6 and 5-7. For both tests, the 24x24 mesh is satisfactory when the correlation length is greater than $0.1L$. When the correlation length is smaller than $0.1L$, the 24x24 mesh leads to significant errors. As for both examples of chapter 4 (see sections 4.2.1.4 and 4.2.2.5), this is due to the fact that the variation of the random parameters is very fast in this case. Again, these results show that the strategy which consists in identifying the optimal mesh for the nominal case and use it for the calculation of the variability is valid, except when the correlation length is extremely small.

λ	$0.01L$	$0.1L$	L	$10\,L$	$100\,L$
$err_{mesh}\big(m(U)\big)$ (%)	0.5	0.5	0.5	0.5	0.2
$err_{mesh}\big(\sigma(U)\big)$ (%)	66	1.6	0.7	0.2	0.0

Table 5-6 Simply supported square bending plate under uniformly distributed load (E random, $c.o.v.(E)$ = 10%) – error on the mean value and the standard deviation of displacement at point A for the 24x24 mesh

λ	$0.01L$	$0.1L$	L	$10\,L$	$100\,L$
$err_{mesh}\big(m(U)\big)$ (%)	0.6	0.6	0.6	0.6	0.6
$err_{mesh}\big(\sigma(U)\big)$ (%)	65	3.8	0.9	0.8	0.0

Table 5-7 Simply supported square bending plate under uniformly distributed load (ν random, $c.o.v.(\nu)$ = 10%) – error on the mean value and the standard deviation of displacement at point A for the 24x24 mesh

5.2.1.5. Performance of the CGSM in computational time

As far as computational time is concerned, for this example, the acceleration factor obtained with the CGSM is about 400 compared to the direct Monte Carlo simulation.

5.2.1.6. Errors on the strain energy

As for the membrane plates, both error criteria $err1^e$ and $err2^e$ defined in equations 3-37 and 3-38 are observed. Figures 5-5 and 5-6 show the results obtained for $err1$ and $err2$ respectively, the elasticity modulus being the random parameter. As for the membrane plates, for both criteria, when the correlation length is very large, errors are quite small, while they are bigger for a small correlation length. For a given correlation length we also observe that the first criteria leads to slightly lower maximum errors than the second criteria. In conclusion, when the correlation length is small, the CGSM assumption can lead to significant local errors, but the errors on the mean and standard deviation of displacement remain small (see Tables 5-3 and 5-5).

a. Correlation length, $\lambda = 0.01L$ b. Correlation length, $\lambda = 100L$

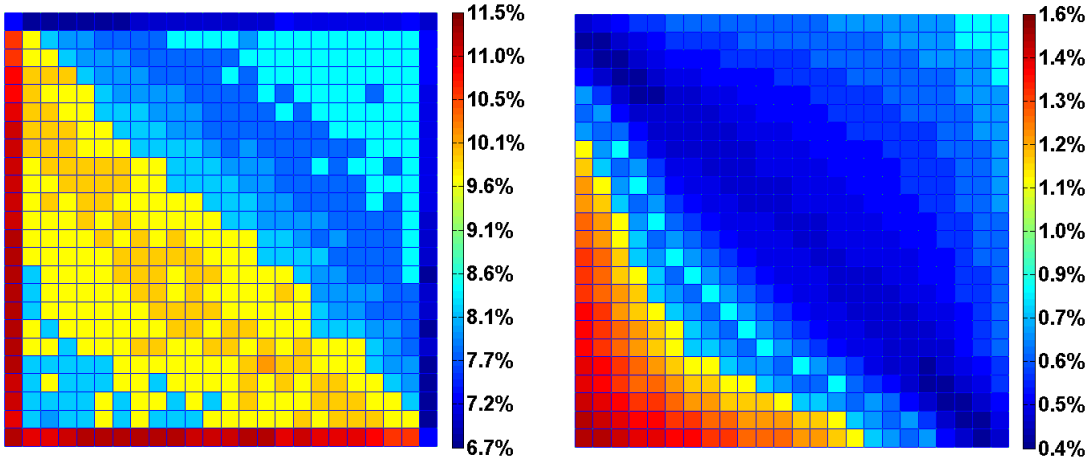

Figure 5-5 Simply supported square bending plate under uniformly distributed load (E random, $c.o.v.(E) = 10\%$) – error criteria $err1^e$

a. Correlation length, $\lambda = 0.01L$ b. Correlation length, $\lambda = 100L$

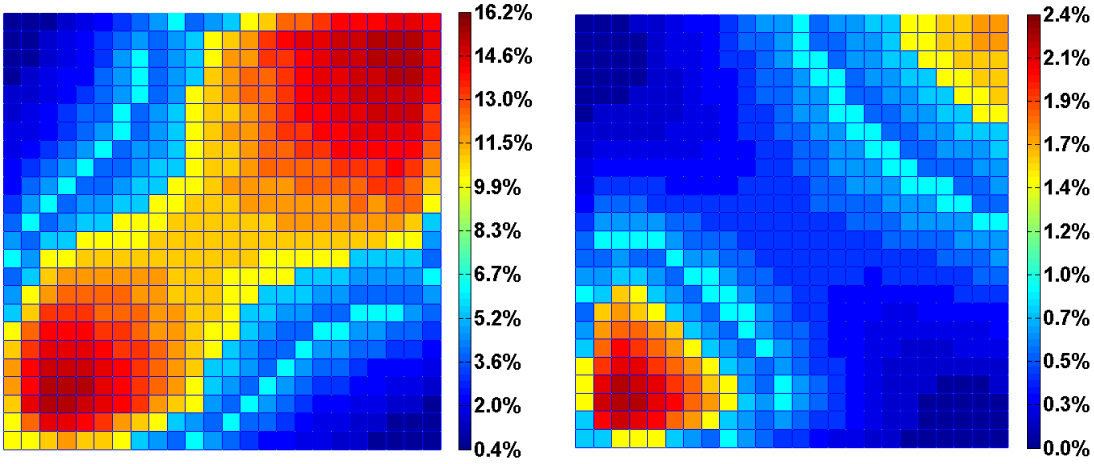

Figure 5-6 Simply supported square bending plate under uniformly distributed load (E random, $c.o.v.(E) = 10\%$) – error criteria $err2^e$

5.2.2. Square bending plate under concentrated load

5.2.2.1. Presentation of the example

We consider here a square bending plate (Figure 5-7), simply supported and subjected to a concentrated load $P = 10$ kN. This example has been treated by Argyris et al. [79]. The geometrical characteristics are as follows: $L = 10$ m and $h = 0.1$ m. The mean elasticity modulus is $m(E) = 10.92 \times 10^5$ kN/m^2 and Poisson's ratio is 0.3. The random parameter is the elasticity modulus, represented by an anisotropic random field. The coefficient of variation is 10% and different correlation lengths, $\lambda = 0.005L$ to $10L$, are considered. The square exponential correlation function (equation 3-27) is used. The direct Monte Carlo simulations and the CGSM + Monte Carlo simulations are made with 10,000 runs. The variability of the vertical displacement of the center point A is calculated. For this example the whole plate is discretized.

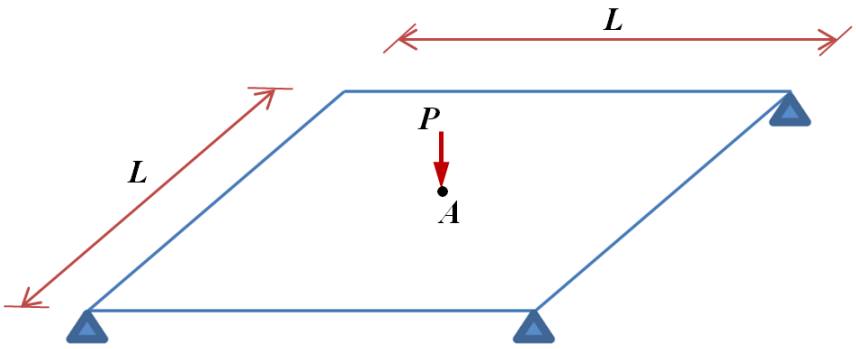

Figure 5-7 Simply supported square bending plate under concentrated load

5.2.2.2. Finite element mesh

As in previous examples, we first search for the optimal nominal mesh and then we verify that this mesh is adapted to calculate the variability. In this example, the DKMQ element proposed by Katili [115] is used and all the results presented below have been obtained with this element. Table 5-8 shows the results of a convergence study of nominal displacement at point *A* performed with the CGSM formulation in the nominal configuration (equation 5-27). The reference solution is given by a very fine mesh (48x48). The 24x24 mesh, leading to an error of 0.3%, is satisfactory for the nominal calculation. Consequently this mesh is exploited to calculate the variability. We will check a posteriori whether this mesh is also well suited for the calculation of the variability.

Node	Mesh: 6x6		Mesh: 12x12		Mesh: 24x24		Mesh 48x48
	Displacement	Error (%)	Displacement	Error (%)	Displacement	Error (%)	Displacement (reference)
A	0.3705	5.1	0.3859	1.3	0.3900	0.3	0.3910

Table 5-8 Simply supported square bending plate under concentrated load – convergence study of displacement at point *A* in nominal configuration

5.2.2.3. Variability of displacement

The CGSM results are compared to a reference solution obtained by direct Monte Carlo simulation. For each correlation length, the mean value, standard

deviation and coefficient of variation of displacements at point *A* are reported in Table 5-9. Errors are given in Table 5-10. The CGSM provides very accurate results for the whole correlation length range.

λ	0.005*L*		0.05 *L*		0.1 *L*		0.2 *L*		2 *L*	
	CGSM	dMC	CGSM	dMC	CGSM	dMC	CGSM	dMC	CGSM	dMC
$m(U)$	0.3941	0.393	0.394	0.394	0.394	0.394	0.394	0.394	0.395	0.396
$\sigma(U)$	0.002	0.002	0.002	0.002	0.006	0.006	0.015	0.015	0.039	0.039
c.o.v.(U) (%)	0.5	0.5	0.6	0.6	1.5	1.5	3.8	3.8	9.9	9.9

Table 5-9 Simply supported square bending plate under concentrated load (E random, *c.o.v.*$(E) = 10\%$) – variability of displacements at point *A*

λ	0.005*L*	0.05 *L*	0.1 *L*	0.2 *L*	2 *L*
Error on $m(U)$) (%)	0.1	0.1	0.0	0.1	0.4
Error on $\sigma(U)$) (%)	0.0	0.0	1.7	0.7	0.5
Error on *c.o.v.*(U) (%)	0.1	0.1	1.7	0.7	0.2

Table 5-10 Simply supported square bending plate under concentrated load (E random, *c.o.v.*$(E) = 10\%$) – errors on the statistical results of displacement at point *A*

Figure 5-8 shows the evolution of the coefficient of variation of displacement at point *A*. The variability of the displacement increases non-linearly with the correlation length. As in the previous example, when the correlation length is smaller than $0.1L$, the variability of the displacement is very small. This is again due to a compensation phenomenon. The CGSM provides results very close to those obtained by the direct Monte Carlo simulation. Our results are also consistent with those presented by Argyris et al. [79]. However some discrepancy is observed when the correlation length is very small ($\lambda=0.005L$). This point is commented and justified in section 5.2.2.4.

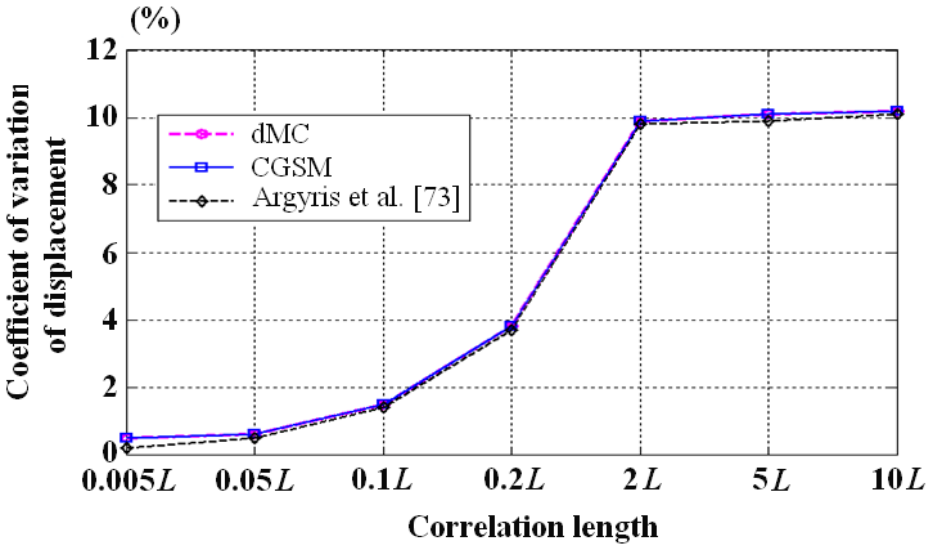

Figure 5-8 Simply supported square bending plate under concentrated load (E random, $c.o.v.(E) = 10\%$) – variability of displacement at point A

Figure 5-9 shows the probability density function of the displacement at point A. Again, the distribution obtained with the CGSM is very close to the reference distribution obtained with the direct Monte Carlo simulation. As already justified, the distribution is not exactly Gaussian.

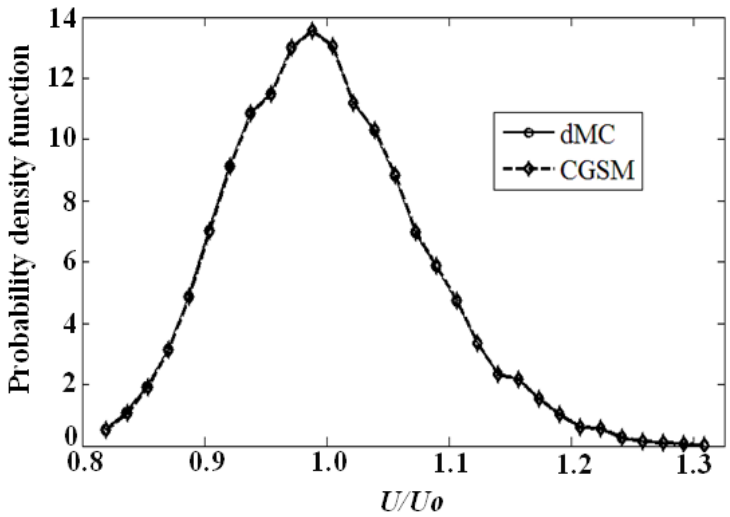

Figure 5-9 Simply supported square bending plate under concentrated load (E random, $c.o.v.(E) = 10\%$, $\lambda = L$) – distribution of the displacement at point A

5.2.2.4. Influence of the mesh for variability computation

We now check that the 24x24 mesh is also well suited for the calculation of the variability. This study is conducted with the CGSM method. The differences between the results obtained with the 24x24 mesh and the 48x48 mesh (reference mesh) on the mean and standard deviation of displacement at point *A,* are shown in Table 5-11. The 24x24 mesh is satisfactory, except for the smallest value of correlation length: 0.005L. These results show again that the strategy which consists in identifying the optimal mesh for the nominal case and use it for the calculation of the variability is valid, except when the correlation length is extremely small.

λ	0.005L	0.05 L	0.1 L	0.2 L	2 L
$err_{mesh}(m(U))$	0.3%	0.3%	0.3%	0.4%	0.2%
$err_{mesh}(\sigma(U))$	122%	0.0%	0.0%	0.7%	0.0%

Table 5-11 Simply supported square bending plate under concentrated load (E random, $c.o.v.(E)$ = 10%) – error on the mean value and the standard deviation of displacement at point A for the 24x24 mesh

5.2.2.5. Performance of the CGSM in computational time

As far as computational time is concerned, for this example, the acceleration factor obtained with the CGSM is about 400 compared to the direct Monte Carlo simulation.

5.2.2.6. Errors on the strain energy

Here we find the same trends previously observed for membrane plates examples (see sections 4.2.1.6 and 4.2.2.7), as well as the first bending plate example (see section 5.2.1.6). For both criteria, the errors are quite small when the correlation length is very large**.** However, when the correlation length is small, the CGSM assumption can lead to significant local errors, but the errors on the mean and standard deviation of displacement remain small (see Table 5-10).

a. Correlation length, $\lambda = 0.005L$ b. Correlation length, $\lambda = 10L$

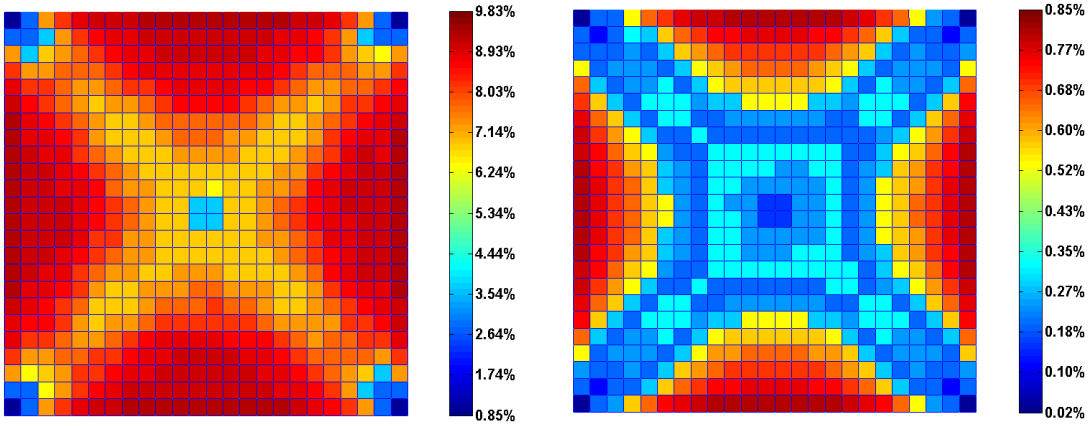

Figure 5-10 Simply supported square bending plate under concentrated load (E random, $c.o.v.(E) = 10\%$) – error criteria $err1^e$

a. Correlation length, $\lambda = 0.005L$ b. Correlation length, $\lambda = 10L$

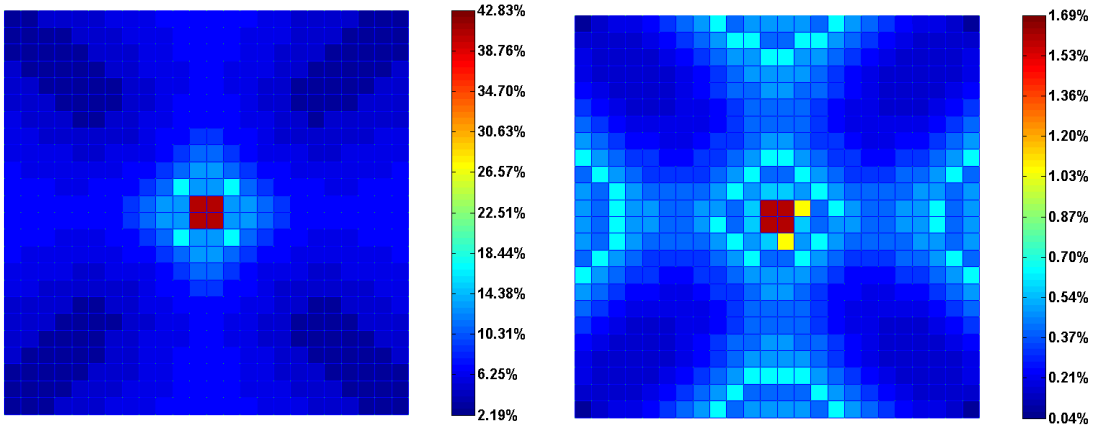

Figure 5-11 Simply supported square bending plate under concentrated load (E random, $c.o.v.(E) = 10\%$) – error criteria $err2^e$

5.2.3. Simply supported circular plate under uniform load

5.2.3.1. Presentation of the example

We consider here a quarter of a circular plate of radius $R = 5$ (Figure 5-12), simply supported and subjected to a uniformly distributed load $f_z = -1$ (data are provided in dimensionless form). Two thicknesses are considered: $h_1 = 0.1$ and $h_2 = 2.5$. The mean elasticity modulus is $m(E) = 10.92$, Poisson's ratio is 0.3 and length of structure is $L = 5$. The random parameter is the elasticity modulus, represented

by an isotropic random field. The coefficient of variation is 10% and different correlation lengths, $\lambda = 0.001L$ to $1000L$, are considered. The linear exponential correlation function (equation 3-26) is used. The direct Monte Carlo simulations and the CGSM + Monte Carlo simulations are made with 10000 runs. The variability of the vertical displacement of the center point *C* is calculated.

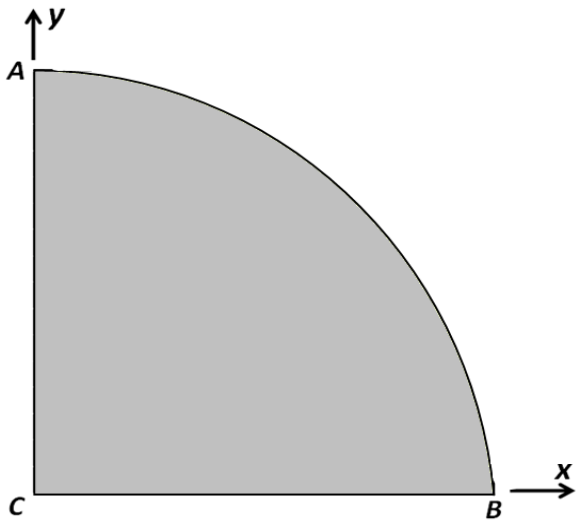

Figure 5-12 Simply supported circular plate under uniform load in the *z* direction

5.2.3.2. Finite element mesh

As in previous examples, we first search for the optimal nominal mesh and then we verify that this mesh is adapted to calculate the variability. In this example, the DKMQ element proposed by Katili [115] is used and all the results presented below have been obtained with this element. Tables 5-12 and 5-13 show the results of a convergence study of nominal displacement at point *C* performed with the CGSM formulation in the nominal configuration (equation 5-27). For this example the exact solution, considered as a reference, is available [115]. The 192 finite elements mesh (Figure 5-13), leading to a maximal error of 0.5%, is satisfactory for the nominal calculation. Consequently this mesh is exploited to calculate the variability.

Node	48 finite elements		108 finite elements		192 finite elements		Exact
	Displacement	Error (%)	Displacement	Error (%)	Displacement	Error (%)	displacement
C	4327	8.6	4017	0.8	4005	0.5	3983

Table 5-12 Simply supported circular plate under uniform load – convergence study of displacement at point *C* in nominal configuration for thin plate with $R/h = 50$

Node	48 finite elements		108 finite elements		192 finite elements		Exact
	Displacement	Error (%)	Displacement	Error (%)	Displacement	Error (%)	displacement
C	3.472	6.4	3.245	0.5	3.250	0.4	3.262

Table 5-13 Simply supported circular plate under uniform load – convergence study of displacement at point *C* in nominal configuration for thick plate with $R/h = 2$

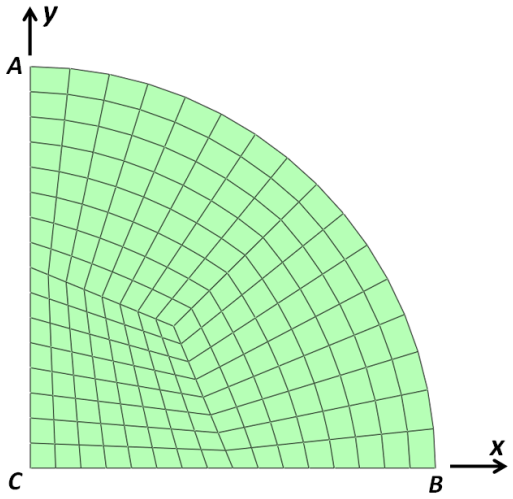

Figure 5-13 Simply supported circular plate under uniform load – the 192 finite elements mesh

5.2.3.3. Variability of displacement

The CGSM results are compared to reference solutions obtained by direct Monte Carlo simulations, for the thin plate and the thick one. The random parameter is *E* and several correlation lengths are considered. For each correlation length, the mean value, standard deviation and coefficient of variation of displacement at point

C are reported in Tables 5-14 and 5-16. Errors are given in Tables 5-15 and 5-17. The CGSM provides very accurate results when the correlation length is bigger than *L*. Nevertheless the errors slightly increase when the correlation length is smaller than *L*. Anyway, even in the extreme case $\lambda = 0.01L$, the errors remain acceptable. The comparison between the results obtained for the thin plate and the thick plate, show that the coefficients of variation are close, as shown in Tables 5-14, 5-16, and Figure 5-15.

λ	0.01*L*		0.1 *L*		*L*		10 *L*		100 *L*	
	CGSM	dMC	CGSM	dMC	CGSM	dMC	CGSM	dMC	CGSM	dMC
$m(U)$	4047	4004	4047	4007	4045	4014	4044	4019	4046	4023
$\sigma(U)$	370.1	343.1	1036	986.5	3220	3197	3977	3949	4113	4089
c.o.v.(U) (%)	0.91	0.86	2.56	2.46	7.96	7.96	9.83	9.82	10.2	10.2

Table 5-14 Simply supported circular plate under uniform load (*E* random, *c.o.v.*$(E) = 10\%$) – variability of displacements at point *C* for thin plate with $R/h = 50$

λ	0.01*L*	0.1 *L*	*L*	10 *L*	100 *L*
Error on $m(U)$ (%)	1.1	1.0	0.7	0.6	0.6
Error on $\sigma(U)$ (%)	7.8	5.1	0.7	0.7	0.6
Error on *c.o.v.*(U) (%)	6.7	4.0	0.3	0.1	0.0

Table 5-15 Simply supported circular plate under uniform load (*E* random, *c.o.v.*$(E) = 10\%$) – errors on the statistical results of displacement at point *C* for thin plate with $R/h = 50$

λ	0.01*L*		0.1 *L*		*L*		10 *L*		100 *L*	
	CGSM	dMC	CGSM	dMC	CGSM	dMC	CGSM	dMC	CGSM	dMC
$m(U)$	3.286	3.278	3.286	3.281	3.287	3.287	3.283	3.291	3.285	3.294
$\sigma(U)$ (x10^{-2})	2.767	2.613	7.795	7.551	25.69	25.55	32.22	32.27	33.39	33.47
c.o.v.(U) (%)	0.84	0.80	2.37	2.30	7.82	7.77	9.81	9.81	10.16	10.16

Table 5-16 Simply supported circular plate under uniform load (*E* random, *c.o.v.*$(E) = 10\%$) – variability of displacements at point *C* for thick plate with $R/h = 2$

λ	0.01*L*	0.1 *L*	*L*	10 *L*	100 *L*
Error on $m(U)$ (%)	0.3	0.2	0.1	0.2	0.2
Error on $\sigma(U)$ (%)	5.9	3.2	0.5	0.2	0.3
Error on *c.o.v.*(U) (%)	5.6	3.1	0.6	0.1	0.0

Table 5-17 Simply supported circular plate under uniform load (*E* random, *c.o.v.*(E) = 10%) – errors on the statistical results of displacement at point *C* for thick plate with $R/h = 2$

Figure 5-14 shows the evolution of the coefficient of variation of displacement at point *C*. The variability of the displacement increases non-linearly with the correlation length. As in the previous example, when the correlation length is smaller than 0. 1*L*, the variability of the displacement is very small. This is again due to a compensation phenomenon.

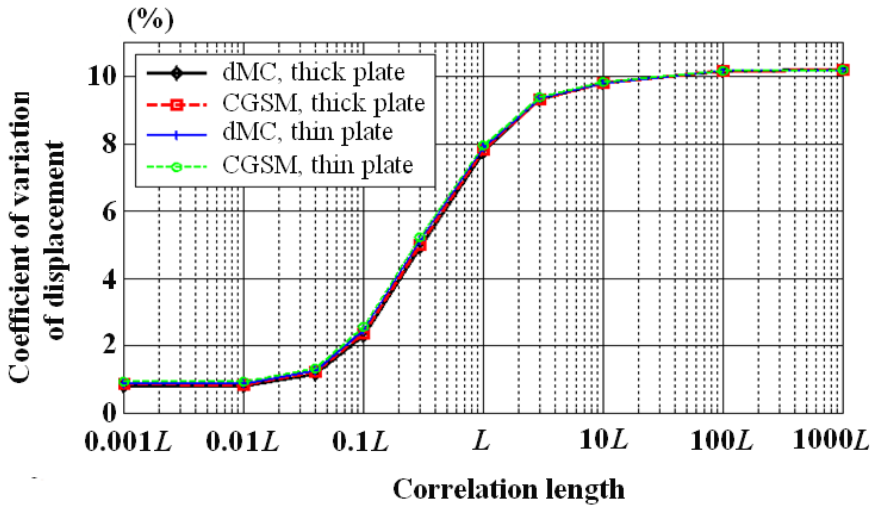

Figure 5-14 Simply supported circular plate under uniform load (*E* random, *c.o.v.*(E) = 10%) – evolution of the variability level of displacement at point *C* versus the correlation length

Figures 5-15 and 5-16 show the probability density function of the displacement at point *C*. Again, the distribution obtained with the CGSM is close to the reference distribution obtained with the direct Monte Carlo simulation. As already justified, the distribution is not exactly Gaussian.

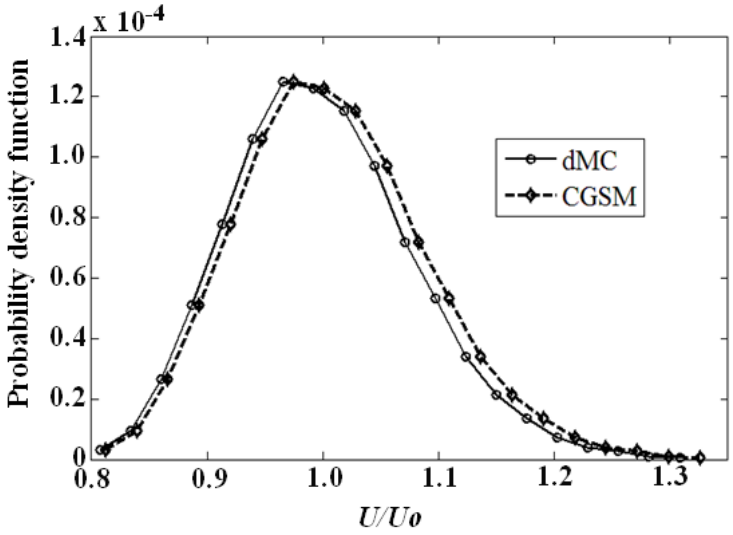

Figure 5-15 Simply supported circular plate under uniform load (*E* random, *c.o.v.*(*E*) = 10%, λ = *L*) – distribution of the displacement at point *C* for thin plate with *R*/*h* = 50

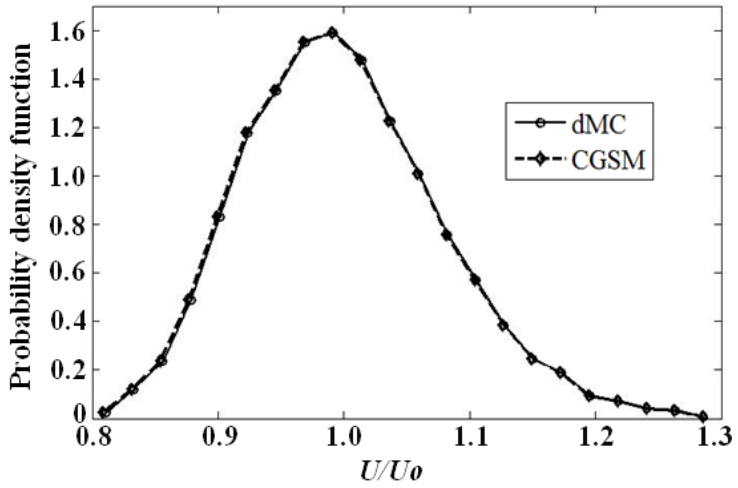

Figure 5-16 Simply supported circular plate under uniform load (*E* random, *c.o.v.*(*E*) = 10%, λ = *L*) – distribution of the displacement at point *C* for thick plate with *R*/*h* = 2

5.2.4. Morley's plate under uniform load

5.2.4.1. Presentation of the example

Morley's acute skew plate (Figure 5-17) is simply supported on all edges and subjected to a uniformly distributed load $f_z = -1$ (data are provided in dimensionless form). The input data are as follows: $L = 100$, $\theta = 30^o$, thickness $h = 0.1$ and Poisson's ratio ν is 0.3. The random parameter is the elasticity modulus, represented by an isotropic random field. The mean elasticity modulus is $m(E) = 10.92$. The coefficient of variation is 10% and different correlation lengths, $\lambda = 0.001L$ to $1000L$, are considered. The isotropic exponential correlation function (equation 3-26) is used. The direct Monte Carlo simulations and the CGSM + Monte Carlo simulations are made with 10,000 runs. The variability of the vertical displacement of the center point C is calculated.

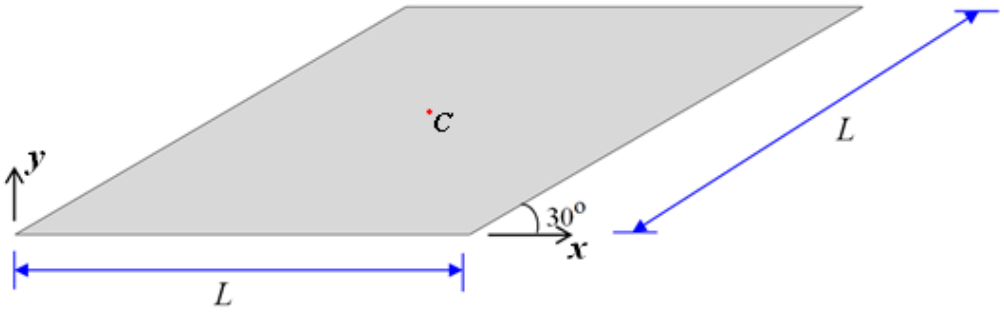

Figure 5-17 Simply supported Morley's plate under uniform load in the z direction

5.2.4.2. Finite element mesh

As in previous examples, we first search for the optimal nominal mesh and then we verify that this mesh is adapted to calculate the variability. Table 5-18 shows the results of a convergence study of nominal displacement at point C performed with the CGSM formulation in the nominal configuration (equation 5-27). For this example the exact solution, considered as a reference, is available [115]. The S3 triangular shell element of Abaqus is used. Table 5-18 shows that for this example a mesh with a uniform size is not efficient. Indeed the error is

significant even for the very fine 128x128 mesh containing 16384 elements. The adaptive mesh with 1263 elements (Figure 5-18), leading to an error of 0.1%, is satisfactory for the nominal calculation. Consequently this mesh is exploited to calculate the variability.

Node	Mesh: 128x128		Adaptive mesh (1263 elements)		Exact
	Displacement	Error (%)	Displacement	Error (%)	Displacement
C	0.4135	1.4	0.4085	0.1	0.408

Table 5-18 Simply supported Morley's plate under uniform load – convergence study of displacement at node *C* in nominal configuration

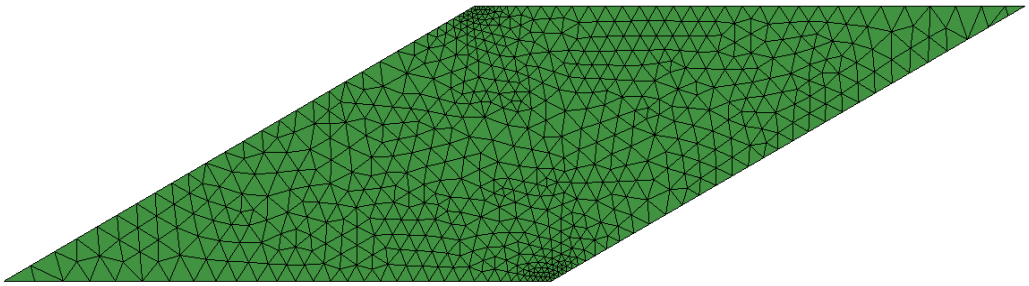

Figure 5-18 Simply supported Morley's plate under uniform load – the adaptive mesh (1263 S3 shell elements of Abaqus)

5.2.4.3. Variability of displacement

The CGSM results are compared to reference solutions obtained by direct Monte Carlo simulations. The random parameter is *E* and several correlation lengths are considered. For each correlation length, the mean value, standard deviation and coefficient of variation of displacement at point *C* are reported in Table 5-19. Errors are given in Table 5-20. The CGSM provides very accurate results for the whole correlation length range. Nevertheless the errors slightly increase when the correlation length is smaller than *L*.

λ	0.01L		0.1 L		L		10 L		100 L	
	CGSM	dMC	CGSM	dMC	CGSM	dMC	CGSM	dMC	CGSM	dMC
$m(U)$	0.4126	0.4092	0.413	0.411	0.413	0.412	0.413	0.413	0.413	0.413
$\sigma(U)$ (x10^{-2})	0.2526	0.2441	1.438	1.409	3.608	3.591	4.158	4.156	4.225	4.226
c.o.v.(U) (%)	0.61	0.60	3.48	3.43	0.87	0.87	10.08	10.08	10.24	10.24

Table 5-19 Simply supported Morley's plate under uniform load (E random, *c.o.v.*(E) = 10%) – variability of displacement at point C

λ	0.01L	0.1 L	L	10 L	100 L
Error on $m(U)$ (%)	0.8	0.6	0.1	0.6	0.0
Error on $\sigma(U)$ (%)	3.5	2.0	0.5	0.7	0.0
Error on *c.o.v.*(U) (%)	2.6	1.4	0.4	0.1	0.0

Table 5-20 Simply supported Morley's plate under uniform load (E random, *c.o.v.*(E) = 10%) – errors on the statistical results of displacement at point C

Figure 5-19 shows the evolution of the coefficient of variation of displacement at point C. The variability of the displacement increases non-linearly with the correlation length. As in the previous example, when the correlation length is smaller than 0.01L, the variability of the displacement is very small. This is again due to a compensation phenomenon.

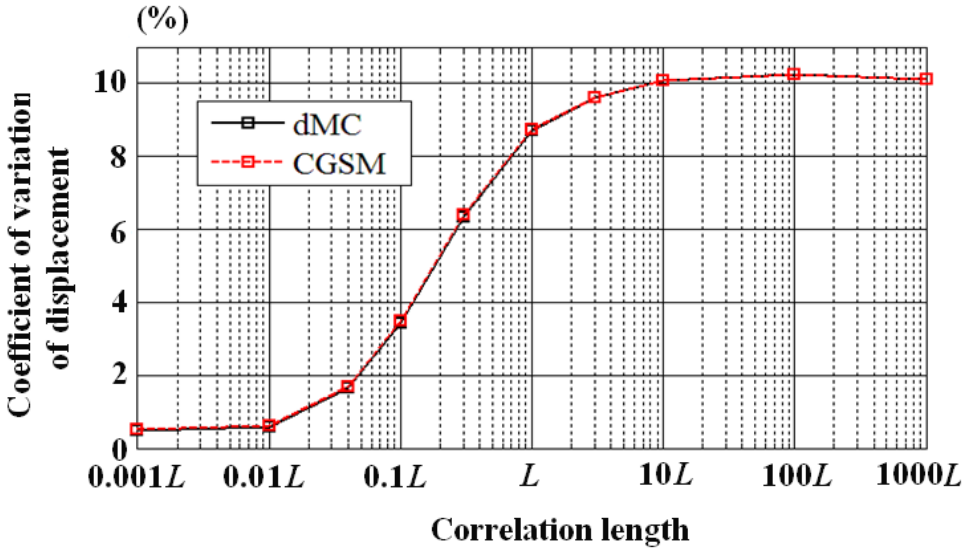

Figure 5-19 Simply supported Morley's plate under uniform load (E random, *c.o.v.*(E) = 10%) – variability of displacement at point C

Figure 5-20 shows the probability density function of the displacement at point *C*. Again, the distribution obtained with the CGSM is close to the reference distribution obtained with the direct Monte Carlo simulation. As already justified, the distribution is not exactly Gaussian.

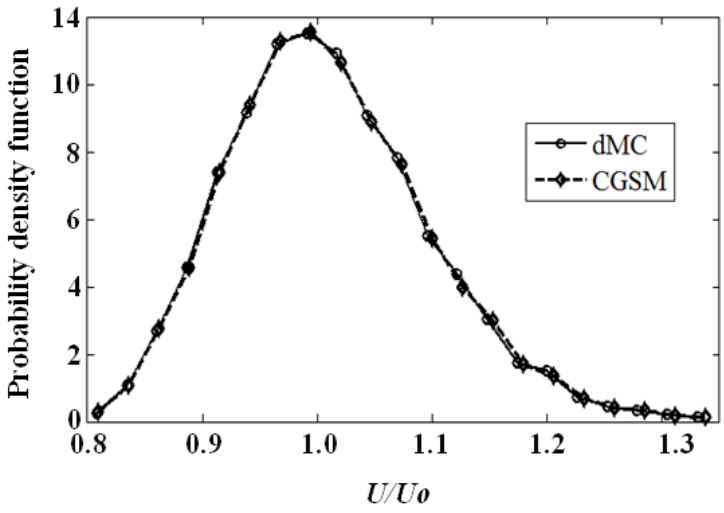

Figure 5-20 Simply supported Morley's plate under uniform load (*E* random, *c.o.v.*(*E*) = 10%, λ = *L*) – distribution of the displacement at point *C*

Chapter 6
Formulation and Applications of CGSM for Shells

6.1. Formulation of the CGSM for shells

As in previous chapters, the CGSM is developed here for three-node triangles (T3) and four-node quadrilaterals (Q4), whatever the formulation of these elements. Two formulations are described, the first one for homogeneous isotropic shells, the second one for multilayered composite shells.

6.1.1. Formulation of the CGSM for homogeneous isotropic shells

The objective is to describe the calculation of the variability of displacement. The overall strain energy for isotropic shells is obtained by combining membrane, bending and transverse shear strain energies.

$$\pi_{int} = \pi_{int}^{m} + \pi_{int}^{b} + \pi_{int}^{tsh} \qquad \textbf{6-1}$$

These contributions to the strain energy can be written as:

membrane $$\pi_{int}^{m} = \frac{1}{2}\int_{V} \langle e \rangle \, [H] \, \{e\} \, dV = \frac{1}{2}\int_{A} \langle e \rangle \, [H] \, \{e\} \, dA$$

bending $$\pi_{int}^{b} = \frac{1}{2}\int_{V} z^2 \langle \chi \rangle \, [H] \, \{\chi\} \, dV = \frac{1}{2}\int_{A} \frac{h^3}{12} \langle \chi \rangle \, [H] \, \{\chi\} \, dA \qquad \textbf{6-2}$$

transverse shear $$\pi_{int}^{tsh} = \frac{1}{2}\int_{V} \langle \gamma \rangle \, [H_s] \, \{\gamma\} \, dV = \frac{1}{2}\int_{A} h \langle \gamma \rangle \, [H_s] \, \{\gamma\} \, dA$$

The relations between generalized strains and generalized stresses are:

$$\begin{aligned} \{e\} &= \frac{1}{h}[H]^{-1}\{N\} \\ \{\chi\} &= \frac{12}{h^3}[H]^{-1}\{M\} \\ \{\gamma\} &= \frac{1}{h}[H_s]^{-1}\{T\} \end{aligned} \qquad \textbf{6-3}$$

Considering equations 6-2 and 6-3, equation 6-1 becomes:

$$\begin{aligned} \pi_{int} = \frac{1}{2}\int_A \frac{1}{h}\langle N\rangle[H]^{-1}\{N\}\,dA + \frac{1}{2}\int_A \frac{12}{h^3}\langle M\rangle[H]^{-1}\{M\}\,dA \\ + \frac{1}{2}\int_A \frac{1}{h}\langle T\rangle[H_s]^{-1}\{T\}\,dA \end{aligned} \qquad \textbf{6-4}$$

with $\langle N\rangle = \langle N_x \;\; N_y \;\; N_{xy}\rangle$ the axial forces, $\langle M\rangle = \langle M_x \;\; M_y \;\; M_{xy}\rangle$ the moments, $\langle T\rangle = \langle T_x \quad T_y\rangle$ the transverse shear forces, $[H]$ the plane stress elasticity matrix defined in equation 4-2, $[H_s]$ the transverse shear elasticity matrix defined in equation 4-14, h the thickness of the structure, and A the area of the structure.

Considering that the domain is spatially discretized and the mesh contains *n* finite elements, taking into account equations 4-7, 5-6, and 5-20 into equation 6-4, gives:

$$\begin{aligned} \pi_{int} = \frac{1}{2}\sum_{i=1}^{n}\int_{A_i}\Bigg(&\frac{1}{E_i h_i}\left({N_{x_i}}^2 - 2v_i N_{x_i}N_{y_i} + {N_{y_i}}^2 + 2(1+v_i){N_{xy_i}}^2\right) \\ &+ \frac{12}{E_i {h_i}^3}\left({M_{x_i}}^2 - 2v_i M_{x_i}M_{y_i} + {M_{y_i}}^2 + 2(1+v_i){M_{xy_i}}^2\right) \\ &+ \frac{2(1+v_i)}{E_i\, k_s\, h_i}\left({T_{x_i}}^2 + {T_{y_i}}^2\right)\Bigg)\,dA \end{aligned} \qquad \textbf{6-5}$$

where *i* is the element number; the subscripts x_i, y_i are the local directions; A_i is the area; E_i is the elasticity modulus; k_s is the transverse shear correction factor; h_i is the thickness and v_i is the Poisson's ratio.

In order to apply the Castigliano's theorem for calculating the displacement U at a point P in a given direction, the forces in each element are decomposed into two contributions:

$$
\begin{aligned}
&\text{for the axial forces} && N_{x_i} = N_{x_i}' + FN_{x_i}^{"} \\
& && N_{y_i} = N_{y_i}' + FN_{y_i}^{"} \\
& && N_{xy_i} = N_{xy_i}' + FN_{xy_i}^{"} \\
&\text{for the moments} && M_{x_i} = M_{x_i}' + FM_{x_i}^{"} \\
& && M_{y_i} = M_{y_i}' + FM_{y_i}^{"} \\
& && M_{xy_i} = M_{xy_i}' + FM_{xy_i}^{"} \\
&\text{for the transverse shear forces} && T_{x_i} = T_{x_i}' + FT_{x_i}^{"} \\
& && T_{y_i} = T_{y_i}' + FT_{y_i}^{"}
\end{aligned}
\qquad \textbf{6-6}
$$

where i is the element number; F is the load applied at point P in the direction of interest (F is a force or a moment if the variability of a displacement or a rotation must be assessed respectively); the subscripts x_i, y_i are the local directions; N', M', T' are the generalized stresses due to loads on the whole structure except at point P in the direction of interest; $N^{"}$, $M^{"}$, $T^{"}$ are the generalized stresses due to a unitary load applied at point P in the direction of interest.

Substituting equation 6-6 into equation 6-5 gives:

$$
\begin{aligned}
\pi_{int} = \frac{1}{2}\sum_{i=1}^{n}\int_{A_i}\Bigg(
&\frac{1}{E_i h_i}\Big(\left(N_{x_i}' + FN_{x_i}^{"}\right)^2 \\
&- 2v_i\left(N_{x_i}'N_{y_i}' + FN_{x_i}'N_{y_i}^{"} + FN_{x_i}^{"}N_{y_i}' + F^2N_{x_i}^{"}N_{y_i}^{"}\right) \\
&+ \left(N_{y_i}' + FN_{y_i}^{"}\right)^2 + 2(1+v_i)\left(N_{xy_i}' + FN_{xy_i}^{"}\right)^2\Big) \\
&+ \frac{12}{E_i {h_i}^3}\Big(\left(M_{x_i}' + FM_{x_i}^{"}\right)^2 \\
&- 2v_i\left(M_{x_i}'M_{y_i}' + FM_{x_i}'M_{y_i}^{"} + FM_{x_i}^{"}M_{y_i}' + F^2M_{x_i}^{"}M_{y_i}^{"}\right) \\
&+ \left(M_{y_i}' + FM_{y_i}^{"}\right)^2 + 2(1+v_i)\left(M_{xy_i}' + FM_{xy_i}^{"}\right)^2\Big) \\
&+ \frac{2(1+v_i)}{E_i\, k_s\, h_i}\left(\left(T_{x_i}' + FT_{x_i}^{"}\right)^2 + \left(T_{y_i}' + FT_{y_i}^{"}\right)^2\right)\Bigg)dA
\end{aligned}
\qquad \textbf{6-7}
$$

As for the membrane plate and the bending plate cases, our objective is to consider simple interpolations of generalized stresses; these interpolations are

independent of the initial formulation of the element. For T3 and Q4 elements considered here, all the generalized stresses are assumed to be constant over one element. Equation 6-7 becomes:

$$\begin{aligned}\pi_{int} = \frac{1}{2}\sum_{i=1}^{n}\frac{A_i}{E_i h_i}\Big(&\left(N_{x_i}' + FN_{x_i}''\right)^2 \\ &- 2v_i\left(N_{x_i}'N_{y_i}' + FN_{x_i}'N_{y_i}'' + FN_{x_i}''N_{y_i}' + F^2N_{x_i}''N_{y_i}''\right) \\ &+ \left(N_{y_i}' + FN_{y_i}''\right)^2 + 2(1+v_i)\left(N_{xy_i}' + FN_{xy_i}''\right)^2\Big) \\ &+ \frac{12}{E_i {h_i}^3}\Big(\left(M_{x_i}' + FM_{x_i}''\right)^2 \\ &- 2v_i\left(M_{x_i}'M_{y_i}' + FM_{x_i}'M_{y_i}'' + FM_{x_i}''M_{y_i}' + F^2M_{x_i}''M_{y_i}''\right) \\ &+ \left(M_{y_i}' + FM_{y_i}''\right)^2 + 2(1+v_i)\left(M_{xy_i}' + FM_{xy_i}''\right)^2\Big) \\ &+ \frac{2(1+v_i)}{E_i\, k_s\, h_i}\left(\left(T_{x_i}' + FT_{x_i}''\right)^2 + \left(T_{y_i}' + FT_{y_i}''\right)^2\right)\end{aligned} \qquad \textbf{6-8}$$

To obtain the displacement at a point *P* in a given direction, the Castigliano's theorem is applied:

$$U = \frac{\pi_{int}}{\partial F} \qquad \textbf{6-9}$$

Finally, for the homogeneous isotropic shells case, the displacement is:

$$\begin{aligned}U = \sum_{i=1}^{n}\frac{A_i}{E_i h_i}\Bigg(&\begin{pmatrix}N_{x_i}''\left(N_{x_i}' + FN_{x_i}''\right) + N_{y_i}''\left(N_{y_i}' + FN_{y_i}''\right) + 2N_{xy_i}''\left(N_{xy_i}' + FN_{xy_i}''\right)\\ +v_i\left(2N_{xy_i}''\left(N_{xy_i}' + FN_{xy_i}''\right) - \left(N_{x_i}'N_{y_i}'' + N_{x_i}''N_{y_i}' + 2FN_{x_i}''N_{y_i}''\right)\right)\end{pmatrix} \\ &+ \frac{12}{{h_i}^2}\begin{pmatrix}M_{x_i}''\left(M_{x_i}' + FM_{x_i}''\right) + M_{y_i}''\left(M_{y_i}' + FM_{y_i}''\right) + 2M_{xy_i}''\left(M_{xy_i}' + FM_{xy_i}''\right)\\ +v_i\left(2M_{xy_i}''\left(M_{xy_i}' + FM_{xy_i}''\right) - \left(M_{x_i}'M_{y_i}'' + M_{x_i}''M_{y_i}' + 2FM_{x_i}''M_{y_i}''\right)\right)\end{pmatrix} \\ &+ \frac{2(1+v_i)}{k_s}\left(T_{x_i}''\left(T_{x_i}' + FT_{x_i}''\right) + T_{y_i}''\left(T_{y_i}' + FT_{y_i}''\right)\right)\Bigg)\end{aligned} \qquad \textbf{6-10}$$

The expression of *U* given in equation 6-10 is used for each trial of the CGSM+Monte Carlo simulation, to calculate the displacement variability at a point of a homogeneous isotropic shell.

6.1.2. Formulation of the CGSM for multilayered shells

The objective is to describe the calculation of the variability of displacement. The strain energy for multilayered composite shells can be written as:

$$\pi_{int} = \frac{1}{2}\int_A \langle e \;\; \chi \;\; \gamma \rangle \begin{bmatrix} A & B & 0 \\ B & D & 0 \\ 0 & 0 & F \end{bmatrix} \begin{Bmatrix} e \\ \chi \\ \gamma \end{Bmatrix} dA \qquad \textbf{6-11}$$

with $\langle e \rangle = \langle e_x \;\; e_y \;\; e_{xy} \rangle$ the in-plane strains, $\langle \chi \rangle = \langle \chi_x \;\; \chi_y \;\; \chi_{xy} \rangle$ the curvatures; $\langle \gamma \rangle = \langle \gamma_{xz} \;\; \gamma_{yz} \rangle$ the out-of-plane shear strains; A, B, D and F the generalized membrane stiffness matrix, membrane-bending coupling stiffness matrix, bending stiffness matrix and transverse shear stiffness matrix respectively.

As introduced in chapter 3 (see equation 3-11), the relationship between the strains and the generalized stresses is:

$$\begin{Bmatrix} e_x \\ e_y \\ e_{xy} \\ \hline \chi_x \\ \chi_y \\ \chi_{xy} \\ \hline \gamma_{xz} \\ \gamma_{yz} \end{Bmatrix} = \left[\begin{array}{ccc|ccc|cc} A_{11} & A_{12} & A_{13} & B_{11} & B_{21} & B_{31} & 0 & 0 \\ A_{12} & A_{22} & A_{23} & B_{12} & B_{22} & B_{32} & 0 & 0 \\ A_{13} & A_{23} & A_{33} & B_{13} & B_{23} & B_{33} & 0 & 0 \\ \hline B_{11} & B_{12} & B_{13} & D_{11} & D_{12} & D_{13} & 0 & 0 \\ B_{21} & B_{22} & B_{23} & D_{12} & D_{22} & D_{23} & 0 & 0 \\ B_{31} & B_{32} & B_{33} & D_{13} & D_{23} & D_{33} & 0 & 0 \\ \hline 0 & 0 & 0 & 0 & 0 & 0 & F_{11} & F_{12} \\ 0 & 0 & 0 & 0 & 0 & 0 & F_{12} & F_{22} \end{array}\right]^{-1} \begin{Bmatrix} N_x \\ N_y \\ N_{xy} \\ \hline M_x \\ M_y \\ M_{xy} \\ \hline T_x \\ T_y \end{Bmatrix} \qquad \textbf{6-12}$$

where $\langle N_x \;\; N_y \;\; N_{xy} \rangle$ are the axial forces, $\langle M_x \;\; M_y \;\; M_{xy} \rangle$ are the bending moments, $\langle T_x \quad T_y \rangle$ are the shear forces.

Equation 6-12 can be written in the following synthetic form:

$$\begin{Bmatrix} e \\ \chi \\ \gamma \end{Bmatrix} = \begin{bmatrix} AI & BI & 0 \\ BI & DI & 0 \\ 0 & 0 & FI \end{bmatrix} \begin{Bmatrix} N \\ M \\ T \end{Bmatrix} \qquad \textbf{6-13}$$

Reporting equation 6-13 into equation 6-11, one obtains:

$$\pi_{int} = \frac{1}{2}\int_A \langle N \;\; M \;\; T \rangle \begin{bmatrix} AI & BI & 0 \\ BI & DI & 0 \\ 0 & 0 & FI \end{bmatrix} \begin{Bmatrix} N \\ M \\ T \end{Bmatrix} dA \qquad \textbf{6-14}$$

The strain energy may be decomposed into several contributions:

membrane $$\pi_{int}^{m} = \frac{1}{2}\int_A \langle N\rangle\,[AI]\,\{N\}\,dA \qquad \textbf{6-15}$$

membrane-bending coupling $$\pi_{int}^{b} = \int_A \langle M\rangle\,[BI]\,\{N\}\,dA \qquad \textbf{6-16}$$

bending $$\pi_{int}^{mb} = \frac{1}{2}\int_A \langle M\rangle\,[DI]\,\{M\}\,dA \qquad \textbf{6-17}$$

transverse shear $$\pi_{int}^{tsh} = \frac{1}{2}\int_A \langle T\rangle\,[FI]\,\{T\}\,dA \qquad \textbf{6-18}$$

Finally the strain energy can be written:

$$\pi_{int} = \frac{1}{2}\int_A \langle N\rangle\,[AI]\,\{N\}\,dA + \int_A \langle M\rangle\,[BI]\,\{N\}\,dA + \frac{1}{2}\int_A \langle M\rangle\,[DI]\,\{M\}\,dA + \frac{1}{2}\int_A \langle T\rangle\,[FI]\,\{T\}\,dA \qquad \textbf{6-19}$$

Considering that the domain is spatially discretized and the mesh contains n finite elements, equation 6-19 gives:

$$\pi_{int} = \frac{1}{2}\sum_{i=1}^{n}\int_A \left(\langle N\rangle[AI]\{N\} + 2\langle N\rangle[BI]\{M\} + \langle M\rangle[DI]\{M\} + \langle T\rangle[FI]\{T\}\right)\,dA \qquad \textbf{6-20}$$

In order to apply the Castigliano's theorem for calculating the displacement U of a point P in a given direction, the generalized stresses in each element are decomposed into two contributions, as described in equations 6-6. By exploiting equation 6-6, equation 6-20 becomes:

$$\pi_{int} = \frac{1}{2}\sum_{i=1}^{n}\int_{A}\left(\begin{Bmatrix} N_{x_i}' + FN_{x_i}'' \\ N_{y_i}' + FN_{y_i}'' \\ N_{xy_i}' + FN_{xy_i}'' \end{Bmatrix}^T \begin{bmatrix} AI_{11} & AI_{12} & AI_{13} \\ AI_{12} & AI_{22} & AI_{23} \\ AI_{13} & AI_{23} & AI_{33} \end{bmatrix} \begin{Bmatrix} N_{x_i}' + FN_{x_i}'' \\ N_{y_i}' + FN_{y_i}'' \\ N_{xy_i}' + FN_{xy_i}'' \end{Bmatrix}\right.$$
$$+ 2\begin{Bmatrix} N_{x_i}' + FN_{x_i}'' \\ N_{y_i}' + FN_{y_i}'' \\ N_{xy_i}' + FN_{xy_i}'' \end{Bmatrix}^T \begin{bmatrix} BI_{11} & BI_{21} & BI_{31} \\ BI_{12} & BI_{22} & BI_{32} \\ BI_{13} & BI_{23} & BI_{33} \end{bmatrix} \begin{Bmatrix} M_{x_i}' + FM_{x_i}'' \\ M_{y_i}' + FM_{y_i}'' \\ M_{xy_i}' + FM_{xy_i}'' \end{Bmatrix} \quad \textbf{6-21}$$
$$+ \begin{Bmatrix} M_{x_i}' + FM_{x_i}'' \\ M_{y_i}' + FM_{y_i}'' \\ M_{xy_i}' + FM_{xy_i}'' \end{Bmatrix}^T \begin{bmatrix} DI_{11} & DI_{12} & DI_{13} \\ DI_{12} & DI_{22} & DI_{23} \\ DI_{13} & DI_{23} & DI_{33} \end{bmatrix} \begin{Bmatrix} M_{x_i}' + FM_{x_i}'' \\ M_{y_i}' + FM_{y_i}'' \\ M_{xy_i}' + FM_{xy_i}'' \end{Bmatrix}$$
$$\left. + \begin{Bmatrix} T_{x_i}' + FT_{x_i}'' \\ T_{y_i}' + FT_{y_i}'' \end{Bmatrix}^T \begin{bmatrix} FI_{11} & FI_{12} \\ FI_{12} & FI_{22} \end{bmatrix} \begin{Bmatrix} T_{x_i}' + FT_{x_i}'' \\ T_{y_i}' + FT_{y_i}'' \end{Bmatrix}\right) dA$$

As for the case of the homogeneous isotropic shells, our objective is to consider simple interpolations of generalized stresses; these interpolations are independent of the initial formulation of the element. For T3 and Q4 elements considered here, the generalized stresses are assumed to be constant over one element. The values calculated at the center of each element are considered. Equation 6-21 becomes:

$$\pi_{int} = \sum_{i=1}^{n}\frac{A_i}{2}\left(\begin{Bmatrix} N_{x_i}' + FN_{x_i}'' \\ N_{y_i}' + FN_{y_i}'' \\ N_{xy_i}' + FN_{xy_i}'' \end{Bmatrix}^T \begin{bmatrix} AI_{11} & AI_{12} & AI_{13} \\ AI_{12} & AI_{22} & AI_{23} \\ AI_{13} & AI_{23} & AI_{33} \end{bmatrix} \begin{Bmatrix} N_{x_i}' + FN_{x_i}'' \\ N_{y_i}' + FN_{y_i}'' \\ N_{xy_i}' + FN_{xy_i}'' \end{Bmatrix}\right.$$
$$+ 2\begin{Bmatrix} N_{x_i}' + FN_{x_i}'' \\ N_{y_i}' + FN_{y_i}'' \\ N_{xy_i}' + FN_{xy_i}'' \end{Bmatrix}^T \begin{bmatrix} BI_{11} & BI_{21} & BI_{31} \\ BI_{12} & BI_{22} & BI_{32} \\ BI_{13} & BI_{23} & BI_{33} \end{bmatrix} \begin{Bmatrix} M_{x_i}' + FM_{x_i}'' \\ M_{y_i}' + FM_{y_i}'' \\ M_{xy_i}' + FM_{xy_i}'' \end{Bmatrix} \quad \textbf{6-22}$$
$$+ \begin{Bmatrix} M_{x_i}' + FM_{x_i}'' \\ M_{y_i}' + FM_{y_i}'' \\ M_{xy_i}' + FM_{xy_i}'' \end{Bmatrix}^T \begin{bmatrix} DI_{11} & DI_{12} & DI_{13} \\ DI_{12} & DI_{22} & DI_{23} \\ DI_{13} & DI_{23} & DI_{33} \end{bmatrix} \begin{Bmatrix} M_{x_i}' + FM_{x_i}'' \\ M_{y_i}' + FM_{y_i}'' \\ M_{xy_i}' + FM_{xy_i}'' \end{Bmatrix}$$
$$\left. + \begin{Bmatrix} T_{x_i}' + FT_{x_i}'' \\ T_{y_i}' + FT_{y_i}'' \end{Bmatrix}^T \begin{bmatrix} FI_{11} & FI_{12} \\ FI_{12} & FI_{22} \end{bmatrix} \begin{Bmatrix} T_{x_i}' + FT_{x_i}'' \\ T_{y_i}' + FT_{y_i}'' \end{Bmatrix}\right)$$

To obtain the displacement at a point P in a given direction, the Castigliano's theorem is applied:

$$U = \frac{\pi_{int}}{\partial F} \quad \textbf{6-23}$$

The displacement contains the following distributions:

$$U = \frac{\pi_{int}^{m}}{\partial F} + \frac{\pi_{int}^{mb}}{\partial F} + \frac{\pi_{int}^{b}}{\partial F} + \frac{\pi_{int}^{tsh}}{\partial F} \quad \textbf{6-24}$$

or

$$U = U_m + U_{mb} + U_b + U_{tsh} \quad \textbf{6-25}$$

where U_m is the displacement due to the axial forces, U_{mb} is the displacement due to coupling between the membrane and bending effects, U_b is the displacement due to the bending moments, and U_{tsh} is the displacement due to the transverse shear forces.

Equation 6-22 is used to calculate the different terms of the displacement U expressed in equation 6-24. Displacement due to the axial forces is:

$$U_m = \sum_{i}^{n} \frac{A_i}{2} \begin{pmatrix} AI_{11}N_i^1 + AI_{22}N_i^2 + AI_{33}N_i^3 \\ +2\left(AI_{12}N_i^4 + AI_{13}N_i^5 + AI_{23}N_i^6\right) \end{pmatrix} \quad \textbf{6-26}$$

where:

$$\begin{aligned} N_i^1 &= 2N_{xi}^{"}\left(N_{xi}' + FN_{xi}^{"}\right) \\ N_i^2 &= 2N_{yi}^{"}\left(N_{yi}' + FN_{yi}^{"}\right) \\ N_i^3 &= 2N_{xyi}^{"}\left(N_{xyi}' + FN_{xyi}^{"}\right) \\ N_i^4 &= N_{xi}'N_{yi}^{"} + N_{yi}'N_{xi}^{"} + 2FN_{xi}^{"}N_{yi}^{"} \\ N_i^5 &= N_{xi}'N_{xyi}^{"} + N_{xyi}'N_{xi}^{"} + 2FN_{xi}^{"}N_{xyi}^{"} \\ N_i^6 &= N_{yi}'N_{xyi}^{"} + N_{xyi}'N_{yi}^{"} + 2FN_{yi}^{"}N_{xyi}^{"} \end{aligned} \quad \textbf{6-27}$$

Displacement due to coupling between the membrane and bending effects is:

$$U_{mb} = \sum_{i}^{n} A_i \begin{pmatrix} BI_{11}MN_i^1 + BI_{22}MN_i^2 + BI_{33}MN_i^3 \\ +BI_{12}MN_i^4 + BI_{13}MN_i^5 + BI_{23}MN_i^6 \\ +BI_{21}MN_i^7 + BI_{31}MN_i^8 + BI_{32}MN_i^9 \end{pmatrix} \quad \textbf{6-28}$$

where

$$\begin{aligned} MN_i^1 &= N'_{xi}M^{"}_{xi} + N^{"}_{xi}M'_{xi} + 2FN^{"}_{xi}M^{"}_{xi} \\ MN_i^2 &= N'_{yi}M^{"}_{yi} + N^{"}_{yi}M'_{yi} + 2FN^{"}_{yi}M^{"}_{yi} \\ MN_i^3 &= N'_{xyi}M^{"}_{xyi} + N^{"}_{xyi}M'_{xyi} + 2FN^{"}_{xyi}M^{"}_{xyi} \\ MN_i^4 &= N'_{yi}M^{"}_{xi} + N^{"}_{yi}M'_{xi} + 2FN^{"}_{yi}M^{"}_{xi} \\ MN_i^5 &= N'_{xyi}M^{"}_{xi} + N^{"}_{xyi}M'_{xi} + 2FN^{"}_{xyi}M^{"}_{xi} \\ MN_i^6 &= N'_{xyi}M^{"}_{yi} + N^{"}_{xyi}M'_{yi} + 2FN^{"}_{xyi}M^{"}_{yi} \\ MN_i^7 &= N'_{xi}M^{"}_{yi} + N^{"}_{xi}M'_{yi} + 2FN^{"}_{xi}M^{"}_{yi} \\ MN_i^8 &= N'_{xi}M^{"}_{xyi} + N^{"}_{xi}M'_{xyi} + 2FN^{"}_{xi}M^{"}_{xyi} \\ MN_i^9 &= N'_{yi}M^{"}_{xyi} + N^{"}_{yi}M'_{xyi} + 2FN^{"}_{yi}M^{"}_{xyi} \end{aligned} \quad \textbf{6-29}$$

Displacement due to the bending moments is:

$$U_b = \sum_{i}^{n} \frac{A_i}{2} \begin{pmatrix} DI_{11}M_i^1 + DI_{22}M_i^2 + DI_{33}M_i^3 \\ +2\left(DI_{12}M_i^4 + DI_{13}M_i^5 + DI_{23}M_i^6\right) \end{pmatrix} \quad \textbf{6-30}$$

where

$$\begin{aligned} M_i^1 &= 2M^{"}_{xi}\left(M'_{xi} + FM^{"}_{xi}\right) \\ M_i^2 &= 2M^{"}_{yi}\left(M'_{yi} + FM^{"}_{yi}\right) \\ M_i^3 &= 2M^{"}_{xyi}\left(M'_{xyi} + FM^{"}_{xyi}\right) \\ M_i^4 &= M'_{xi}M^{"}_{yi} + M'_{yi}M^{"}_{xi} + 2FM^{"}_{xi}M^{"}_{yi} \\ M_i^5 &= M'_{xi}M^{"}_{xyi} + M'_{xyi}M^{"}_{xi} + 2FM^{"}_{xi}M^{"}_{xyi} \\ M_i^6 &= M'_{yi}M^{"}_{xyi} + M'_{xyi}M^{"}_{yi} + 2FM^{"}_{yi}M^{"}_{xyi} \end{aligned} \quad \textbf{6-31}$$

Displacement due to the transverse shear forces is:

$$U_{tsh} = \sum_{i}^{n} \frac{A_i}{2} (FI_{11}S_i^1 + FI_{22}S_i^2 + 2FI_{12}S_i^3) \quad \textbf{6-32}$$

where

$$S_i^1 = 2T_{x_i}^{''}\left(T_{x_i}' + FT_{x_i}^{''}\right)$$
$$S_i^2 = 2T_{y_i}^{''}\left(T_{y_i}' + FT_{y_i}^{''}\right) \quad \textbf{6-33}$$
$$S_i^3 = T_{xi}'T_{yi}^{''} + T_{yi}'T_{xi}^{''} + 2FT_{xi}^{''}T_{yi}^{''}$$

The expression of U summarized in equation 6-25 and detailed in equations 6-26 to 6-33 is used for each trial of the Monte Carlo simulation, to calculate the displacement variability of a point of a multilayered composite shell.

6.2. Shells examples

6.2.1. Scordelis-Lo shell roof

6.2.1.1. Presentation of the example

The homogeneous and isotropic Scordelis-Lo shell roof example has been treated by Stefanou and Papadrakakis [124]**.** It is assumed that the two longitudinal edges are free and the two circular edges are supported by rigid diaphragms. Along the rigid diaphragms it is assumed that the displacements in direction x, y, and z are zero. The roof is subjected to gravity loading with magnitude 4 kPa. The geometric characteristics are: L = 15.2 m, R = 7.6 m, $\theta = 40^o$. The Poisson's ratio ν is deterministic and its value is 0.3. The random parameters are the elasticity modulus E and the thickness h, represented by isotropic random fields. The mean values of these parameters are $m(E) = 2.1\text{x}10^7$ kN/m^2 and $m(h) = 0.76$ m. The coefficients of variation *c.o.v.*(E) and *c.o.v.*(h) are equal to 10%. An isotropic exponential correlation function defined in equation 3-29 and several correlation lengths $\lambda = 0.004L$ to $8.55L$ are considered. The direct Monte Carlo simulations and the CGSM + Monte Carlo simulations are made with 10,000 runs. The vertical displacement variability of point C, located at the middle of the longitudinal edge, is calculated.

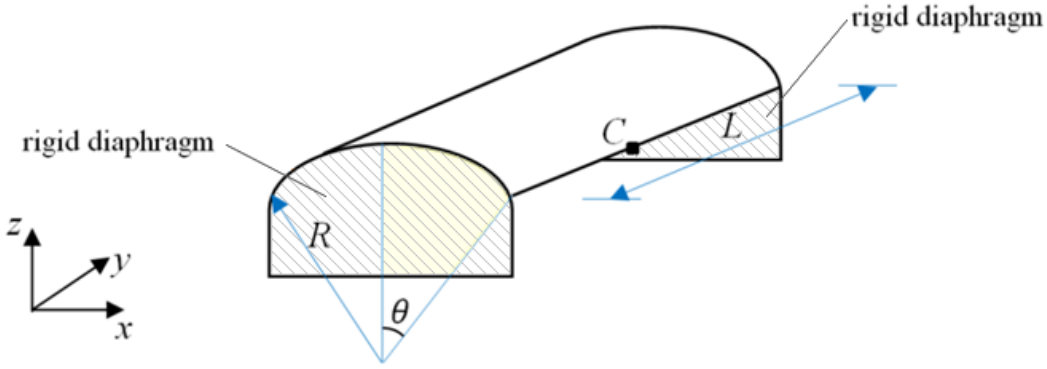

Figure 6-1 Scordelis-Lo shell roof under gravity loading

6.2.1.2. Finite element mesh

As in previous examples, we first search for the optimal nominal mesh and then we verify that this mesh is adapted to calculate the variability. Table 6-1 shows the results of a convergence study of the nominal displacement at point *C* performed with the CGSM formulation in the nominal configuration (equation 6-10). The reference solution is given by a very fine mesh (80x112). An adaptive mesh, shown in Figure 6-3, leading to a good precision for the nominal case, is also proposed. This mesh is selected for the variability calculation. The adaptive mesh is obtained by using the Abaqus software [114]. The adaptive mesh procedure, based on the minimization of the error on the strain energy, leads to a refined mesh in the areas with high strain energy density, as can be seen in Figure 6-4. This mesh is exploited to calculate the variability. The results obtained with the CGSM are compared to reference solutions obtained by direct Monte Carlo simulations.

Node	Mesh: Adaptive 1621 elements		Mesh: 40x56 2240 elements		Mesh: 60x84 5040 elements		Mesh: 80x112 8960 elements
	Displacement	Error (%)	Displacement	Error (%)	Displacement	Error (%)	Displacement (reference)
C	4.606E-2	0.43	4.618E-2	0.69	4.592E-2	0.12	4.587E-2

Table 6-1 Scordelis-Lo shell roof under gravity load – convergence study of displacement at node *C* in nominal configuration

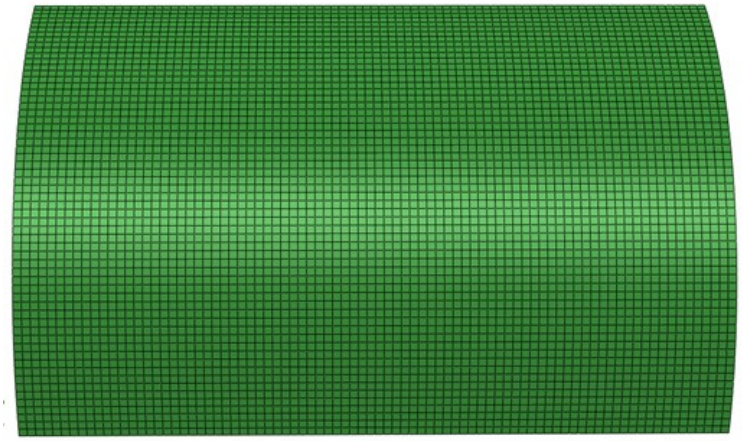

Figure 6-2 Scordelis-Lo shell roof under gravity loading – the 60x84 mesh (5185 nodes and 5040 elements)

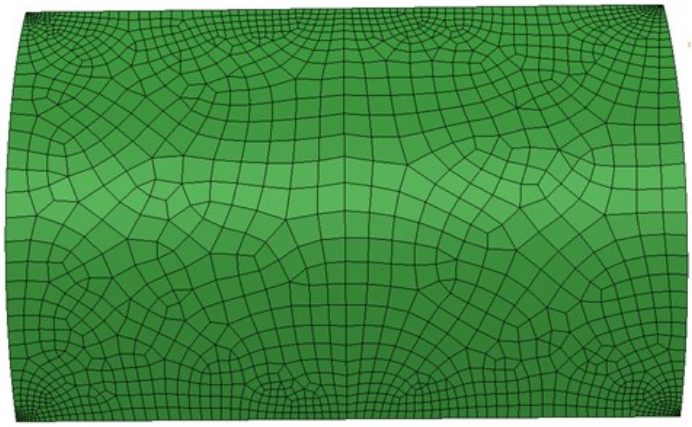

Figure 6-3 Scordelis-Lo shell roof under gravity loading – the adaptive mesh (1722 nodes and 1621 elements)

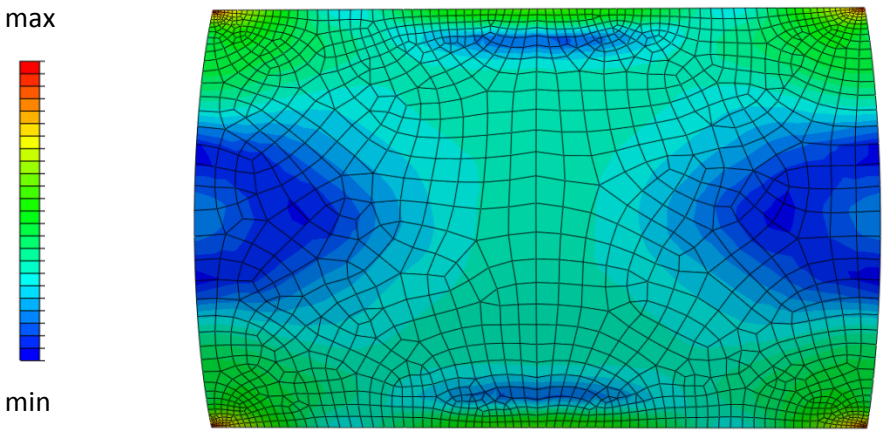

Figure 6-4 Scordelis-Lo shell roof under gravity loading – the envelope of strain energy density of adaptive mesh

6.2.1.3. Displacement variability

The CGSM results are compared to reference solutions obtained by direct Monte Carlo simulations. In the first case, the random parameter is E and several correlation lengths are considered. For each correlation length, the mean value, standard deviation and coefficient of variation of displacement at point C are reported in Table 6-2. Errors are given in Table 6-3. The CGSM provides very accurate results for the whole correlation length range. Nevertheless the errors slightly increase when the correlation length is smaller than L.

λ	$0.004L$		$0.17L$		$8.55\,L$	
	CGSM	dMC	CGSM	dMC	CGSM	dMC
$m(U)$	4.638E-2	4.621E-2	4.639E-2	4.621E-2	4.639E-2	4.643E-2
$\sigma(U)$	1.185E-4	1.156E-4	2.029E-3	1.992E-3	4.749E-3	4.753E-3
$c.o.v.(U)$ (%)	0.26	0.25	0.44	0.43	10.23	10.23

Table 6-2 Scordelis-Lo shell roof under gravity loading (E random, $c.o.v.(E)$ = 10%) – variability of displacement at point C

λ	$0.004L$	$0.17L$	$8.55\,L$
Error on $m(U)$ (%)	0.4	0.4	0.1
Error on $\sigma(U)$ (%)	2.5	1.8	0.1
Error on $c.o.v.(U)$ (%)	2.2	1.4	0.0

Table 6-3 Scordelis-Lo shell roof under gravity loading (E random, $c.o.v.(E)$ = 10%) – errors on the statistical results of displacement at point C

In the second case, the random parameter is h and again several correlation lengths are considered. Table 6-4 shows the mean value, standard deviation and coefficient of variation of displacement obtained by the CGSM and the Monte Carlo simulations. Errors, reported in Table 6-5, increase for small values of the correlation length. However, in all cases they remain acceptable. We observe that considering the thickness h as a random parameter leads to larger errors, compared to the situation where the elasticity modulus E is random. This demonstrates that the CGSM assumption is less valid when the random parameter is the thickness.

λ	0.004*L*		0.17*L*		8.55 *L*	
	CGSM	dMC	CGSM	dMC	CGSM	dMC
$m(U)$	4.754E-2	4.629E-2	4.757E-2	4.632E-2	4.756E-2	4.721E-2
$\sigma(U)$	1.585E-4	1.424E-4	4.769E-3	4.359E-3	9.934E-3	9.513E-3
c.o.v.(U) (%)	0.33	0.31	10.02	0.94	20.09	20.14

Table 6-4 Scordelis-Lo shell roof under gravity loading (h random, *c.o.v.*(h) = 10%) – variability of displacement at point C

λ	0.004*L*	0.17*L*	8.55 *L*
Error on $m(U)$ (%)	2.7	2.7	0.7
Error on $\sigma(U)$ (%)	11	9.4	4.4
Error on *c.o.v.*(U) (%)	8.4	6.5	3.6

Table 6-5 Scordelis-Lo shell roof under gravity loading (h random, *c.o.v.*(h) = 10%) – errors on the statistical results of displacement at point C

Figure 6-5 shows the evolution of the coefficient of variation of displacement at point C, when the correlation length varies. The variability of the displacement increases non-linearly with the correlation length. For small correlation lengths, the variability level is very low. This is due to a compensation phenomenon. This figure clearly highlights that the displacement variability level is significantly higher when the random parameter is the thickness, compared to the situation where the random parameter is the elasticity modulus. Figure 6-5 shows the CGSM, direct Monte Carlo, and Stefanou and Papadrakakis [124] results are globally consistent. However, a slight gap exists between the Stefanou and Papadrakakis results [124] and the CGSM or direct Monte Carlo ones. This is perhaps due to the fact that Stefanou used a quite coarse mesh. Indeed we have verified that this type of mesh is not fine enough to observe a good convergence of displacements. We observe that the adaptive mesh and the mapped mesh lead to similar results, except when the correlation length is very small (0.004*L)*. The results of both meshes are discussed in section 6.2.1.4.

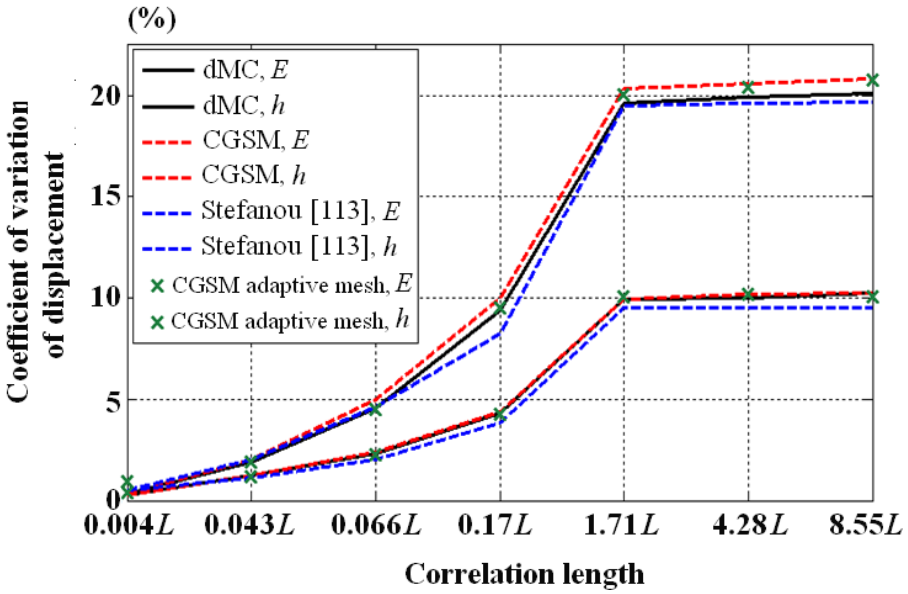

Figure 6-5 Scordelis-Lo shell roof under gravity loading (E or h random, $c.o.v.(E) = 10\%$, $c.o.v.(h) = 10\%$) – variability of displacement at point C

Figure 6-6 shows the probability density function of the displacement at point C, with E or h considered as uncertain. As for the examples of chapter 4 and chapter 5 (sections 4.2.1.3, 4.2.2.3, 5.2.1.3 and 5.2.2.3), the distributions obtained with the CGSM are very close to the reference distributions obtained with the direct Monte Carlo simulation. However, due to larger errors when the thickness is the random parameter, more significant differences appear in this case. Again, for the same reasons as described in the previous sections, the distributions are not exactly Gaussian.

a. *E* random, *c.o.v.*(*E*) = 10%, λ = 0.171*L*

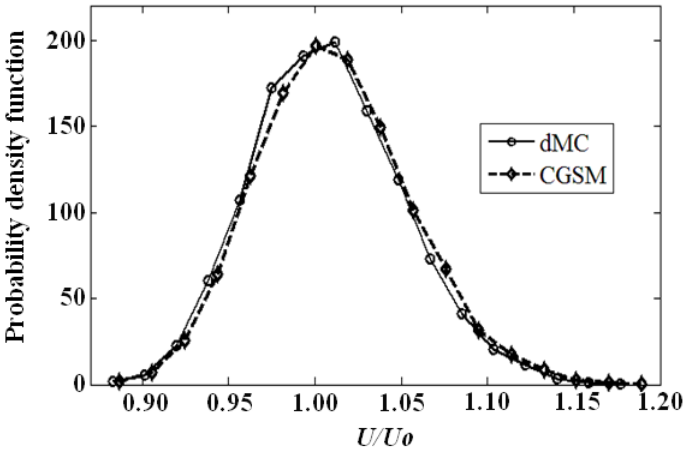

b. *h* random, *c.o.v.*(*h*) = 10%, λ = 0.171*L*

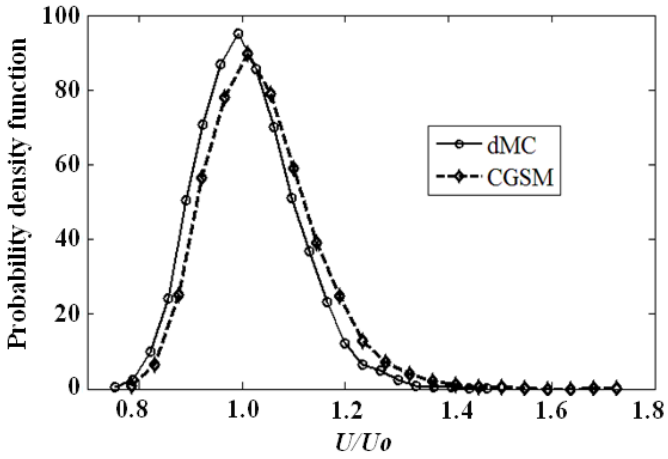

Figure 6-6 Scordelis-Lo shell roof under gravity loading – distribution of the displacement at point *C*

6.2.1.4. Influence of the mesh for variability computation

This section deals with the influence of the mesh on the calculation of the displacement variability. The study is conducted with the CGSM method. In this test, adaptive mesh and mapped mesh (see Figures 6-2 and 6-3) are compared with the reference mesh (80x112). The objective of the tests presented in this section is to verify a posteriori whether the adaptive mesh, which is optimal for the nominal configuration, is also correct for the calculation of variability. In the first case, the random parameter is the elasticity modulus (*c.o.v.*(*E*) = 10%) and in the second case, the random parameter is the thickness (*c.o.v.*(*h*) = 10%). The errors obtained

with adaptive mesh and 60x84 mapped mesh on the mean value and standard deviation of displacement at point *C*, are shown in Tables 6-6 and 6-7.

For both tests, the 60x84 mapped mesh is satisfactory when the correlation length is greater than 0.004*L*. The adaptive mesh leads to bigger errors when the correlation length is small and it is satisfactory only for correlation lengths bigger than *L*. Indeed, the mesh selected must be able to correctly model the random field. This is not a problem when the correlation is large, however it may be a real constraint for small correlation lengths. Matthies et al. [18] suggest to use a uniform mesh over the whole structure studied. We think that it is not absolutely necessary to meet this rule, however all the elements must be small enough for a good representation of the random field. This is not in contradiction with the development of adaptive meshing. The best approach is certainly an adaptive procedure which takes into account random fields, leading to a stochastic adaptive meshing approach. The errors due to a non uniform mesh could also be reduced by using another approach for the representation of random fields. Indeed, the midpoint method is disadvantageous from this point of view.

λ	0.004*L*		0.043*L*		0.171*L*		1.71*L*		8.55*L*	
Mesh	adaptive 1621	mapped 60x84	adaptive 1621	mapped 60x84	adaptive 1621	mapped 60x84	adaptive 1621	mapped 60x84	adaptive 1621	mapped 60x84
Error on $m(U)$ (%)	0.5	0.2	0.5	0.2	0.5	0.2	0.6	0.1	0.4	0.1
Error on $\sigma(U)$ (%)	54	29	3.8	0.4	3.7	0.8	0.4	0.2	0.6	0.5

Table 6-6 Scordelis-Lo shell roof under gravity loading (*E* random, *c.o.v.*(*E*) = 10%) – mesh errors on the statistical results of displacement at point *C*

λ	0.004*L*		0.043*L*		0.171*L*		1.71*L*		8.55*L*	
Mesh	adaptive 1621	mapped 60x84	adaptive 1621	mapped 60x84	adaptive 1621	mapped 60x84	adaptive 1621	mapped 60x84	adaptive 1621	mapped 60x84
Error on $m(U)$ (%)	0.5	0.2	0.5	0.2	0.4	0.1	0.4	0.0	0.3	0.0
Error on $\sigma(U)$ (%)	78	36	7.2	0.2	3.6	0.9	1.9	0.4	1.2	0.5

Table 6-7 Scordelis-Lo shell roof under gravity loading (*h* random, *c.o.v.*(*h*) = 10%) – mesh errors on the statistical results of displacement at point *C*

6.2.2. Windscreen

6.2.2.1. Presentation of the example

The windscreen is a sandwich structure, as shown in Figure 6-7. It is subjected to pressure loading with magnitude 1.9 kPa. The windscreen is assumed clamped along its whole periphery. The sandwich structure consists of 5 layers of material (as shown in Figure 6-8):

- the exterior layers 1 and 5 are made of glass.
- the intermediate layers 2 and 4 are made of a polymer PVB (Polyvinyl butyl).
- the layer 3 is made of an acoustic polymer.

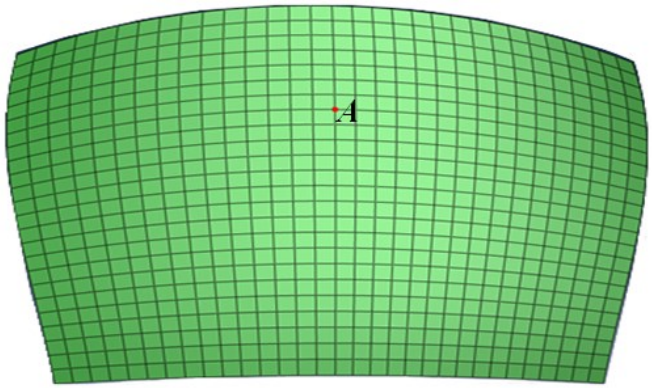

Figure 6-7 Car windscreen under pressure loading

The material properties and variability levels are shown in Table 6-8. The variability of material properties and thicknesses are represented by random variables. The variables are defined for each layer and all random parameters are independent. Results are observed at point *A* where the displacement is maximal. The variability of the vertical displacement of the central point *A* is calculated by direct Monte Carlo simulations and the CGSM, which are both performed with 10,000 runs.

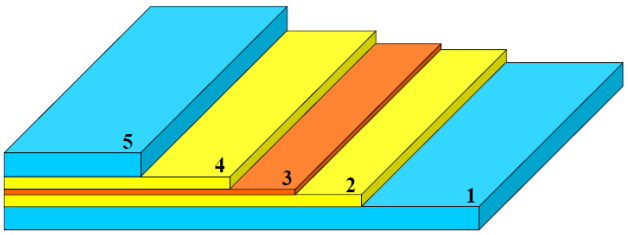

Figure 6-8 Car windscreen under pressure loading – stacking sequence

Layers	Elasticity modulus (MPa)	Poisson's ratio v	Thickness (mm)	*c.o.v.* (h_i) (%)	*c.o.v.* (E_i) (%)
glass	70000	0.215	2.1	2	2
polymer PVB	346	0.491	0.33	5	20
acoustic polymer	12	0.491	0.1	15	20
polymer PVB	346	0.491	0.33	5	20
glass	70000	0.215	2.1	2	2

Table 6-8 Car windscreen under pressure loading – material properties**,** physical properties and variability levels

6.2.2.2. Finite element mesh

As in previous examples, we first search for the optimal nominal mesh and then we verify that this mesh is adapted to calculate the variability. Table 6-9 shows the results of a convergence study of nominal displacement at point *A* performed with the CGSM formulation in the nominal configuration (equation 6-25). The reference solution is given by a very fine mesh (13200 elements). Mesh II with 744 elements, leading to an error of 0.14%, is satisfactory for the nominal calculation. Consequently this mesh is exploited to calculate the variability. We will check a posteriori whether this mesh is also well suited for the calculation of the variability.

Node	Mesh I 192 elements		Mesh II 744 elements		Reference mesh 13200 elements
	Displacement	Error (%)	Displacement	Error (%)	Displacement (reference)
A	0.1494	1.7	0.1469	0.1	0.1469

Table 6-9 Car windscreen under pressure loading – convergence study of displacement at node *C* in nominal configuration

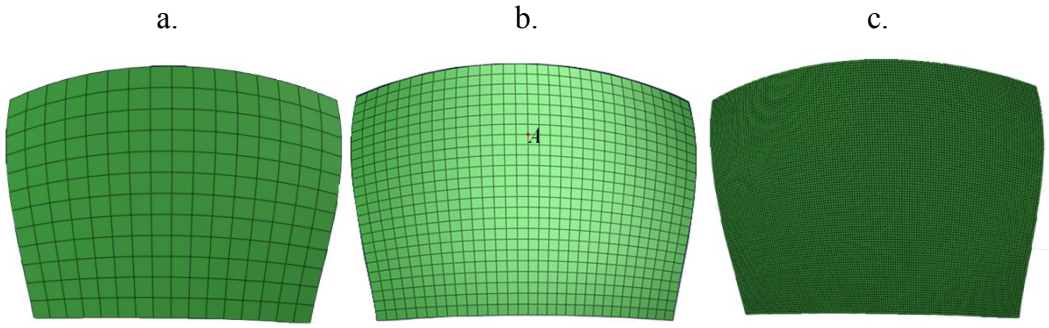

Figure 6-9 Car windscreen under pressure loading – Mesh I: 192 elements (a), Mesh II: 744 elements (b), Mesh III: 13200 elements (c)

6.2.2.3. Displacement variability

The CGSM results are compared to a reference solution obtained by direct Monte Carlo simulation. Three cases are treated: the uncertain parameters are the elasticity modulus, the thickness and both these parameters for cases 1, 2 and 3 respectively (see Table 6-8). The fourth case is treated with changing of variability levels of the glass layers ($c.o.v.(E_i)$ and $c.o.v.(h_i)$ are 10%), the uncertain parameters are both the elasticity modulus and the thickness. Cases 1, 2, 3, 4 lead to 5, 5, 10 and 10 independent random parameters respectively. For each test, the mean value, standard deviation and coefficient of variation of displacements at point *A* are reported in Tables 6-10, 6-11 and 6-12. The CGSM provides very accurate results in all cases.

	Uncertain parameters: E_i		
	CGSM	dMC	Error (%)
$m(U)$	0.1470	0.1468	0.1
$\sigma(U)$	2.014E-03	2.014E-03	0.0
$c.o.v.(U)$ (%)	1.37	1.37	0.13

Table 6-10 Car windscreen under pressure loading (case 1: E random) – variability of displacement at point A

	Uncertain parameters: E_i		
	CGSM	dMC	Error (%)
$m(U)$	0.1470	0.1468	0.1
$\sigma(U)$	2.285E-03	2.282E-03	0.1
$c.o.v.(U)$ (%)	1.55	1.55	0.0

Table 6-11 Car windscreen under pressure loading (case 2: h random) – variability of displacement at point A

	Uncertain parameters: E_i and h_i		
	CGSM	dMC	Error (%)
$m(U)$	0.1471	0.1469	0.1
$\sigma(U)$	3.051E-03	3.049E-03	0.1
$c.o.v.(U)$ (%)	2.07	2.08	0.1

Table 6-12 Car windscreen under pressure loading (case 3: E and h random) – variability displacement at point A

Figure 6-10 shows the probability density function of the displacement at point A. Again, the distribution obtained with the CGSM is very close to the reference distribution obtained with the direct Monte Carlo simulation. In order to test the robustness of the CGSM, a complementary case, with a larger input variability level, has been treated. The data are identical to those reported in Table 6-8, except for the glass layers which manage the mechanical behavior of the windscreen. The coefficients of variation are now increased: $c.o.v.(E_i) = c.o.v.(h_i) = 10\%$ for the glass layers.

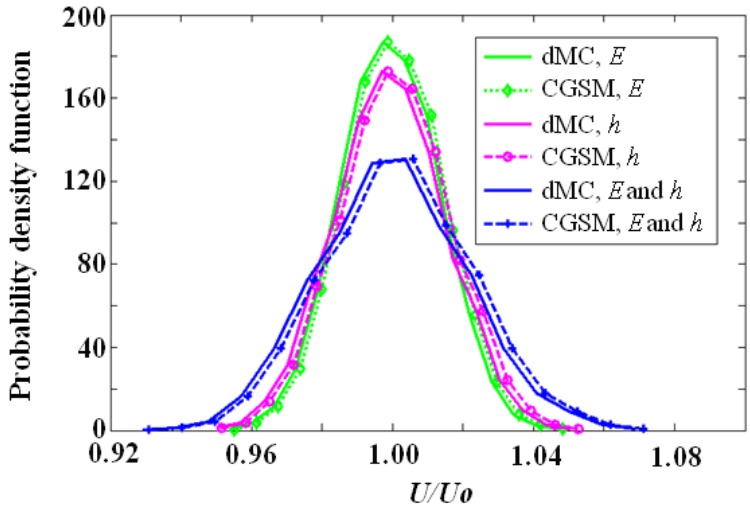

Figure 6-10 Car windscreen under pressure loading – distribution of displacement at point *A*

Table 6-13 shows that the output variability level is quite high. Anyway, errors remain quite limited. Figure 6-11 shows the probability density function of the displacement at point *A*. Again, the distribution obtained with the CGSM is very close to the reference distribution obtained with the direct Monte Carlo simulation.

These results highlight that for this example, the CGSM assumption, that is to say the generalized stresses are certain, is quite valid. The CGSM is particularly precise in this example because for one given layer, the perturbation is uniformly distributed over the whole structure. Consequently, the perturbed generalized stresses are quite certain.

	Uncertain parameters: E_i and h_i		
	CGSM	dMC	Error (%)
$m(U)$	0.1494	0.1484	0.6
$\sigma(U)$	1.582E-02	1.560E-02	1.4
$c.o.v.(U)$ (%)	10.59	10.50	0.8

Table 6-13 Car windscreen under pressure loading (case 4: *E* and *h* uncertain, for glass $c.o.v.(E_i) = c.o.v.(h_i) = 10\%$) – variability of displacement at point *A*

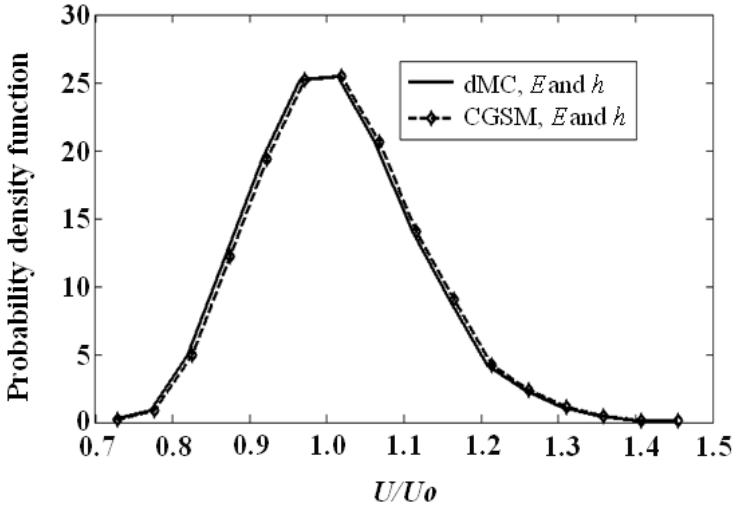

Figure 6-11 Car windscreen under pressure loading (case 4: E and h uncertain, for glass $c.o.v.(E_i) = c.o.v.(h_i) = 10\%$) – distribution of displacement at point A

6.3. Synthesis of the performances of the CGSM in computational time

The tests are performed for two examples: the Scordelis-Lo shell roof (see section 6.1) and the winscreen (see section 6.2). Several numbers of trials and several meshes are considered. In the first example, input variability is described by random fields. In the second example, only random variables are considered.

For the Scordelis-Lo shell roof example, results are presented in Figures 12 and 13 and in Table 6-14. Two tests are performed to highlight the influence of random fields. First the acceleration factor (acceleration factor 1) between the direct Monte Carlo simulations and the CGSM is calculated taking into account the total computational time. Then the acceleration factor (acceleration factor 2) is calculated again by removing the computational time due to the autocovariance decomposition. This autocovariance decomposition is specific of random fields, it is performed only once but is very time consuming.

Figure 6-12 shows the results for acceleration factor 1. It increases with the number of trials and decreases with the mesh refinement level. For a number of trials classically considered and equal to 10000, the acceleration factor is comprised between 148 and 251, depending on the mesh refinement level. Figure 6-13 shows

the results for the acceleration factor 2. It increases with the number of trials and the mesh refinement level. This is a very hopeful characteristic. For a number of trials equal to 10000, the acceleration factor is comprised between 330 and 413, depending on the mesh refinement level. In summary, for this example, the acceleration factors are always bigger than 148 and this performance is satisfactory. Anyway, the CGSM is slowed here by the presence of random fields. To increase further the efficiency of the CGSM in computational time, one perspective of this research is to improve the approach to calculate and manage random fields.

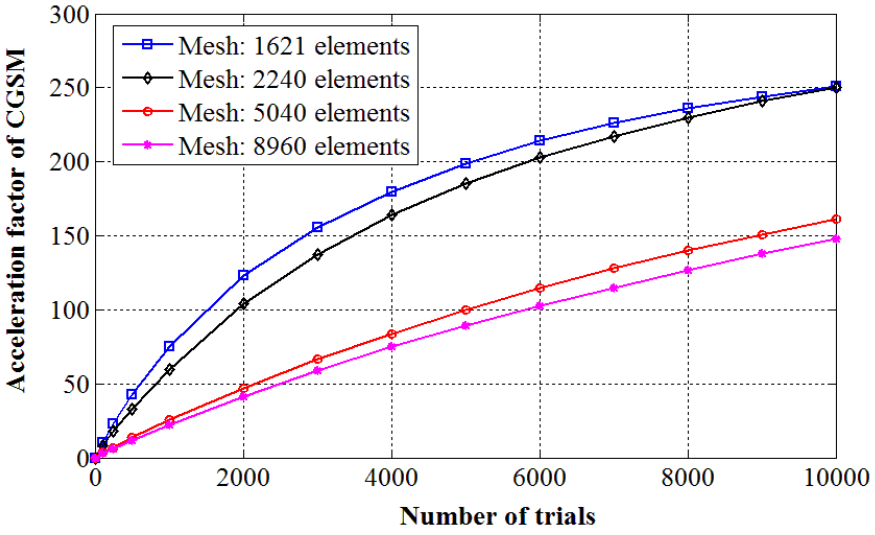

Figure 6-12 Scordelis-Lo shell roof under gravity loading – acceleration factor 1

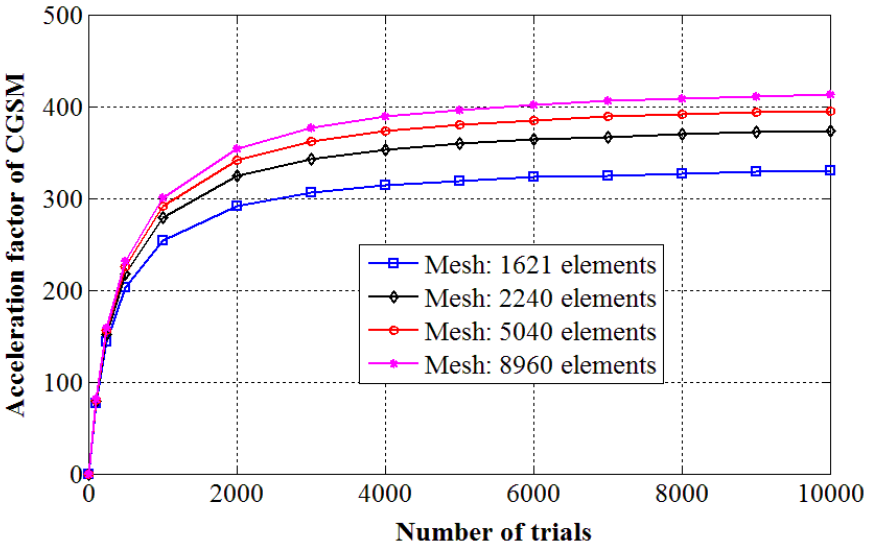

Figure 6-13 Scordelis-Lo shell roof under gravity loading – acceleration factor 2

	Mesh: Adaptive 1621 elements			Mesh: 40x56 2240 elements			Mesh: 60x84 5040 elements			Mesh: 80x112 8960 elements		
	CGSM (sec)	MCd (sec)	Acceleration factor of CGSM	CGSM (sec)	MCd (sec)	Acceleration factor of CGSM	CGSM (sec)	MCd (sec)	Acceleration factor of CGSM	CGSM (sec)	MCd (sec)	Acceleration factor of CGSM
Computational time due to autocovariance decomposition	45	45		95	95		801	801		2344	2344	
Computational time due to the trials No. of trials												
1	5	5	1	7	7	1	22	22	1	54	54	1
250	8	1186	144	12	1805	152	35	5393	156	85	13378	158
500	12	2372	203	17	3610	218	48	10787	226	116	26756	231
1000	19	4743	254	26	7219	279	74	21573	292	178	53511	301
5000	74	23716	319	100	36096	360	284	107867	380	675	267557	396
10000	144	47432	330	193	72192	373	546	215734	395	1296	535114	413
Total computational time No. of trials												
1	50	50	1	103	103	1	822	822	1	2397	2397	1
250	53	1231	23	107	1900	18	835	6194	7	2428	15722	6
500	57	2417	43	112	3705	33	848	11587	14	2459	29099	12
1000	64	4788	75	121	7315	60	875	22374	26	2522	55855	22
5000	119	23761	199	196	36191	185	1084	108668	100	3019	269901	89
10000	189	47477	251	289	72287	250	1346	216534	161	3640	537458	148

Table 6-14 Scordelis-Lo shell roof under gravity loading – comparison of computational time between CGSM and direct Monte Carlo simulation

For the windscreen example, results are presented in Figures 6-14 and in Table 6-15. Figure 6-14 shows that the acceleration factor increases with the number of trials and with the mesh refinement level. This hopeful characteristic of CGSM is clearly highlighted in this example described by random input variables but without any random field. For a number of trials classically considered and equal to 10000, the acceleration factor is comprised between 1129 and 1473, depending on the mesh refinement level. This result reveals the high efficiency of the CGSM in computational time, for an industrial application.

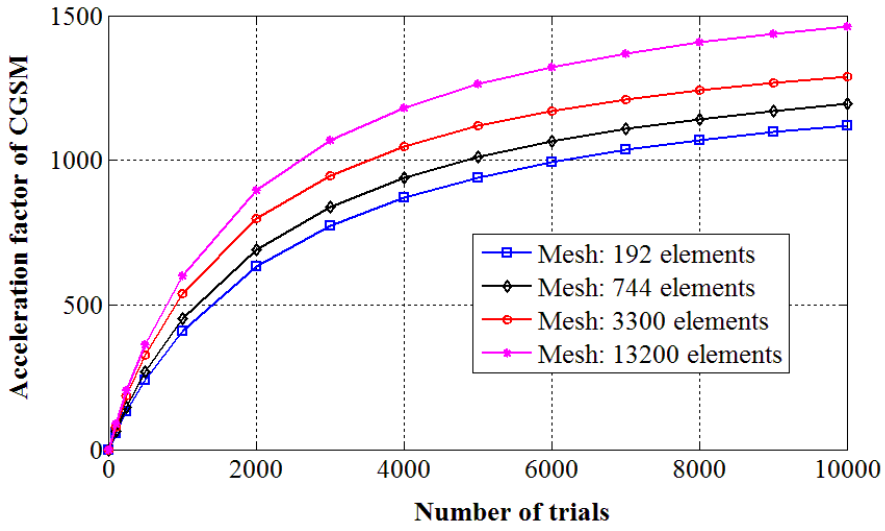

Figure 6-14 Car windscreen under pressure loading – acceleration factor of CGSM

Number of trials	Mesh I 192 elements			Mesh II 744 elements			Mesh III 3300 elements			Reference mesh 13200 elements		
	CGSM (sec)	MC (sec)	Acceleration factor of CGSM	CGSM (sec)	MC (sec)	Acceleration factor of CGSM	CGSM (sec)	MC (sec)	Accelerati-on factor	CGSM (sec)	MC (sec)	Acceleration factor of CGSM
1	1	1	1	2	1	1	4	3	1	10	9	1
250	1	189	132	2	264	148	4	767	184	12	2342	204
500	2	378	242	2	529	269	5	1534	329	13	4684	365
1000	2	756	412	2	1058	454	6	3068	542	16	9369	604
5000	4	3778	946	5	5289	1017	14	15338	1124	37	46845	1270
10000	7	7556	1129	9	10578	1203	24	30676	1299	64	93689	1473

Table 6-15 Car windscreen under pressure loading – comparison of computational time between CGSM and direct Monte Carlo simulation

Chapter 7

Conclusions and Perspectives

This research focused on the development and the assessment of the Certain Generalized Stresses Method for the probabilistic analysis of thin-walled structures, that is to say plates and shells. Aleatory uncertainties have been considered and uncertain inputs have been defined by probabilistic laws. The uncertain input parameters are elasticity moduli, Poisson's ratios and thicknesses. Uniform random parameters as well as random fields have been considered. The outputs are statistical quantities: mean value, standard deviation and probability density functions of the structural responses. The output parameters retained for the study are displacements and strains. The statistical results are obtained by Monte Carlo simulations, using a semi-analytical formula. They have been compared with the direct Monte Carlo simulation considered as a reference.

Several examples of membrane plates, bending plates, and homogeneous as well as multilayered shells, have been treated. The results have been compared with the direct Monte Carlo simulation. Very satisfactory results have been obtained for the mean value, standard deviation and probability density of displacements and strains. The limitations of the methodology developed have also been highlighted. In particular, when uncertainty is defined by random fields, some drawbacks have been observed for short correlation lengths, due to the selected midpoint method. From a computational time point of view, the CGSM is very efficient compared to the direct Monte Carlo simulation. In particular, for the windscreen which is an industrial example, the acceleration factor is more than 1000. This represents a large reduction of the high computational costs that characterize most of the existing approaches. Moreover, the larger the size of the problem, the bigger the acceleration factor. Anyway, the performance in computational time is not as good if random fields are considered.

Several prospects in this work can be considered. The performance of the CGSM in presence of random fields has to be further improved. In particular, for

the representation of random fields, alternatives to the midpoint methods shoud be used. The CGSM can be extended to composite structures made of anisotropic materials. A method inspired by CGSM can also be developed for non linear analysis. An extension of the CGSM to possibilistic approach to take into account epistemic uncertainties is also desirable. The development of error indicators would also be a useful perspective in order to assess the quality of the results obtained. The choice of the optimal finite element mesh is also an important issue. In this study, relevant results have been obtained using an adaptive meshing technique based on deterministic analyses. The best approach would certainly be an adaptive procedure which takes into account potential random fields, leading to a stochastic adaptive meshing procedure. Finally, to improve further the precision of the results by keeping the main advantages of the methodology developed, alternative assumptions leading to variants of the CGSM could be tested.

List of Figures

List of Tables

References

[1] Wood, L.A. & Joachim, C.A. (1984). Variability of interior noise levels in passenger cars. *Proceding of the Conference on Vehicle Noise and Vibration, Mechanical Engineering Publications Limited***,** 197-206.

[2] Kompella, M.S. & Bernhard, R.J. (1996). Variation of structural acoustic characteristics of automotive vehicles. *Noise Control Engineering Journal***,** 93–99.

[3] Lionnet, C. & Lardeur, P. (2007). A hierarchical approach to the assessment of the variability of interior noise levels measured in passenger cars. *Noise Control Engineering Journal,* 55**,** 29-37.

[4] Scigliano, R., Scionti, M. & Lardeur, P. (2011). Verification, validation and variability for the vibration study of a car windscreen modeled by finite elements. *Finite Elements in Analysis and Design,* 47**,** 17-29.

[5] Arnoult, É., Lardeur, P. & Martini, L. (2011). The modal stability procedure for dynamic and linear finite element analysis with variability. *Finite Elements in Analysis and Design,* 47**,** 30-45.

[6] Sudret, B. (2007). Uncertainty propagation and sensitivity analysis in mechanical models. *Report: Habilitation à diriger des recherches,* Université Blaise Pascal.

[7] Bae, H.-R., Grandhi, R.V. & Canfield, R.A. (2003). Uncertainty quantification using evidence theory with a cost-effective algorithm. *Second M.I.T. Conference on Computational Fluid and Solid Mechanics*.

[8] Batoz, J.-L. & Dhatt, G. (1992). Modelisation des structures par elements finis, volume 1-3. *Edition Hermes, Paris*.

[9] Katili, I. (2004). Metode elemen hingga untuk pelat lentur. *UI Press, Jakarta*.

[10] Helton, J.C. (2011). Quantification of margins and uncertainties: Conceptual and computational basis. *Reliability Engineering & System Safety,* 96**,** 976-1013.

[11] Thacker, B.H., Doebling, S.W., Hemez, F.M., Anderson, M.C., Pepin, J.E. & Rodriguez, E.A. (2004). Concepts of model verification and validation. *Los Alomos, National Laboratory*.

[12] Roy, C.J. & Oberkampf, W.L. (2011). A comprehensive framework for verification, validation, and uncertainty quantification in scientific computing. *Computer Methods in Applied Mechanics and Engineering,* 200**,** 2131-2144.

[13] Iaccarino, G. (2009). Introduction to uncertainty quantification in computational science. *Department of Mechanical Engineering, Stanford University*.

[14] Lardeur, P., Oudjene, M. & Arnoult, É. (2003). La méthode MEGC pour le calcul de dispersion du comportement statique des treillis. *Colloque national en calcul des structures,* Giens.

[15] Lardeur, P., Demri, A., Lionnet, E. & Arnoult, É. (2005). Application de la méthode MEGC aux treillis de barres hyperstatiques, Colloque national en calcul des structures. *Colloque national en calcul des structures,* Giens.

[16] Lardeur, P., Arnoult, É., Martini, L. & Knopf-Lenoir, C. (2012). The Certain Generalized Stresses Method for the static finite element analysis of bar and beam trusses with variability. *Finite Elements in Analysis and Design,* 50**,** 231-242.

[17] Schuëller, G.I. (1997). A state-of-the-art report on computational stochastic mechanics. *Probabilistic Engineering Mechanics,* 12**,** 197-321.

[18] Matthies, H.G., Brenner, C.E., Bucher, C.G. & Guedes Soares, C. (1997). Uncertainties in probabilistic numerical analysis of structures and solids-Stochastic finite elements. *Structural Safety,* 19**,** 283-336.

[19] Sudret, B. & Der Kiureghian, A. (2000). Stochastic finite element methods and reliability: A state of the art report. *A report on research, Department of Civil & Environmental Engineering, University of California*.

[20] Keese, A. (2003). A review of recent developments in the numerical solution of stochastic partial differential equations (stochastic finite elements). *Technical University Braunschweig, Institute of Scientific Computing*.

[21] Stefanou, G. (2009). The stochastic finite element method: Past, present and future. *Computer Methods in Applied Mechanics and Engineering,* 198**,** 1031-1051.

[22] Moens, D. & Hanss, M. (2011). Non-probabilistic finite element analysis for parametric uncertainty treatment in applied mechanics: Recent advances. *Finite Elements in Analysis and Design,* 47**,** 4-16.

[23] Li, B. & Chen, X. (2014). Wavelet-based numerical analysis: A review and classification. *Finite Elements in Analysis and Design,* 81**,** 14-31.

[24] Schuëller, G.I. & Shinozuka, M. (1987). Stochastic methods in structural dynamics. *Martinus Nijhoff publishers*.

[25] To Cho, W.S. (2014). Stochastic structural dynamics: Application of finite element methods. *John Wiley & Sons Singapore Pte. Ltd*.

[26] Elishakoff, I. (1999). Probabilistic theory of structures. *Dover Publications, Inc*.

[27] Papoulis, A. (2002). Probability, random variables and stochastic processes. *McGraw-Hill Higher Education*.

[28] Gatti, P.L. (2005). Probability theory and mathematical statistics for engineers. *Spon Press*.

[29] Field, J.R.V. (2008). Stochastic models: Theory and simulation. *Sandia National Laboratories*.

[30] Schenk, C.A. & Schuëller, G.I. (2005). Uncertainty assessment of large finite element systems. *Lecture notes in applied and computational mechanics,* 24.

[31] Hammersley, J.M. & Handscomb, D.C. (1965). Monte Carlo Methods. *John Wiley & Sons Ltd*.

[32] Fishman, G.S. (2003). Monte Carlo: Concepts, algorithms, and applications. *Springer series*.

[33] Ghanem, R.G. & Spanos, P.D. (2003). Stochastic finite elements method : A spectral Approach. *Dover Publications, Inc*.

[34] Dongbin, X. (2010). Numerical methods for stochastic computations: A spectral method approach. *Priceton University Press*.

[35] Shen, H.-S. (2013). A two-step perturbation method in nonlinear analysis of beams, plates, and shells. *John Wiley & Sons Singapore Pte. Ltd*.

[36] Vanmarcke, E.H. (1983). Random fields: analysis and synthesis. *The MIT Press, Cambridge, Mass*.

[37] Abrahamsen , P. (1997). A review Gaussian random fields and correlation functions. *Research fellowship from The Research Council of Norway*.

[38] Grigoriu, M. (2012). Stochastic systems: uncertainty quantification and propagation. *Springer Series in Reliability Engineering*.

[39] Mulani, S.B. (2006). Uncertainty quantification in dynamic problems with large uncertainties. *Doctoral Thesis,* Aerospace Engineering, Virginia Polytechnic Institute and State University.

[40] Moore, R.E. (1979). Methods and application of interval analysis. *SIAM, Philadelphia*.

[41] Oberkampf, W.L., Deland, S.M., Rutherford, B.M., Diegert, K.V. & Alvin, K.F. (2002). Error and uncertainty in modeling and simulation. *Reliability Engineering & System Safety,* 75**,** 333-357.

[42] Oberkampf, W.L., Helton, J.C., Joslyn, C.A., Wojtkiewicz, S.F. & Ferson, S. (2004). Challenge problems: uncertainty in system response given uncertain parameters. *Reliability Engineering & System Safety,* 85**,** 11-19.

[43] Panayirci, H.M. (2010). Computational strategies for efficient stochastic finite element analysis of engineering structures. *Doctoral Thesis,* Institute of Engineering Mechanics, University of Innsbruck, Austria, EU.

[44] Jones, S. & Hunt, H. (2012). Predicting surface vibration from underground railways through inhomogeneous soil. *Journal of Sound and Vibration,* 331**,** 2055-2069.

[45] Hills, E., Mace, B.R. & Ferguson, N.S. (2004). Response statistics of stochastic built-up structures. *Proceedings of ISMA 2004, Katholieke Universiteit Leuven, Leuven, Belgium*.

[46] Sudret, B. & Der Kiureghian, A. (2002). Comparison of finite element reliability methods. *Probabilistic Engineering Mechanics,* 17**,** 337-348.

[47] Der Kiureghian, A. & Ke, J.-B. (1988). The stochastic finite element method in structural reliability. *Probabilistic Engineering Mechanics,* 3**,** 83-91.

[48] Liu, W.K., Belytschko, T. & Mani, A. (1986). Random field finite elements. *International Journal for Numerical Methods in Engineering,* 23**,** 1831-1845.

[49] Liu, W.K., Belytschko, T. & Mani, A. (1986). Probabilistic finite elements for nonlinear structural dynamics. *Computer Methods in Applied Mechanics and Engineering,* 56**,** 61-81.

[50] Brenner, C.E. & Bucher, C. (1995). A contribution to the SFE-based reliability assessment of nonlinear structures under dynamic loading. *Probabilistic Engineering Mechanics,* 10**,** 265-273.

[51] Lee, T.-H. & Mosalam, K.M. (2004). Probabilistic fiber element modeling of reinforced concrete structures. *Computers & Structures,* 82**,** 2285-2299.

[52] Charmpis, D.C., Schuëller, G.I. & Pellissetti, M.F. (2007). The need for linking micromechanics of materials with stochastic finite elements: A challenge for materials science. *Computational Materials Science,* 41**,** 27-37.

[53] Ching, J. & Phoon, K.-K. (2013). Effect of element sizes in random field finite element simulations of soil shear strength. *Computers & Structures,* 126**,** 120-134.

[54] Li, C. & Der Kiureghian, A. (1993). Optimal Discretization of Random Fields. *Journal of Engineering Mechanics,* 119**,** 1136-1154.

[55] Vanmarcke, E. & Grigoriu, M. (1983). Stochastic Finite Element Analysis of Simple Beams. *Journal of Engineering Mechanics,* 109**,** 1203-1214.

[56] Vanmarcke, E., Shinozuka, M., Nakagiri, S., Schuëller, G.I. & Grigoriu, M. (1986). Random fields and stochastic finite elements. *Structural Safety,* 3**,** 143-166.

[57] Deodatis, G. (1991). Weighted Integral Method. I: Stochastic Stiffness Matrix. *Journal of Engineering Mechanics,* 117**,** 1851-1864.

[58] Deodatis, G. & Shinozuka, M. (1991). Weighted Integral Method. II: Response Variability and Reliability. *Journal of Engineering Mechanics,* 117 (8)**,** 1865–1877.

[59] Gerbrands, J.J. (1981). On the relationships between SVD, KLT and PCA. *Pattern Recognition,* 14**,** 375-381.

[60] Loève, M. (1978). Probability theory II. *Springer-Verlag*.

[61] Shinozuka, M. & Deodatis, G. (1991). Simulation of stochastic processes by spectral representation. *Applied Mechanics Reviews,* 44 | 4**,** 191-204.

[62] Grigoriu, M. (1993). On the spectral representation method in simulation. *Probabilistic Engineering Mechanics,* 8**,** 75-90.

[63] Wiener, N. (1938). The homogeneous chaos. *American Journal of Mathematics,* 60**,** 897-936.

[64] Sakamoto, S. & Ghanem, R. (2002). Polynomial Chaos Decomposition for the Simulation of Non-Gaussian Nonstationary Stochastic Processes. *Journal of Engineering Mechanics,* 128**,** 190-201.

[65] Baker, K. (2013). Singular value decomposition tutorial. *https://www.ling.ohio-state.edu/~kbaker*.

[66] Phoon, K.K., Huang, H.W. & Quek, S.T. (2004). Comparison between Karhunen–Loeve and wavelet expansions for simulation of Gaussian processes. *Computers & Structures,* 82**,** 985-991.

[67] Pranesh, S. & Ghosh, D. (2015). Faster computation of the Karhunen–Loève expansion using its domain independence property. *Computer Methods in Applied Mechanics and Engineering,* 285**,** 125-145.

[68] Li, L.B., Phoon, K.K. & Quek, S.T. (2007). Comparison between Karhunen–Loève expansion and translation-based simulation of non-Gaussian processes. *Computers & Structures,* 85**,** 264-276.

[69] Metropolis, N. & Ulam, S. (1949). The Monte Carlo method. *Journal of the American Statistical Association,* Vol. 44, No. 247**,** 335-341.

[70] Olsson, A. & Sandberg, G. (2002). Latin Hypercube Sampling for Stochastic Finite Element Analysis. *Journal of Engineering Mechanics,* 128**,** 121-125.

[71] Helton, J.C., Johnson, J.D., Sallaberry, C.J. & Storlie, C.B. (2006). Survey of sampling-based methods for uncertainty and sensitivity analysis. *Reliability Engineering & System Safety,* 91**,** 1175-1209.

[72] Au, S.K. & Beck, J.L. (1999). A new adaptive importance sampling scheme for reliability calculations. *Structural Safety,* 21**,** 135-158.

[73] Wang, B., Wang, D., Jiang, J., Zhang, J. & Sun, P. (2015). Efficient functional reliability estimation for a passive residual heat removal system with subset simulation based on importance sampling. *Progress in Nuclear Energy,* 78**,** 36-46.

[74] Au, S.K. & Beck, J.L. (2001). First excursion probabilities for linear systems by very efficient importance sampling. *Probabilistic Engineering Mechanics,* 16**,** 193-207.

[75] Ching, J., Au, S.K. & Beck, J.L. (2005). Reliability estimation for dynamical systems subject to stochastic excitation using subset simulation with splitting. *Computer Methods in Applied Mechanics and Engineering,* 194**,** 1557-1579.

[76] Pradlwarter, H.J., Schuëller, G.I., Koutsourelakis, P.S. & Charmpis, D.C. (2007). Application of line sampling simulation method to reliability benchmark problems. *Structural Safety,* 29**,** 208-221.

[77] Martini, L. (2008). Développement et évaluation de l'hypothèse de stabilité modale pour la variabilité du comportement vibratoire des structures minces modélisées par éléments finis. In: *Doctoral Thesis*, Université de Technologie de Compiègne, Compiègne, France.

[78] Blatman, G. & Sudret, B. (2010). Efficient computation of global sensitivity indices using sparse polynomial chaos expansions. *Reliability Engineering & System Safety,* 95**,** 1216-1229.

[79] Argyris, J., Papadrakakis, M. & Stefanou, G. (2002). Stochastic finite element analysis of shells. *Computer Methods in Applied Mechanics and Engineering,* 191**,** 4781-4804.

[80] Charmpis, D.C. & Papadrakakis, M. (2005). Improving the computational efficiency in finite element analysis of shells with uncertain properties. *Computer Methods in Applied Mechanics and Engineering,* 194**,** 1447-1478.

[81] Papadrakakis, M. & Papadopoulos, V. (1996). Robust and efficient methods for stochastic finite element analysis using Monte Carlo simulation. *Computer Methods in Applied Mechanics and Engineering,* 134**,** 325-340.

[82] Noh, H.-C. & Park, T. (2006). Monte Carlo simulation-compatible stochastic field for application to expansion-based stochastic finite element method. *Computers & Structures,* 84**,** 2363-2372.

[83] Chakraborty, S. & Dey, S.S. (1996). Stochastic finite element simulation of random structure on uncertain foundation under random loading. *International Journal of Mechanical Sciences,* 38**,** 1209-1218.

[84] Avila Da S. Jr, C.R. & Beck, A.T. (2015). New method for efficient Monte Carlo–Neumann solution of linear stochastic systems. *Probabilistic Engineering Mechanics,* 40**,** 90-96.

[85] Yamazaki, F., Shinozuka, M. & Dasgupta, G. (1988). Neumann Expansion for Stochastic Finite Element Analysis. *Journal of Engineering Mechanics,* 114**,** 1335-1354.

[86] Cambou, B. (1975). Application of first-order uncertainty analysis in the finite element method in linear elasticity. *Proceedings of 2nd International Conference on: Applications of Statistics and Probability in Soil and Structural Engineering, Archen***,** 87-97.

[87] Rahman, S. & Rao, B.N. (1991). A perturbation method for stochastic meshless analysis in elastostatics. *International Journal for Numerical Methods in Engineering,* 50**,** 1969-1991.

[88] Elishakoff, I., Ren, Y.J. & Shinozuka, M. (1995). Improved finite element method for stochastic problems. *Chaos, Solitons & Fractals,* 5**,** 833-846.

[89] Falsone, G. & Impollonia, N. (2002). A new approach for the stochastic analysis of finite element modelled structures with uncertain parameters. *Computer Methods in Applied Mechanics and Engineering,* 191**,** 5067-5085.

[90] Kamiński, M. (2007). Generalized perturbation-based stochastic finite element method in elastostatics. *Computers & Structures,* 85**,** 586-594.

[91] Chang, T.P., Liu, M.F. & Chang, H.C. (2008). Finite element analysis of nonlinear shell structures with uncertain material property. *Thin-Walled Structures,* 46**,** 1055-1065.

[92] Henriques, A.A. (2008). Efficient analysis of structural uncertainty using perturbation techniques. *Engineering Structures,* 30**,** 990-1001.

[93] Xia, B., Yu, D. & Liu, J. (2014). Transformed perturbation stochastic finite element method for static response analysis of stochastic structures. *Finite Elements in Analysis and Design,* 79**,** 9-21.

[94] Ghanem, R. & Spanos, P. (1991). Spectral Stochastic Finite-Element Formulation for Reliability Analysis. *Journal of Engineering Mechanics,* 117**,** 2351-2372.

[95] Ghanem, R.G. & Kruger, R.M. (1996). Numerical solution of spectral stochastic finite element systems. *Computer Methods in Applied Mechanics and Engineering,* 129**,** 289-303.

[96] Pellissetti, M.F. & Ghanem, R.G. (2000). Iterative solution of systems of linear equations arising in the context of stochastic finite elements. *Advances in Engineering Software,* 31**,** 607-616.

[97] Nouy, A., Clément, A., Schoefs, F. & Moës, N. (2008). An extended stochastic finite element method for solving stochastic partial differential

equations on random domains. *Computer Methods in Applied Mechanics and Engineering,* 197**,** 4663-4682.

[98] Nouy, A. (2008). Generalized spectral decomposition method for solving stochastic finite element equations: Invariant subspace problem and dedicated algorithms. *Computer Methods in Applied Mechanics and Engineering,* 197**,** 4718-4736.

[99] Ghiocel, D. & Ghanem, R. (2002). Stochastic finite element analysis of seismic soil–structure interaction. *Journal of Engineering Mechanics,* 128**,** 66-77.

[100] Berveiller, M., Sudret, B. & Lemaire, M. (2006). Stochastic finite element: a non-intrusive approach by regression. *Rev. Européenne Mécanique Numérique,* 15.

[101] Dessombz, O., Thouverez, F. & Lainé, J.P. (1999). Interval structural analysis of uncertain mechanical systems: static and dynamic cases. *Actes du congrès : Euromech 405, Valenciennes, France***,** 65-74.

[102] Koyliioglu, H.U., Cakmak, A.S. & Nielsen, S.R.K. (1995). Interval algebra to deal with pattern loading and structural uncertainties. *Journal of Engineering Mechanics,* 121**,** 1149-1157.

[103] Mullen, R.L. & Muhanna, R.L. (1999). Bounds of structural response for all possible loading combinations. *Journal of Structural Engineering,* 125**,** 98-106.

[104] Dessombz, O., Thouverez, F., Laine, J.P. & Jezequel, L. (2001). Analysis of mechanical systems using interval computations applied to finite element methods. *Journal of Sound and Vibration,* 239**,** 949-968.

[105] Majumder, L. & Rao, S.S. (2009). Interval-based optimization of aircraft wings under landing loads. *Computers & Structures,* 87**,** 225-235.

[106] Xu, M. & Qiu, Z. (2013). Free vibration analysis and optimization of composite lattice truss core sandwich beams with interval parameters. *Composite Structures,* 106**,** 85-95.

[107] Santoro, R., Muscolino, G. & Elishakoff, I. (2015). Optimization and anti-optimization solution of combined parameterized and improved interval analyses for structures with uncertainties. *Computers & Structures,* 149**,** 31-42.

[108] Zadeh, L.A. (1965). Fuzzy sets. *Information and Control,* 8**,** 338-353.

[109] Moens, D. & Vandepitte, D. (2005). A survey of non-probabilistic uncertainty treatment in finite element analysis. *Computer Methods in Applied Mechanics and Engineering,* 194**,** 1527-1555.

[110] Sawyer, J.P. & Rao, S.S. (1999). Strength-based reliability and fracture assessment of fuzzy mechanical and structural systems. *AIAA Journal,* 37.

[111] Massa, F., Tison, T. & Lallemand, B. (2006). A fuzzy procedure for the static design of imprecise structures. *Computer Methods in Applied Mechanics and Engineering,* 195**,** 925-941.

[112] Massa, F., Ruffin, K., Tison, T. & Lallemand, B. (2008). A complete method for efficient fuzzy modal analysis. *Journal of Sound and Vibration,* 309**,** 63-85.

[113] Farkas, L., Moens, D., Vandepitte, D. & Desmet, W. (2010). Fuzzy finite element analysis based on reanalysis technique. *Structural Safety,* 32**,** 442-448.

[114] Abaqus (2011). Standard User's Manual. *Dassault Systèmes Simulia*.

[115] Katili, I. (1993). A new discrete Kirchhoff-Mindlin element based on Mindlin–Reissner plate theory and assumed shear strain fields—part II: An extended DKQ element for thick-plate bending analysis. *International Journal for Numerical Methods in Engineering,* 36**,** 1885-1908.

[116] Matlab (2015). MATLAB tutorials and learning resources. *1994-2015 The Math Works, Inc*.

[117] Engineering.Purdue.Edu Castigliano's theorem. *https://engineering.purdue.edu/~ce474/Docs/The%20Theorem%20of%20Least%20Work_2012.pdf*.

[118] Ashton, J.E. & Whitney, J.M. (1970). Theory of laminated plates. *Technomics Publishing*.

[119] Nettles, A.T. (1994). Basics mechanics of laminated composite plates. *NASA Reference Publication 1351*.

[120] Reddy, J.N. (2004). Mechanics of laminated composite plates and shells. *CRC Press*.

[121] Berthelot, J.M. (2005). Matériaux composites: Comportement mécanique et analyse des structures. *Tec & Doc Lavoisier*.

[122] Rahman, S. & Xu, H. (2005). A meshless method for computational stochastic mechanics. *International Journal of Computational Methods in Engineering Science and Mechanics,* 6**,** 41-58.

[123] Noh, H.C. (2006). Effect of multiple uncertain material properties on the response variability of in-plane and plate structures. *Computer Methods in Applied Mechanics and Engineering,* 195**,** 2697-2718.

[124] Stefanou, G. & Papadrakakis, M. (2004). Stochastic finite element analysis of shells with combined random material and geometric properties. *Computer Methods in Applied Mechanics and Engineering,* 193**,** 139-160.